CONSTRUCTION, ANALYSIS AND VALIDATION OF A MATHEMATICAL MODEL OF HUMAN METABOLISM

A Dissertation

Submitted to the Graduate School
of the University of Notre Dame
in Partial Fulfillment of the Requirements
for the Degree of

Doctor of Philosophy

by

Dayu Lv

Bill Goodwine, Director

Graduate Program in Aerospace and Mechanical Engineering
Notre Dame, Indiana
April 2011

CONSTRUCTION, ANALYSIS AND VALIDATION OF A MATHEMATICAL MODEL OF HUMAN METABOLISM

Abstract

by

Dayu Lv

This thesis develops a mechanistic model of glucose metabolism in the human body, representing transport and oxidization of glucose to maintain energy balance. The model is a set of differential equations. The forms of these equations are primarily based on qualitative understanding of the relevant physiological process and the related chemical reactions and experimental data. The parameters in these differential equations represent physiological characteristics and therefore have physical meanings.

The first part of this thesis develops a model of glucose metabolism, which includes the brain, the liver, skeletal muscle and the pancreas. The model is mechanistic because it includes, among other things, detailed representations of glucose transporters and the metabolic pathways. The transporters have different properties in different organs. The parameters in the model come from chemical balances, ranges of normal values published in the literature, curve fitting of experimental data and tuning. In simulation protocols of meals and various exercise intensities, the results demonstrate a qualitative agreement with the dynamics of glucose metabolism in healthy subjects.

The next part of this thesis develops a sub-model of the pancreas which includes more differential equations representing additional physiological processes.

The parameters of this pancreas model are obtained by a global optimization method. Parallel computing is implemented to handle the large computational cost of the optimization method. The simulation results demonstrate that this pancreas model can capture the transient response in intravenous glucose tolerance tests (IVGTT), which is an important characteristic of a healthy pancreas. The values of the parameters can categorize subjects such as normal ones, as well as mild, moderate and treated type 2 diabetics. Unlike much of the literature, the model is validated by comparison to experimental results that are not used in the parameters identification process.

The sub-model of glucose transport in skeletal muscle is also refined to incorporate more physiological information. Its parameters are also obtained by the optimization method. The simulation results demonstrate varied rates of glucose transport into muscle under different exercise intensities.

CONTENTS

FIGURES

TABLES

ACKNOWLEDGMENTS

I would like to express my gratitude to my advisor, Dr. Bill Goodwine, for his direction and help in my research. His advice and guidance help me finish the project and the writing of this thesis. Also I would to thank Dr. Mihir Sen, Dr. Glen Niebur and Dr. Mark Alber for serving in my thesis committee. And thank them for their time and efforts to improve this thesis.

I would also like to thank my lab colleagues, Neil Petroff, Baoyang Deng, Jason Nightingale and Alice Nightingale for all of their help and support, which make our lab a wonderful place to work in.

I would like to give great thanks to my wife for her continuous support and encouragement. I would also thank my parents and my family for giving me support, education and love.

Finally, I would thank God to give me wisdom and patience throughout the study.

CHAPTER 1

INTRODUCTION

Recent decades have witnessed an increasing trend of research focus on human metabolism, which provides energy and nutrition to the body. Irregularities or dysfunction in metabolic pathways may cause many health problems and impair our quality of life. One of these metabolic diseases is diabetes mellitus which is characterized by the body improperly regulating glucose concentration in plasma. As a chronic consequence, high glucose concentration may bring about severe diseases such as cardiovascular diseases, kidney diseases, blindness, *etc.* The cost related to diabetes in the United States was about $174 billion in 2007 (American Diabetes Association, 2007). Another metabolic problem, obesity, is gradually becoming a world wide concern. One of its forming reasons is due to an unhealthy life style of excess calories uptake and insufficient energy consumption. This may result in fat accumulation which may result in metabolic disturbance. Inside the human body, nutrients are extracted and oxidized to provide energy or to be converted into metabolites which are stored for future use. The balance between energy production and consumption is a key to understanding the dynamics of metabolism. When glucose and fatty acid uptake alone cannot meet energy demand, such as during high intensity exercise (such as sprinting), glycogen and triacylglycerol (TAG) stored in organs will be broken down to supply more substrates for energy production; on the other hand, if energy production

from uptake exceeds the consumption, such as having a sugar-rich meal in basal state, the metabolic pathways will prefer the storage direction.

Insulin plays a critical role in the balance between glucose and fatty acid metabolism. Insulin is produced by β-cells in the pancreas, stored in vesicle granules, and released to plasma to regulate concentrations of glucose and fatty acids. There are two different pathways of energy generation, aerobic respiration and anaerobic respiration, to produce molecular units of energy as adenosine triphosphate (ATP) which releases energy when hydrolyzed. It is clear that these two pathways are related to the sufficiency of the supplies of oxygen. Energy production is more efficient in aerobic respiration than that in anaerobic one.

The human body is a largely interconnected complicated system: the gut digests the food; the liver extracts nutrients and produces bile; the pancreas produces important hormones including insulin, glucagon and somatostatin; skeletal muscle and cardiac muscle utilize nutrients to provide required energy and store the excess as glycogen; and the kidneys work as filters to recycle nutrients. These organs play different roles in metabolism and as a whole, they work together in an integrated way to support daily life.

Diabetes is one of the metabolic disorder diseases. There are mainly two types of diabetes, Type 1 and Type 2. Type 1 diabetes is insulin dependent which is due to autoimmune destruction of β-cells leading to the failure of insulin production. Related research is focused on the control of exogenous insulin injection rate to maintain glucose concentration at a certain level (Campos-Delgado et al., 2005; Chee et al., 2005; Parker et al., 2000; Ruiz-Velázquez et al., 2004). As for Type 2 diabetes, it is a non-insulin-dependent disease with characteristics such that organs cannot react to insulin properly which results in glucose intolerance,

insulin resistance, *etc.* One motivation of this research is to reduce the impact of Type 2 diabetes. Constructing a mechanistic mathematical model to represent relations and dynamics of glucose and insulin concentrations in various subjects may give us guidelines to find efficient control parameters to maintain metabolites concentrations at healthy levels.

The whole systematic metabolism model is composed of several organ models including the brain, the pancreas, skeletal muscle and the liver. In the pancreas, insulin is produced, stored and released to regulate both glucose and fatty acids metabolism. A reliable model, which represents how glucose stimulates the activities of insulin and how insulin regulates glucose concentration, may play an important role at the metabolic simulation in the human body. In the 1970s, Bergman *et al.* proposed the so-called *minimal model* to quantitatively describe the relation between glucose and insulin which was given by

$$\frac{dG}{dt}(t) = -(p_1 + X(t))G(t) + p_1 G_b \tag{1.1}$$

$$\frac{dX}{dt}(t) = -p_2 X(t) + p_3(I(t) - I_b) \tag{1.2}$$

$$\frac{dI}{dt}(t) = -nI(t) + \gamma(G(t) - h)t, \tag{1.3}$$

with $G(0)$=$G_0, X(0)$=0 and $I(0)$=I_0 where $G(t), X(t)$ and $I(t)$ represent the concentrations of glucose in the plasma, the remote insulin and insulin in the plasma respectively and $p_1, p_2, p_3, G_0, n, \gamma, h$ and I_0 are parameters (Pacini and Bergman, 1986). Based on the minimal model, some metabolic characteristics were proposed, such as glucose effectiveness and insulin sensitivity. Due to the idea of this minimal model using the fewest number of parameters to represent the dynamics of glucose and insulin, it was constructed empirically rather than mechanistically.

One of its drawbacks is that it failed to provide detailed physiological pathways information, e.g., the pathways of glucose transport into the pancreas and glucose stimulation in the pancreas. Also the minimal model can not represent transient phenomenon such as insulin release in an intravenous glucose tolerance test (IVGTT). This will prevent it from being used in longer term simulations which include meals because the peak of insulin release is one of the important characteristics of the pancreas. Simulation results of insulin response of the minimal model are illustrated in Figure 1.1. Stars represent the clinical data of glucose concentrations; empty squares represent the clinical data of insulin concentrations; and dash-dotted line represents the simulation result of insulin concentration in the minimal model. Observe that in the plot, the minimal model fails to capture the insulin transient response. This is because the low order of the minimal model cannot represent a long term dynamics of insulin concentration. In contrast to the minimal model, the pancreas model presented in this thesis describes insulin activities in a mechanistic way and it can represent the important characteristics of the pancreas such as insulin release peak and insulin clearance.

After the development of the minimal model, further research was based upon it. Cobelli added glucagon as another variable in the model (Cobelli et al., 1982). Additional models were proposed for some specific organs, such as skeletal muscle (Dash et al., 2007). In his paper, Dash designed a computational model to simulate responses of skeletal muscle to chronically loaded and unloaded exercises, which may reflect metabolic adaptations.

In 2000, the weight of β-cells was introduced to the system of glucose and insulin concentrations (Topp et al., 2000). The model included three ordinary

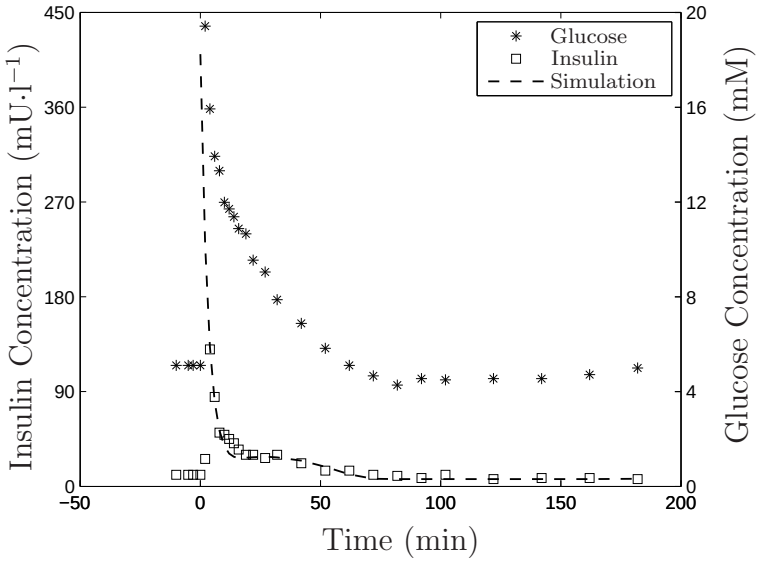

Figure 1.1. Experimental data and simulation results of insulin response to IVGTT from minimal model (Pacini and Bergman, 1986). Data before time $t = 0$ are extended from the basal states.

differential equations,

$$\frac{dG}{dt}(t) = R_0 - (E_{G_0} + S_I I)G(t) \tag{1.4}$$

$$\frac{dI}{dt}(t) = \frac{\beta\sigma G(t)^2}{\alpha + G(t)^2} - kI(t) \tag{1.5}$$

$$\frac{d\beta}{dt}(t) = (-d_0 + r_1 G(t) - r_2 G(t)^2)\beta(t), \tag{1.6}$$

where $G(t)$ and $I(t)$ represent the concentrations of glucose and insulin respectively; $\beta(t)$ represents the mass of β-cells; R_0 represents the net rate of production at zero glucose; E_{G_0} represents the total glucose effectiveness at zero insulin concentration; S_I represents the total insulin sensitivity; σ represents the maximal insulin releasing rate; α represents the glucose concentration, $G = \alpha^{1/2}$, when insulin reaches half its maximal value; d_0 represents the death rate of β-

cells at zero glucose; and k, r_1 and r_2 are constants. This model is characterized by bifurcations brought about by the parameter r_1, which may be related to the physiological progression of Type 2 diabetes. There are two stable fixed points representing physiological and pathological steady states. Stability analysis was performed based on Topp's model (Adrover et al., 2006; Creta et al., 2006; Giona et al., 2006; Petrosyan, 2003) shows the system has two stable equilibrium points and one saddle point. According to the properties of the system eigenvalues, the Intrinsic Low Dimensional Manifold method was utilized to find slow manifolds of the system.

Other research has focused on kinetic properties of hormones, particularly insulin (Duckworth et al., 1998; Finegood and Topp, 2001). An insulin model with glucose clamped and constant transport rates among compartments was introduced by Sherwin (Sherwin et al., 1974). There exists oscillation in insulin release which appeared as the variation of glucose concentration (Tolić et al., 2000). Another mathematical model was established to describe long term β-cell dysfunction (Bagust and Beale, 2003), which may represent the development of Type 2 diabetes.

As for aerobic and anaerobic respiration, the dynamical relation between oxygen and lactate has also been investigated (Cabrera et al., 1998). Oxygen is a very important molecule participating in various metabolic reactions, especially in aerobic respiration to generate energy. Cabrera *et al.* constructed a mathematical model to represent the dynamics of oxygen from the kinetics of mass and reactions in muscle, splanchnic organs, *etc.*

Researchers were also interested at constructing a Compartmental Physiological Model (CPM) to achieve the goal of adjusting or changing the whole phys-

iological system. A systematic metabolism model was first proposed by Guyton (Guyton et al., 1978). The model was developed to represent glucose-insulin relation in normal subjects and Type 1 diabetics (Parker et al., 2001; Sorensen, 1985) and Type 2 diabetics (Vahidi et al., 2010). The model was specified for the Type 1 diabetics, so it did not include the pancreas due to the failure of insulin production in Type 1 diabetics. The methods of feedback control, robust control, fuzzy control, *etc.* were implemented to analyze characteristics of the metabolic system, such as system stability (Campos-Delgado et al., 2006; Owens et al., 2006; Park et al., 1999; Parker et al., 2000; Quiroz and Femat, 2007; Ruiz-Velázquez et al., 2004). A simplified model was established for insulin sensitivity analysis (Panunzi et al., 2007).

Many of the proposed models outlined above were mainly restricted to substrates such as glucose and insulin while the properties of transporters' activities were not incorporated, e.g., the tissue-specific glucose transporters. In contrast, this thesis presents a mechanistic model which incorporates more physiological information such as the characteristics of glucose transporters. Its goals are to track the dynamics of energy which determines the change of substrates and metabolites, and investigate pathways and relations between glucose and fatty acids. It shows different dimensions for the metabolic regulation of glucose in the human body. Also, this model attempts to improve the understanding about metabolic pathways in Type 2 diabetes mellitus which is also called non-insulin-dependent diabetes mellitus. A deterministic optimization method called DIRECT (DIviding RECTangles) (Jones et al., 1993) is used to obtain model parameters. DIRECT searches for global optimal solutions in the parameters space.

Glucose in the plasma may come from meals or be released from the liver.

It is carried through cell membranes facilitated by tissue-specific glucose transporters (GLUTs). Then it is converted to glucose-6-phosphate (G6P) which is a key metabolite described in this model. In liver, G6P may be converted back to glucose and released to plasma as a supply for organs (Frayn, 2003; Schaftingen and Gerint, 2002). In skeletal muscle and the liver, G6P may also be stored in the form of glycogen through glycogenesis, which can be described as a highly branched polymer of glucose residues. As an energy storage, glycogen may be broken down to generate G6P *via* glycogenolysis. Through aerobic glycolysis and anaerobic glycolysis, G6P may be metabolized to generate energy units (ATP). Anaerobic glycolysis is stimulated when aerobic respiration cannot produce enough energy as required by activities.

Fatty acid metabolism includes the metabolites of fatty acids and lipoprotein particles in the plasma. Lipoprotein particles are composed of chylomicrons (CLM), very-low-density lipoproteins (VLDL), *etc.* The CLM is taken up from the gut and released to the circulation system through lymphatic ducts. VLDL is secreted endogenously from the liver. Lipoprotein particles are too large to enter the interstitial fluid directly so they need to be hydrolyzed into fatty acids by lipoprotein lipase located in skeletal muscle, the heart and adipose. After that, fatty acids are carried into cells by the transporter FAT/CD36 and may be esterified as triacylglycerol (TAG).

Insulin regulates many of pathways in metabolism of glucose and fatty acid. It is produced by β-cells in the pancreas and is stimulated by glucose. Insulin in the plasma will enter organs such as the liver and the kidneys, inside which insulin will be degraded by enzymes. There exist connections between glucose metabolism and fatty acid metabolism. As one of the connecting metabolites,

Acetyl-CoA (ACA) can enter the citric acid cycle (TCA cycle) to be oxidized for energy production. ACA may come from G6P or β-oxidization of fatty acids.

The whole-body human metabolic model is composed of several organs: the brain, the pancreas, skeletal muscle and the liver. Mechanistic modeling of these organs may provide a convenient tool to provide insight into human physiology and also the pathophysiology of disease. Also, it will allow for inexpensive biosimulation, which might provide guidance to *in vivo* and *in vitro* experimentation.

CHAPTER 2

OVERALL MODEL OF GLUCOSE METABOLISM

In this thesis, the mechanistic modeling of metabolism is based on energy balance by assuming that the energy generation meets the demand. The whole metabolism model is represented by the integration of models of various organs. As the first step, the metabolism of glucose and the hormone of insulin are investigated. In this chapter, the glucose metabolism models in the brain, the pancreas, muscle and the liver are proposed. Simulation results illustrating qualitatively reasonable physiological behavior are included. Chapter 3 will refine the model in greater detail with the goal of quantitative validation.

2.1 The Brain

The brain does not appear to use fatty acids as a metabolic fuel. Instead, glucose is the primary source of energy in the brain. It is the case that in starvation, ketone bodies may be used to compensate for insufficient glucose (Frayn, 2003), but that is an extreme case not incorporated into the model in this thesis. Most of glucose uptake in the brain will be oxidized completely to sustain neural activities. As stated previously, glucose is carried into cells by a family of proteins called glucose transporters (GLUTs). In the brain, there are two main isoforms of glucose transporters called GLUT1 and GLUT3. GLUT1 is mainly expressed

in the endothelial cells while GLUT3 is located in the neurons. The blood-brain barrier receives its name from acting like a barrier to prevent some substances entering the brain while some others can (Frayn, 2003). For example, it can block the entrance of lipid-soluble molecules to the brain.

The mathematical representation of the well-known Michaelis-Menten function is given by Equation 2.1 (Frayn, 2003)

$$Rate = V_{\max}\frac{[S]}{[S] + K_m}, \tag{2.1}$$

where $V_{\max}$ represents the maximum reaction rate; K_m represents the substrate concentration when the rate is half-maximal; and $[S]$ represents the substrate concentration. A Michaelis-Menten curve is illustrated in Figure 3.19. This is a common representation for glucose transport by carrier-mediated diffusion because GLUTs follow the Michaelis-Menten relationship to carry glucose into cells in various organs.

Since the brain completely consumes most of glucose in it, in this model the direction of glucose transport is considered as entering the brain inward only. It is assumed that glucose entering into the interstitial fluid space (IFS) will be completely oxidized. The normal glucose concentration in the plasma is a little bit under 5 mM (Frayn, 2003). Since K_m of GLUT1 (5$\sim$7 mmol$\cdot$l^{-1}) is considerably larger than that of GLUT3 (1.6 mmol$\cdot$l^{-1}), which means that the neurons can take up glucose *via* GLUT3 at a relatively constant rate under normal glucose concentration. Thus, the limitation of glucose transport is determined almost completely by GLUT1. So for simplification, only GLUT1 is considered here for glucose transport and the effect of GLUT3 will be represented by V_{maxb1} and K_{mb1} which are given as $V_{maxb1} = 62 \pm 19$ mmol$\cdot$100Kg-brain$^{-1}\cdot$min^{-1} and $K_{mb1} =$

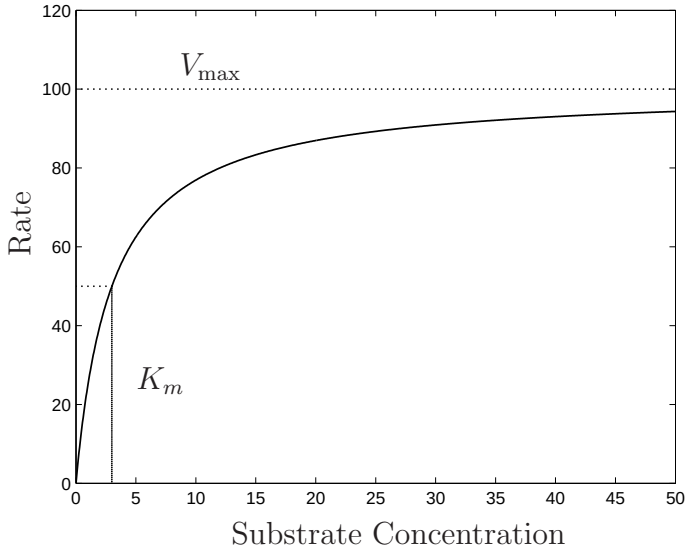

Figure 2.1. Michaelis-Menten Characteristics.

4.1 ± 2.3 mM (Blomqvist et al., 1991). Thus the glucose transport rate into the brain is defined as

$$G_b(t) = V_{maxb1} m_b \frac{G(t)}{K_{mb1} + G(t)}, \tag{2.2}$$

where $G_b(t)$ (mmol·min^{-1}) represents the glucose transport rate in the brain; $G(t)$ (mmol·l^{-1}) represents the glucose concentration in plasma; and m_b (Kg) represents the mass of the brain.

2.2 The Pancreas

From *in vitro* experimental data (Frayn, 2003), insulin is released from β-cells, which follows a sigmoid-like function illustrated by the open boxes in Figure 2.2. Thus, a mathematical representation of insulin increasing concentration ($I_1(t)$,

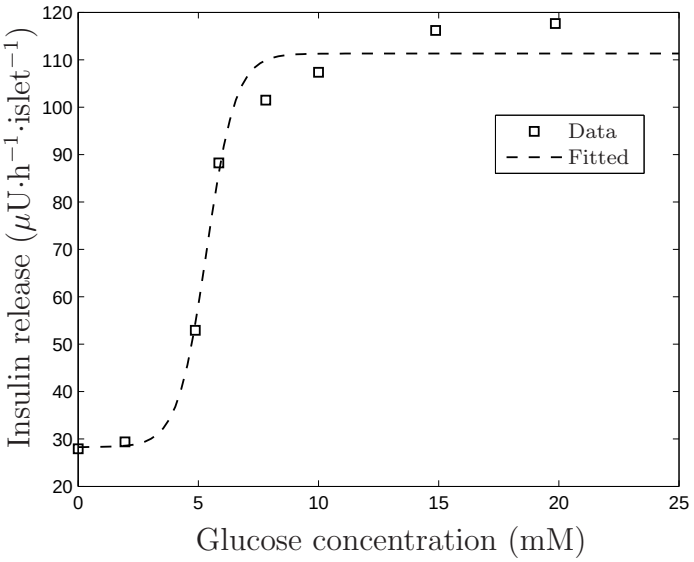

Figure 2.2. Insulin release with respect to glucose concentrations. Data fitted from (Frayn, 2003).

mU·l^{-1}) is given by

$$\frac{dI_1}{dt}(t) = \left(\frac{79.21}{1 + e^{-1.934G(t)+10.52}} + 29.84 \right) \frac{0.7n}{60V_p}, \tag{2.3}$$

as illustrated by the dashed line in Figure 2.2 where $G(t)$ (mM) represents the glucose concentration in the plasma; $n \approx 10^6$ represents the number of Langerhans cells in the pancreas (Gray, 1985); and V_p (l) represents the volume of the plasma which is assumed to be linearly correlated with a subject's mass (Levitt, 2003). The other parameters' values were obtained from the curve fit, which was computed using the Matlab *fit*() function.

Insulin in the plasma is cleared by the organs such as the liver and the kidneys (Duckworth et al., 1998; Wilcox, 2005). In the literature, the decreasing rate

of insulin concentration ($I_2(t)$, mU·l^{-1}) was proposed as an exponential function:

$$\frac{dI_2}{dt}(t) = I(t)e^{-20t}, \tag{2.4}$$

where $I(t)$ (mU·min^{-1}) represents the insulin concentration in the plasma. Since the data of insulin release in from an *in vitro* test of β-cells, the real insulin release rate from the pancreas may not reach the level as in Equation 2.3. The parameter in Equation 2.4 was determined by trial and error. Thus, the changing rate of insulin concentration ($I(t)$ mU·l^{-1}) is determined by

$$\frac{dI}{dt}(t) = \frac{dI_1}{dt}(t) + \frac{dI_2}{dt}(t). \tag{2.5}$$

2.3 Skeletal Muscle

Skeletal muscle is the main place of energy demand because carrying on physical activities requires contractions of muscle which consume energy at the appropriate time. Inside cells, there is a pool of phosphocreatine which can be used to maintain the ATP concentration at a relatively constant level such that it can provide enough energy before other pathways do. So the concentration of ATP remains at a constant level (Frayn, 2003).

2.3.1 Glucose Transport

The model of glucose transport in muscle is divided into three compartments: the plasma, the interstitial fluid space (IFS) and the intracellular space (ICS), which is illustrated in Figure 2.3. Glucose transport between the plasma and the IFS is by diffusion whereas from the IFS to the ICS, it is facilitated by GLUTs (Frayn, 2003). There are two main glucose transporters expressed in

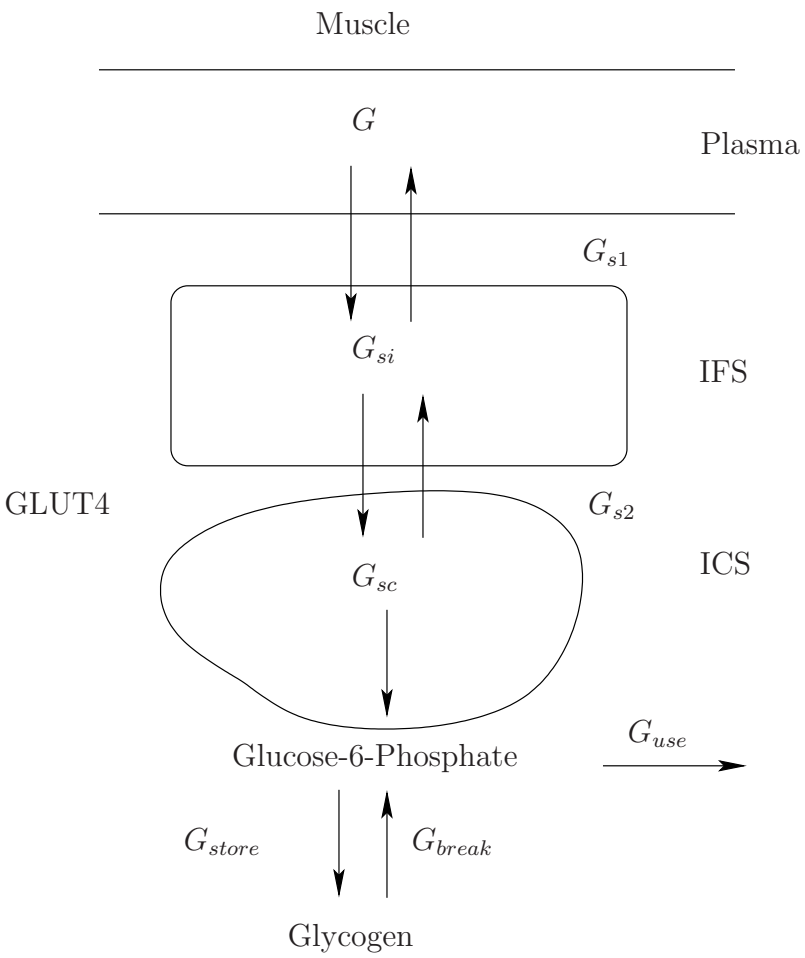

Figure 2.3. Glucose transport into skeletal muscle.

the membranes of muscle cells: GLUT1 and GLUT4. The Michaelis constants of GLUT1 and GLUT4 are similar, but GLUT4 plays a more important role due to its responses with respect to the hormone insulin and exercise. Therefore, this model considers GLUT4 only and the effects of GLUT1 may be integrated into the basal rate of GLUT4.

The volumes of the IFS and the ICS are represented by V_{si} (l) and V_{sc} (l) respectively and may be related to the mass of skeletal muscle by (Aukland and Reed,

1993; Binzoni et al., 1998)

$$V_{si} = 0.1 m_s \tag{2.6}$$

$$V_{sc} = 0.185 m_s, \tag{2.7}$$

where m_s (Kg) represents the mass of skeletal muscle. The Michaelis-Menten characteristics, $V_{maxs-basal}$ (mmol·min^{-1}) and K_{ms4} (mM), are given in (Frayn, 2003; Govers et al., 2001),

$$V_{maxs-basal} = 1.0 m_s \tag{2.8}$$

$$K_{ms4} = 5.7. \tag{2.9}$$

The maximal velocity (V_{max}) is highly influenced by the insulin concentration and the intensity of exercise (Fujimoto et al., 2003; Sarabia et al., 1992). The approximate oxygen consumption rate during rest is about 25% of the maximum oxygen consumption rate and the corresponding glucose uptake rate is about 32 μmmol·kg^{-1}·min^{-1} (Brooks, 1998; Swain, 2000). The mathematical representations of effects of insulin and exercise on GLUT4, denoted by y_{in} and y_{exe} respectively, can be fitted from the data given in the literature, which are expressed in Equation 2.10 and 2.11. And the corresponding plots are illustrated in Figure 2.4 and 2.5

$$y_{in} = \frac{1.433}{1 + e^{-0.2473 \log_{10} I(t) - 3.271}} \tag{2.10}$$

$$y_{exe} = \frac{4.453}{1 + e^{0.2(-198.5\mathrm{FO(t)} + 60.95)}} + 1, \tag{2.11}$$

where I (mU·dl^{-1}) represents the insulin concentration; and FO (flag of oxygen

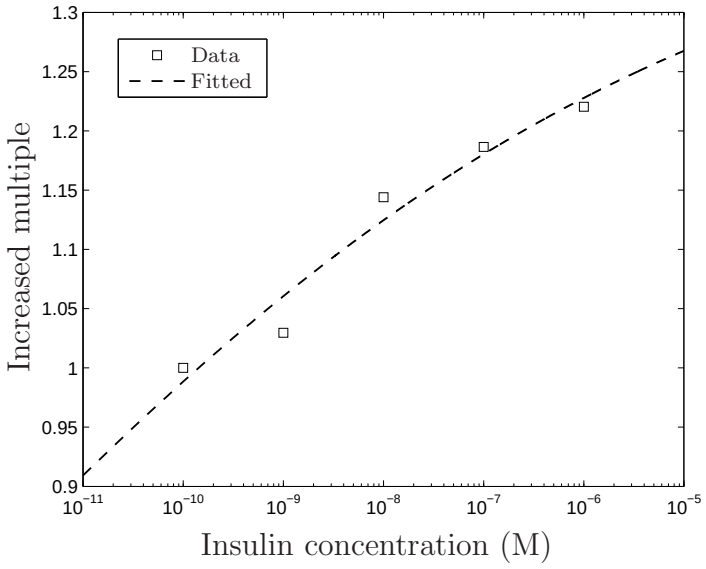

Figure 2.4. GLUT4 activity with respect to insulin concentrations. Data fitted from (Sarabia et al., 1992).

consumption rate, which is equal to the ratio of $\dot{V}_{O_2}/\dot{V}_{O_2\,\max}$) represents the ratio of oxygen consumption rate with respect to the maximal value, which reflects the exercises intensity. The parameters values in Equations 2.10 and 2.11 were computed using the Matlab *fit*() function.

Therefore glucose transport in skeletal muscle can be determined as following:

1. The glucose transport rate from the plasma to the IFS is denoted by f_{gs} (mmol·min^{-1}). It is positive when the glucose is moving from the plasma to the IFS. It may be represented by

$$f_{gs}(t) = 3.0(G(t) - G_{si}(t)), \tag{2.12}$$

where $G(t)$ and $G_{si}(t)$ represent glucose concentrations in the plasma and the IFS respectively. The coefficient of 3.0 l·min^{-1} is because the cardiac

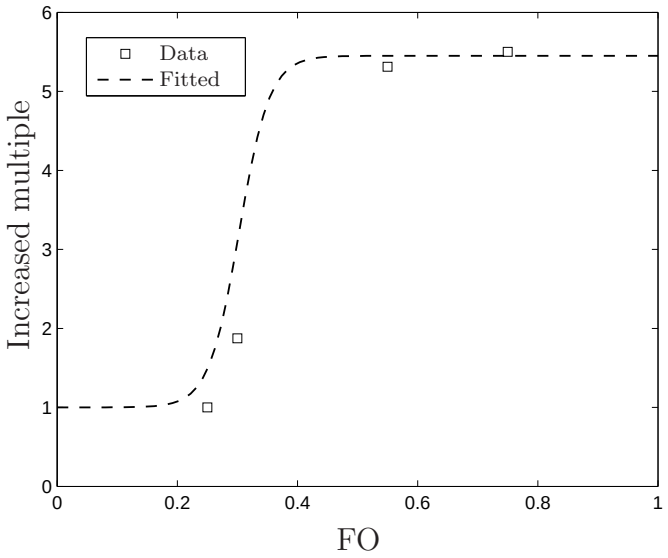

Figure 2.5. GLUT4 activity with respect to oxygen consumption ratio. Data fitted from (Brooks, 1998; Fujimoto et al., 2003)

output of blood is about 5∼25 l·min^{-1} in various exercise intensities (Frayn, 2003).

2. The glucose transport rate from the IFS to the ICS is denoted by f_{gsi} (mmol·min^{-1}). It is positive when the glucose is moving from the IFS to the ICS. It may be represented by

$$f_{gsi}(t) = V_{maxs-basal}\frac{G_{si}(t)}{K_m + G_{si}(t)}y_{in}y_{exe}, \tag{2.13}$$

where $G_{si}(t)$ represents the glucose concentration in the IFS; $V_{maxs-basal}$ and K_{ms4} represent the characteristics of GLUT4 in the Michaelis-Menten transport.

3. Thus, the change rate of the concentration of glucose in the IFS (mM·min^{-1})

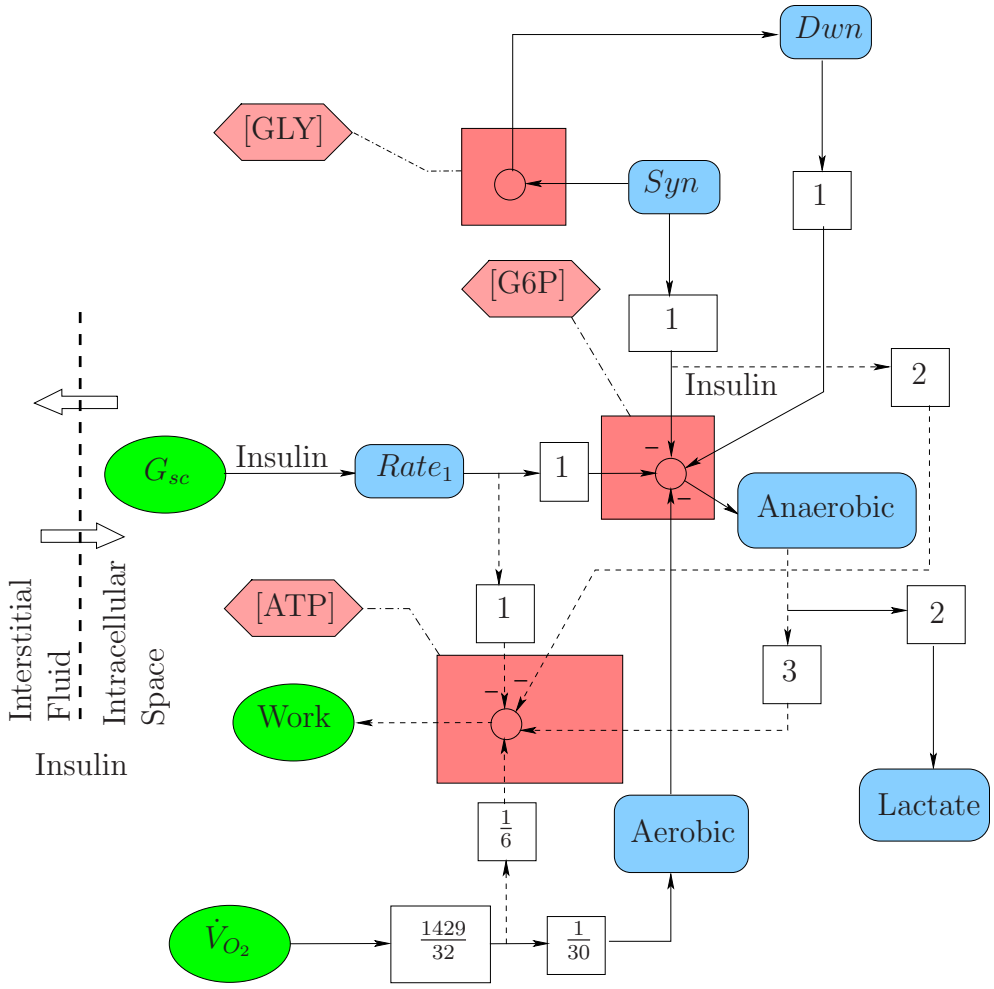

Figure 2.6. Glucose metabolism in skeletal muscle.

is given by

$$\frac{dG_{si}}{dt}(t) = \frac{1}{V_{sc}} \left(f_{gs}(t) - f_{gsi}(t) \right). \tag{2.14}$$

2.3.2 Glucose Utilization

Regulated by insulin in the ICS, glucose (G_{sc}) will be utilized as a fuel or stored as glycogen for future use. A block diagram of intracellular glucose metabolism is illustrated in Figure 2.6.

This model represent the intracellular glucose metabolism in skeletal muscle. It has three main metabolites represented by hexagons, which are ATP (energy units), G6P (Glucose-6-Phosphate, the key metabolite in glucose metabolism) and GLY (Glycogen, a branched glucose polymer). The energy requirement (units of ATP) for performing muscle contractions is represented by Work ($\text{mmol}\cdot\text{min}^{-1}$) which can be converted from energy output (units of Watt) by ATP energy release of 57 $\text{KJ}\cdot\text{mol}^{-1}$ during hydration (Stryer, 2002); the oxygen consumption rate is denoted by $\dot{V}_{O_2}$ ($\text{l}\cdot\text{min}^{-1}$) and the unit conversion from $\text{l}\cdot\text{min}^{-1}$ to $\text{mmol}\cdot\text{min}^{-1}$ is achieved by $\dot{V}_{O_2} \times \frac{1.429}{32} \times 1000$ with oxygen density of 1.429 $\text{g}\cdot\text{l}^{-1}$ and oxygen molar mass of 32 $\text{g}\cdot\text{mol}^{-1}$ (Mellor, 2010). As a key metabolite in the glucose metabolism, the G6P can either be converted to glycogen as storage for future use or be metabolized as a fuel in two routes: aerobic respiration and anaerobic respiration.

In the pathway of glycolysis, G6P is converted to pyruvate, which is metabolized to acetyl-CoA in aerobic respiration to enter the citric acid cycle (also called Krebs Cycle) to be fully oxidized. It is assumed that the oxygen delivered to metabolic sites is completely utilized. The quantification of aerobic respiration is determined by the reaction as below

$$1\ \text{G6P} + 30\ \text{O}_2 \rightarrow 5\ \text{ATP}. \tag{2.15}$$

Therefore as illustrated in Figure 2.6, in the pathway of aerobic respiration, the rates of energy production ($ATP_{aerobic}$, $\text{mmol}\cdot\text{min}^{-1}$) and G6P consumption

($G6P_{aerobic}$, mmol·min^{-1}), are represented by

$$ATP_{aerobic}(t) = \left(\frac{1429}{32} \times \frac{1}{6}\right) \mathrm{FO}(t)\dot{V}_{O_2\,\max} \tag{2.16}$$

$$G6P_{aerobic}(t) = \left(\frac{1429}{32} \times 130\right) \mathrm{FO}(t)\dot{V}_{O_2\,\max}, \tag{2.17}$$

where FO represents the oxygen consumption ratio of $\dot{\mathrm{V}}_{\mathrm{O2\,max}}$ and $\dot{\mathrm{V}}_{\mathrm{O2\,max}}$ (l·min^{-1}) represents the maximal oxygen consumption rate. Also, energy is consumed in the pathways of converting glucose into G6P and glycogen synthesis.

The process of converting glucose into G6P is mediated by the enzyme hexokinase (HK), which is stimulated by insulin. The activity of HK follows the Michaelis-Menten dynamics with the constant $K_m = 0.07$ mM and the maximal reaction rate $V_{\max} = 8.9$ mmol·kg-muscle^{-1}·min^{-1} (Govers et al., 2001). Hence the conversion rate in the basal state ($Rate_0$, mmol·min^{-1}) is represented by

$$Rate_0(t) = 8.9 m_s \frac{G_{sc}(t)}{0.07 + G_{sc}(t)}, \tag{2.18}$$

where m_s (Kg) represents the mass of skeletal muscle and $G_{sc}(t)$ (mM) represents the glucose concentration in the ICS.

There are two expression of HK in skeletal muscle: HK-1 and HK-2. The distribution of HK-2 is about 40%-70%. HK-1 is unaffected by insulin while HK-2 is stimulated by insulin (Kruszynska et al., 1998). Therefore the activity of HK-1 may be represented in the basal converting rate $Rate_0$. HK activity is inhibited by the product G6P (Frayn, 2003; Govers et al., 2001; Kruszynska et al., 1998). The effects of stimulation and inhibition may be saturated due to the substrates capacities (Govers et al., 2001; Kruszynska et al., 1998). The data are illustrated in Figure 2.7 and 2.8.

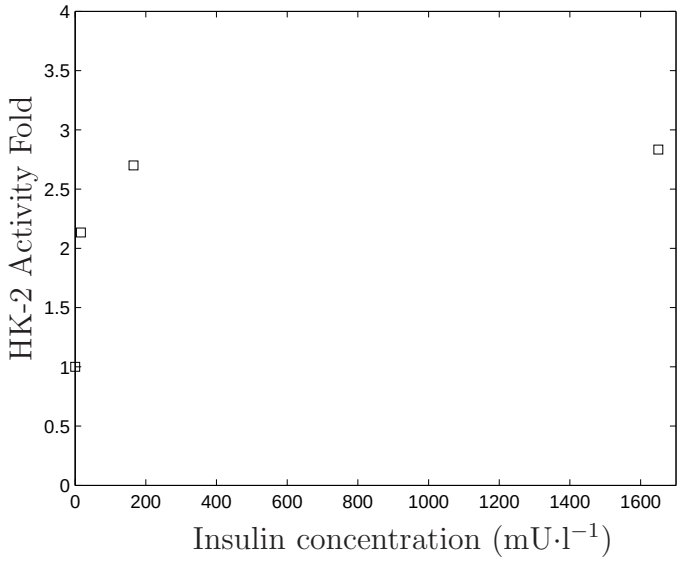

Figure 2.7. Insulin stimulates HK-II activity. Data fitted from (Printz et al., 1993).

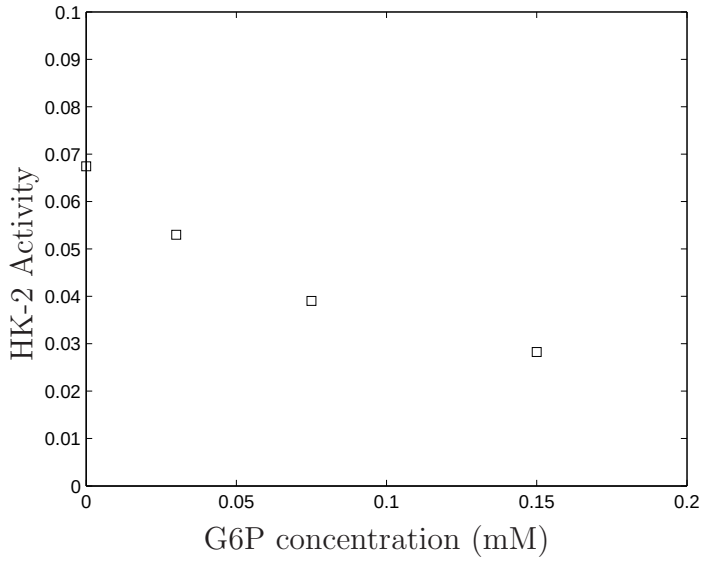

Figure 2.8. G6P inhibits HK-II activity. Data fitted from (Gregoriou et al., 1986).

Thus, the mathematical representations of the effects of insulin (I_R, unitless) and G6P ($G6P_R$, unitless) may be represented by sigmoid functions given as

$$I_R(t) = \frac{2}{1 + e^{(-I(t)+40.0)/20}} \tag{2.19}$$

$$G6P_R(t) = \frac{2}{1 + e^{(G6P_s(t)-0.12m_s/V_{sc})/10}}, \tag{2.20}$$

where I (mU·l^{-1}) represents insulin concentration in the plasma; $G6P_s$ (mM) represents G6P concentration in the ICS; and V_{sc} (l) represents the volume of the ICS. The parameters were determined by trail and error. Thus, G6P production rate from glucose ($Rate_1$, mmol·min^{-1}) may be determined by

$$Rate_1(t) = Rate_0(t)I_R(t)G6P_R(t). \tag{2.21}$$

The conversion processes between G6P and glycogen are expressed as Syn and Dwn, which represent the rates of glycogen synthesis and breakdown respectively. They are affected by the concentrations of insulin, G6P and glycogen. The mathematical representations are established as follows,

1. Syn (mmol·min^{-1}) represents the rate of glycogen synthesis called as glycogenesis.

   (a) The process of glycogenesis is stimulated by G6P (Kelley and Mandarino, 1990; Villar-Palasi, 1991). The data are illustrated in Figure 2.9. Thus, the mathematical representation of the effect ($G6P_{Syn}$, unitless) may be represented by

$$G6P_{Syn}(t) = 0.15e^{\log_{10}\left(\frac{G6P_s(t)}{0.133}\right)}, \tag{2.22}$$

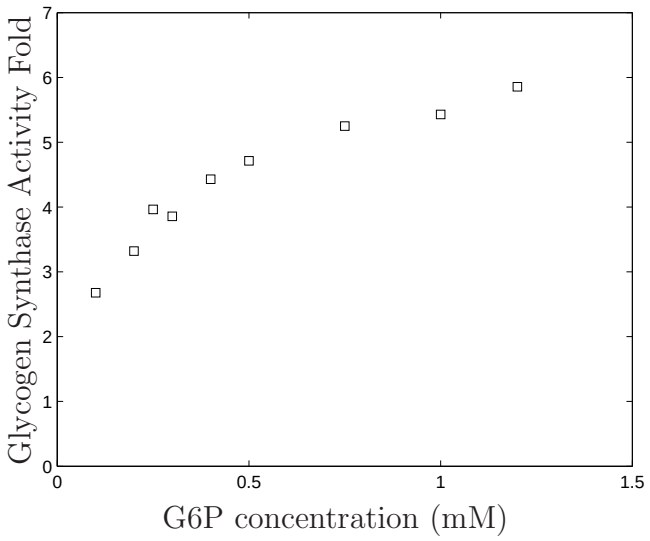

Figure 2.9. G6P stimulates the activity of glycogen synthase. Data fitted from (Villar-Palasi, 1991).

where $G6P_s(t)$ (mM) represents the G6P concentration in skeletal muscle. The parameters were determined by trail and error. The rate of glycogenesis is stimulated when the concentration of G6P increases.

(b) Glycogenesis is stimulated by insulin (Kelley and Mandarino, 1990; Mandarino et al., 1987). The data are illustrated in Figure 2.10. Thus, the mathematical representation of insulin effect ($I_{Syn}(t)$, unitless) may be represented by

$$I_{Syn}(t) = \frac{1.625}{1 + e^{-(I(t)-3.24)/38.2}}, \tag{2.23}$$

where $I(t)$ ($\mathrm{mU \cdot l^{-1}}$) represents the insulin concentration. The parameters were determined by trail and error.

(c) Glycogenesis is mediated by the enzyme glycogen synthase. It is as-

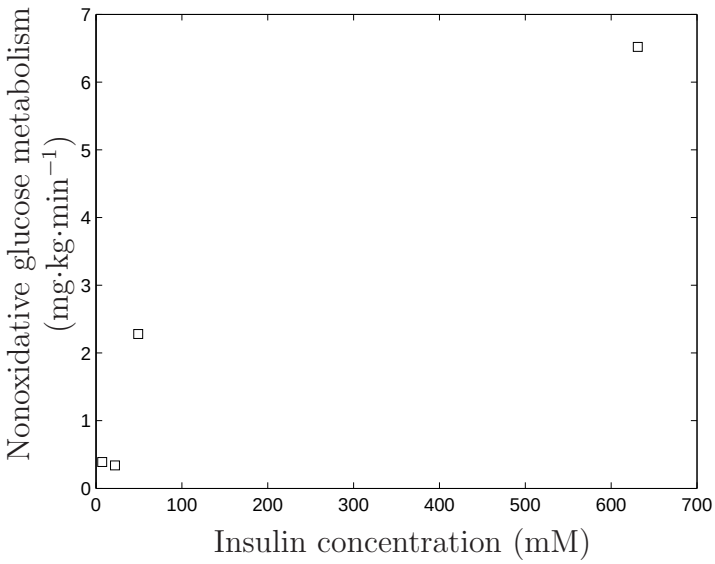

Figure 2.10. Insulin stimulates nonoxidative glucose metabolism which is similar to glycogen synthase. Data fitted from (Mandarino et al., 1987).

sumed that the glycogenesis rate may be saturated as the concentration of glycogen increases. The glycogen concentration effect ($GLY_{Syn}(t)$, unitless) may be represented by

$$GLY_{Syn}(t) = \frac{2}{1 + e^{GLY_s(t) - 0.95GLY_{smax}}}, \tag{2.24}$$

where $GLY_s(t)$ (mM) represents current glycogen concentration in skeletal muscle; and $GLY_{s\max}$ (mM) represents the possible maximal glycogen concentration in skeletal muscle. When the glycogen concentration is increasing and approaching to the maximal value, the synthesis will slow down. The parameters were determined by trail and error.

Together the rate of glycogenesis ($Syn(t)$, mmol·min^{-1}) is represented by

$$Syn(t) = Syn_0(t) \cdot I_{Syn}(t) \cdot G6P_{Syn}(t) \cdot GLY_{Syn}(t), \tag{2.25}$$

where Syn_0 (mmol·min^{-1}) represents the basal glycogen synthesis rate. It is about 0.02 mM·min^{-1} (Mandarino et al., 1987).

2. The rate of glycogen breakdown, also called glycogenolysis, is processed by glycogen phosphorylase. The rate is represented by Dwn (mmol·min^{-1}). It is influenced by G6P, insulin and exercise intensity.

   (a) G6P is the product of glycogenolysis. It works as a substrate supply of energy production. The concentration of G6P inhibits the breakdown of glycogen (Aiston et al., 2003). The data are illustrated in Figure 2.11. Thus, the mathematical representation of G6P effect on glycogenolysis may be given by

   $$G6P_{Dwn}(t) = \frac{2}{1 + e^{(G6P_s(t) - 1.8)/3}}, \tag{2.26}$$

   where $G6P_s(t)$ represents the concentration of G6P. The parameters were determined by trail and error.

   (b) The activity of glycogen phosphorylase is inhibited by insulin (Kelley and Mandarino, 1990; Syed and Khandelwal, 2000). The data are illustrated in Figure 2.12. Thus, the mathematical representation of insulin effect on glycogenolysis may be represented by

   $$In_{Dwn}(t) = \frac{2}{1 + e^{(I(t) - 12)/3}}, \tag{2.27}$$

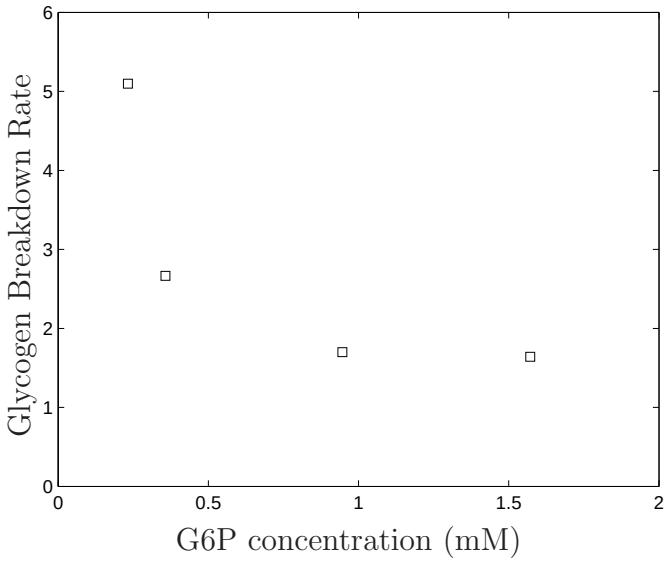

Figure 2.11. G6P effect on glycogenolysis. Data fitted from (Aiston et al., 2003).

where $I(t)$ (mU·l^{-1}) represents the insulin concentration. The parameters were determined by trail and error.

(c) The breakdown rate of glycogen is positively correlated with glycogen concentration (Hespel and Richter, 1992). The data are illustrated in Figure 2.13. The glycogen effect on glycogenolysis $GLY_{Dwn}(t)$ (unitless) may be represented by

$$GLY_{Dwn}(t) = \frac{1}{1 + e^{(-GLY_s(t)+0.1GLY_{\max s})/3}}, \tag{2.28}$$

where $GLY_s(t)$ (mM) represents the concentration of glycogen and $GLY_{s\max}$ (mM) represents the maximal glycogen concentration in skeletal muscle. The parameters were determined by trail and error.

(d) Glycogenolysis is also stimulated by exercise. It is exponentially related

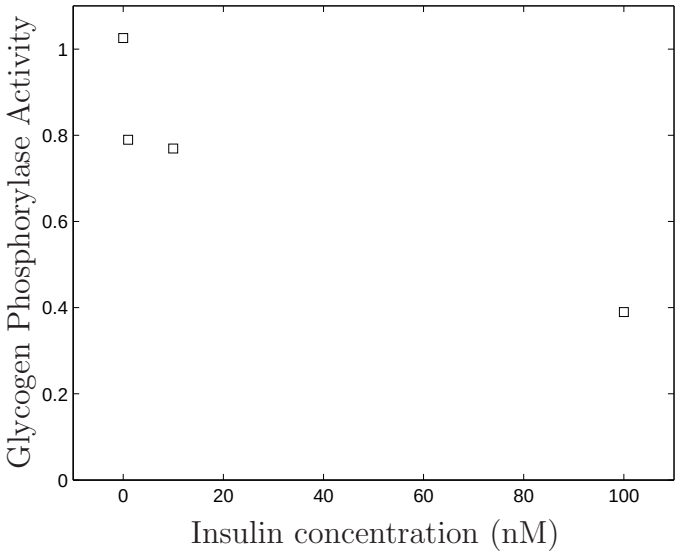

Figure 2.12. Insulin effect on glycogenolysis. Data fitted from (Syed and Khandelwal, 2000).

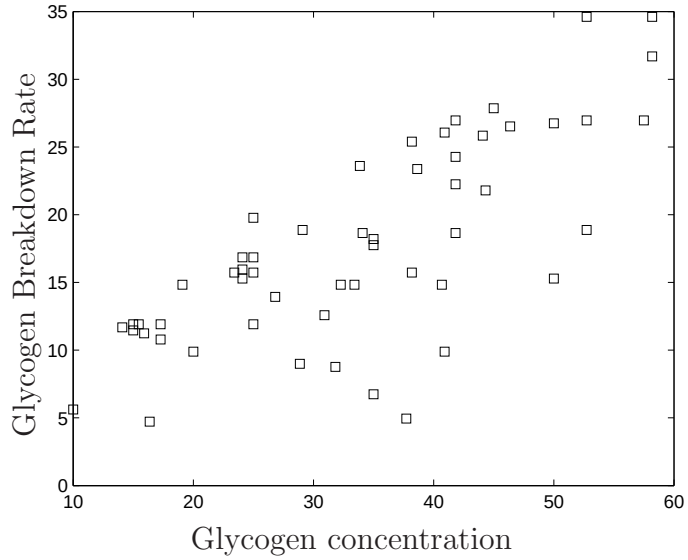

Figure 2.13. Glycogen concentration effect on glycogenolysis. Data fitted from (Hespel and Richter, 1992).

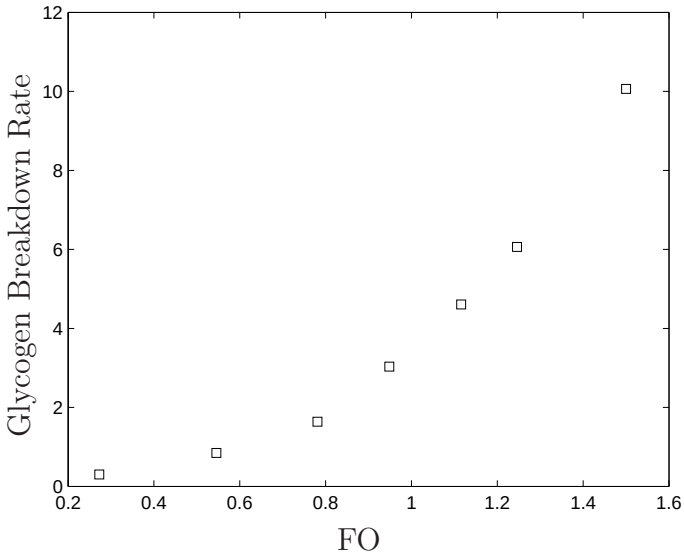

Figure 2.14. Exercise effect on glycogen breakdown. Data fitted from (Brooks, 1998).

to the oxygen consumption rate (Brooks, 1998). The data are illustrated in Figure 2.14. The mathematical relationship is assumed to be linearly related to the weight of skeletal muscle. Hence the glycogenolysis rate under the effects of exercise, $Dwn_0(t)$ (mmol·min^{-1}), may be represented by

$$Dwn_0(t) = 0.0638 m_s e^{3.881\mathrm{FO}(t)}, \tag{2.29}$$

where $\mathrm{FO}(t)$ represents the oxygen consumption ratio of $\dot{\mathrm{V}}_{\mathrm{O_2\,max}}$; and m_s (Kg) represents the mass of skeletal muscle. The parameters were determined by trail and error.

As a whole, the rate of glycogenolysis ($Dwn(t)$, mmol·min^{-1}) is expressed as

$$Dwn(t) = Dwn_0(t) G6P_{Dwn}(t) I_{Dwn}(t) GLY_{Dwn}(t). \tag{2.30}$$

If the body demands more energy than the production from the pathway of the aerobic respiration, the energy can be derived rapidly from the anaerobic direction of glycolysis. The rate can be determined from the law of energy balance which maintains a constant ATP concentration. It states that the rate of energy production equals to what is needed by activities, $\Delta ATP = 0$. The mathematical relationships may be represented by

$$K_{RC}Work(t) = ATP_a(t) + ATP_{an}(t) - ATP_{Rate_1}(t) - ATP_{Syn}(t) \tag{2.31}$$

$$ATP_{Rate_1}(t) = Rate_1(t) \tag{2.32}$$

$$ATP_{Syn}(t) = 2Syn(t), \tag{2.33}$$

where K_{RC} represents the ratio of energy provided by glucose metabolism (energy may also be produced by fatty acid metabolism); $Work(t)$ (mmol·min^{-1}) represent the work output in the unit of ATP; $ATP_a(t)$ (mmol·min^{-1}) represents ATP generation rate in aerobic respiration; $Rate_1(t)$ and $Syn(t)$ are defined in Equations 2.21 and 2.25. Therefore the rate of ATP production from anaerobic respiration is determined by Equation 2.31. When ATP production from aerobic respiration cannot fulfill energy demand of $Work$, the pathway of anaerobic respiration will be active. In contrast, if ATP_a is greater than $Work$, then the ATP generation rate from anaerobic respiration (ATP_{an}) is set to 0. The excess ATP production may be converted to Adenosine diphosphate (ADP) to be used in future as a substrate of ATP production. The parameter of K_{RC} represents the competition of fuel utilization in human body called the *Randle Cycle* (Frayn, 2003). At the exercise of 25% $V_{O2\,\max}$, the percentage of glucose utilization in energy expenditure is about 10%; while in the exercise of 65% $V_{O2\,\max}$, the energy supply of glucose and muscle glycogen is about 40% (Frayn, 2003). Hence, the

values of K_{RC} are given as in Table 2.1.

TABLE 2.1

DEFINITION OF K_{RC}.

Status	Basal State	Light Work	Heavy Work
K_{RC}	0.05	0.2	0.5

Thus, the dynamics of G6P and glycogen concentrations, $G6P_s(t)$ (mM) and $GLY_s(t)$ (mM), may be represented by

$$\frac{dG6P_s}{dt}(t) = \frac{1}{V_{sc}}\left(Rate_1(t) - Syn(t) + Dwn(t) - G6P_a(t) - G6P_{an}(t)\right) \quad (2.34)$$

$$\frac{dGLY_s}{dt}(t) = \frac{1}{V_{sc}}\left(Syn(t) - Dwn(t)\right) \quad (2.35)$$

$$G6P_{an}(t) = \frac{1}{3}ATP_{an}(t), \quad (2.36)$$

where V_{sc} (l) represents the volume of the ICS; $Rate_1$ (mmol·min^{-1}) represents the conversion rate from glucose to G6P which is defined in Equation 2.21; Syn (mmol·min^{-1}) and Dwn (mmol·min^{-1}) represent the rates of glycogenesis and glycogenolysis defined in Equation 2.25 and 2.30 respectively; $G6P_a$ (mmol·min^{-1}) and $G6P_{an}$ (mmol·min^{-1}) represent the rates of G6P consumption in the pathways of the aerobic respiration and the anaerobic respiration which are defined in Equation 2.17 and 2.36 respectively.

As illustrated in Figure 2.6, lactate is one of the products of the anaerobic respiration. It also plays an important role in metabolism. Lactate not only can be converted back to pyruvate and enter the aerobic respiration of Citric Acid Cycle (TCA Cycle) thereafter, but also it can be moved out of skeletal muscle and delivered to the other organs, for example, the heart. One of the most important roles of lactate is that it may enter the liver and be converted to glucose *via* the route of gluconeogenesis (Frayn, 2003). As a simplified assumption, it is assumed that all generated lactate in skeletal muscle will enter the circulation. The anaerobic respiration is expressed as

$$1\ \text{G6P} \rightarrow 2\ \text{Lactate} + 3\ \text{ATP}. \tag{2.37}$$

Thus, the rate of the lactate generation, Lac_s (mmol·min^{-1}), can be determined by

$$\frac{dLac_s}{dt}(t) = 2G6P_{an}(t). \tag{2.38}$$

As a whole, glucose metabolism in skeletal muscle may be modeled by Equation 2.16 through Equation 2.38 printed together as below

$$\begin{aligned}
f_{gs}(t) &= 3.0(G(t) - G_{si}(t)) \\
f_{gsi}(t) &= V_{maxs-basal}\frac{G_{si}(t)}{K_m + G_{si}(t)}y_{in}y_{exe} \\
\frac{dG_{si}}{dt}(t) &= \frac{1}{V_{sc}}\left(f_{gs}(t) - f_{gsi}(t)\right) \\
ATP_{aerobic}(t) &= \left(\frac{1429}{32} \times \frac{1}{6}\right)\text{FO}(t)\dot{V}_{O_2\,\max} \\
G6P_{aerobic}(t) &= \left(\frac{1429}{32} \times 130\right)\text{FO}(t)\dot{V}_{O_2\,\max} \\
Rate_0(t) &= 8.9m_s\frac{G_{sc}(t)}{0.07 + G_{sc}(t)}
\end{aligned}$$

$$
\begin{aligned}
I_R(t) &= \frac{2}{1+e^{(-I(t)+40.0)/20}} \\
G6P_R(t) &= \frac{2}{1+e^{(G6P_s(t)-0.12m_s/V_{sc})/10}} \\
Rate_1(t) &= Rate_0(t)I_R(t)G6P_R(t) \\
G6P_{Syn}(t) &= 0.15e^{\log(G6P_s(t)/0.133)} \\
I_{Syn}(t) &= \frac{1.625}{1+e^{-(I(t)-3.24)/38.2}} \\
GLY_{Syn}(t) &= \frac{2}{1+e^{GLY_s(t)-0.95GLY_{smax}}} \\
Syn(t) &= Syn_0(t)I_{Syn}(t)G6P_{Syn}(t)GLY_{Syn}(t) \\
G6P_{Dwn}(t) &= \frac{2}{1+e^{(G6P_s(t)-1.8)/3}} \\
In_{Dwn}(t) &= \frac{2}{1+e^{(I(t)-12)/3}} \\
GLY_{Dwn}(t) &= \frac{1}{1+e^{(-GLY_s(t)+0.1GLY_{\max s})/3}} \\
Dwn_0(t) &= 0.0638m_s e^{3.881\mathrm{FO}(t)} \\
Dwn(t) &= Dwn_0(t)G6P_{Dwn}(t)I_{Dwn}(t)GLY_{Dwn}(t) \\
K_{RC}Work(t) &= ATP_a(t) + ATP_{an}(t) - ATP_{Rate_1}(t) - ATP_{Syn}(t) \\
ATP_{Rate_1}(t) &= Rate_1(t) \\
ATP_{Syn}(t) &= 2Syn(t) \\
\frac{dG6P_s}{dt}(t) &= \frac{1}{V_{sc}}\left(Rate_1(t) - Syn(t) + Dwn(t) - G6P_a(t) - G6P_{an}(t)\right) \\
\frac{dGLY_s}{dt}(t) &= \frac{1}{V_{sc}}\left(Syn(t) - Dwn(t)\right) \\
G6P_{an}(t) &= \frac{1}{3}ATP_{an(t)} \\
\frac{dLac_s}{dt}(t) &= 2G6P_{an}(t).
\end{aligned}
$$

2.4 The Liver

As the largest organ in the body, the liver has two major blood vessels: the hepatic artery and the hepatic portal vein. The hepatic artery brings about 20% of the blood to the liver. The hepatic portal vein brings the blood first to the liver from the other organs such as the stomach and the small intestine before entering the general circulation (Frayn, 2003). These give the liver the important role in the circulatory system.

Glucose is carried into the liver by glucose transporters (GLUTs). It can be stored in the form of glycogen for future use. In contrast to glycogen in skeletal muscle, glycogen in the liver may work as a glucose provider for the other organs. Also lactate in the plasma can enter the liver and take the pathway of gluconeogenesis, which uses lactate as a precursor of glucose production.

2.4.1 Glucose Transport

The model of glucose transport in the liver is composed of three compartments: the plasma, the interstitial fluid space (IFS) and the intracellular space (ICS). The glucose transporter expressed in the liver cell membranes is GLUT2 (Frayn, 2003). Since there are no GLUTs in capillaries, the transport between the plasma and the IFS is assumed as free diffusion which is illustrated in Figure 2.15. The volumes of the IFS and the ICS are given as V_{li} (l) and V_{lc} (l) respectively. The volumes are linearly related to the mass of the liver (Qian and Brosnan, 1996) which are given by

$$V_{li} = 0.0764 m_l \tag{2.39}$$

$$V_{lc} = 0.4514 m_l, \tag{2.40}$$

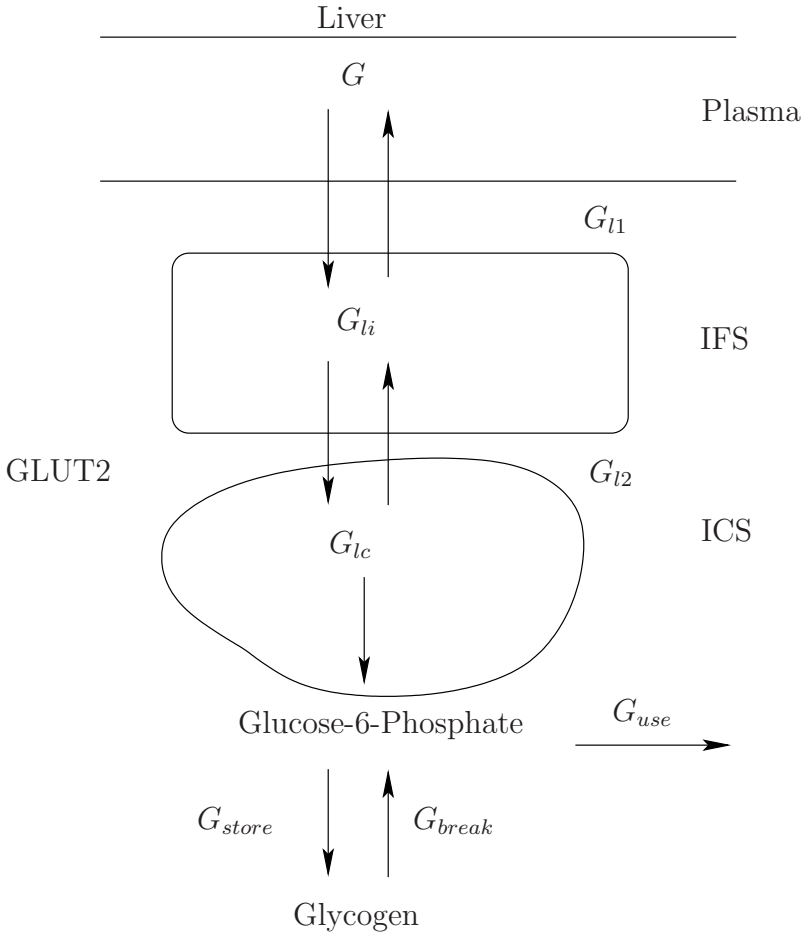

Figure 2.15. Glucose transport into the liver.

where m_l (Kg) represents the mass of the liver. The Michaelis-Menten characteristics of GLUT2 are referred from the data of rats (Guillam et al., 1998), which are given as $V_{\max l2} = 42.6$ mmol·kg-liver protein^{-1}·min^{-1} and the constant $K_{ml2} = 20$mM (Frayn, 2003). GLUT2 has a high K_m and its activity is not affected by insulin. This property can keep transporting glucose into the liver under the normal glucose concentrations.

The glucose transport relationships in the liver are expressed as follows:

1. The glucose transport rate between the plasma and the IFS is represented by $f_{gl1}(t)$ (mmol·min^{-1}). It is positive when glucose is carried from the plasma to the IFS. The mathematical representation of $f_{gl1}(t)$ is

$$f_{gl1}(t) = 10.0(G(t) - G_{li}(t)), \tag{2.41}$$

where G and G_{li} represent the glucose concentrations in the plasma and the IFS respectively. The coefficient of 10.0 l·min^{-1} is picked for simulations since that the cardiac output of blood is about 5$\sim$25 l·min^{-1} in various exercise intensities (Frayn, 2003). A larger parameter represents the important role of delivering metabolites such as glucose to other organs.

2. Glucose transport rate from the IFS to the ICS is represented by G_{l2} (mmol·min^{-1}). It is positive when glucose is carried from the IFS to the ICS. The Michaelis constant $K_{ml2} = 20$ mM (Frayn, 2003). Since the liver also provides glucose for other organs, there is an outward flow of intracellular glucose facilitated by GLUT2. Since the mass of water is about 70% of the liver (Levitt, 2003), it is assumed that half of the rest is protein. And the maximal inward uptake rate is 42 mmol·min^{-1}·kg-liver-protein^{-1} in rats (Guillam et al., 1998). The mass of the liver of human is about 1$\sim$1.5 kg (Frayn, 2003), thus the maximal inward transport rate is given as

$$(42)(1.4)(0.15) \approx 8.82 \tag{2.42}$$

The maximal outward transport rate was determined by trail and error. The

glucose transport function may be expressed as

$$f_{gl2}(t) = 8.82\frac{G_{li}(t)}{K_{ml2} + G_{li}(t)} - 61.7\frac{G_{lc}(t)}{K_{ml2} + G_{lc}(t)}, \tag{2.43}$$

where $G_{li}(t)$ (mM) and $G_{lc}(t)$ (mM) represent the glucose concentrations in the IFS and the ICS respectively.

2.4.2 Glucose Utilization

After glucose enters the liver cells (also called hepatocytes), it can be metabolized or stored as the glycogen for use in the future. The processes are illustrated in Figure 2.16. The dash lines represent cell membranes. In the liver, glucose can be produced and released as a supply for the other organs through the process of gluconeogenesis.

Glucose metabolism in the liver is different than that in skeletal muscle. Most of the energy required in the liver comes from the oxidation of amino acids and fatty acids instead of glucose (Frayn, 2003). In the model of the liver, ATP is produced to meet the basic energy requirement of the organ. Therefore the compartment of ATP is omitted for simplification while the dynamics of G6P and glycogen (GLY) are still very important.

1. As illustrated in Figure 2.16, glucose is converted into G6P by an enzyme called glucokinase (GK), which is different than HK in skeletal muscle. In skeletal muscle, the activity of HK is stimulated by insulin while the activity of GK in the liver is not affected by insulin (Frayn, 2003). Also the activity of GK in the liver follows a Hill equation instead of the Michaelis-Menten dynamics of HK in skeletal muscle (Cárdenas, 1995). The Hill equation has

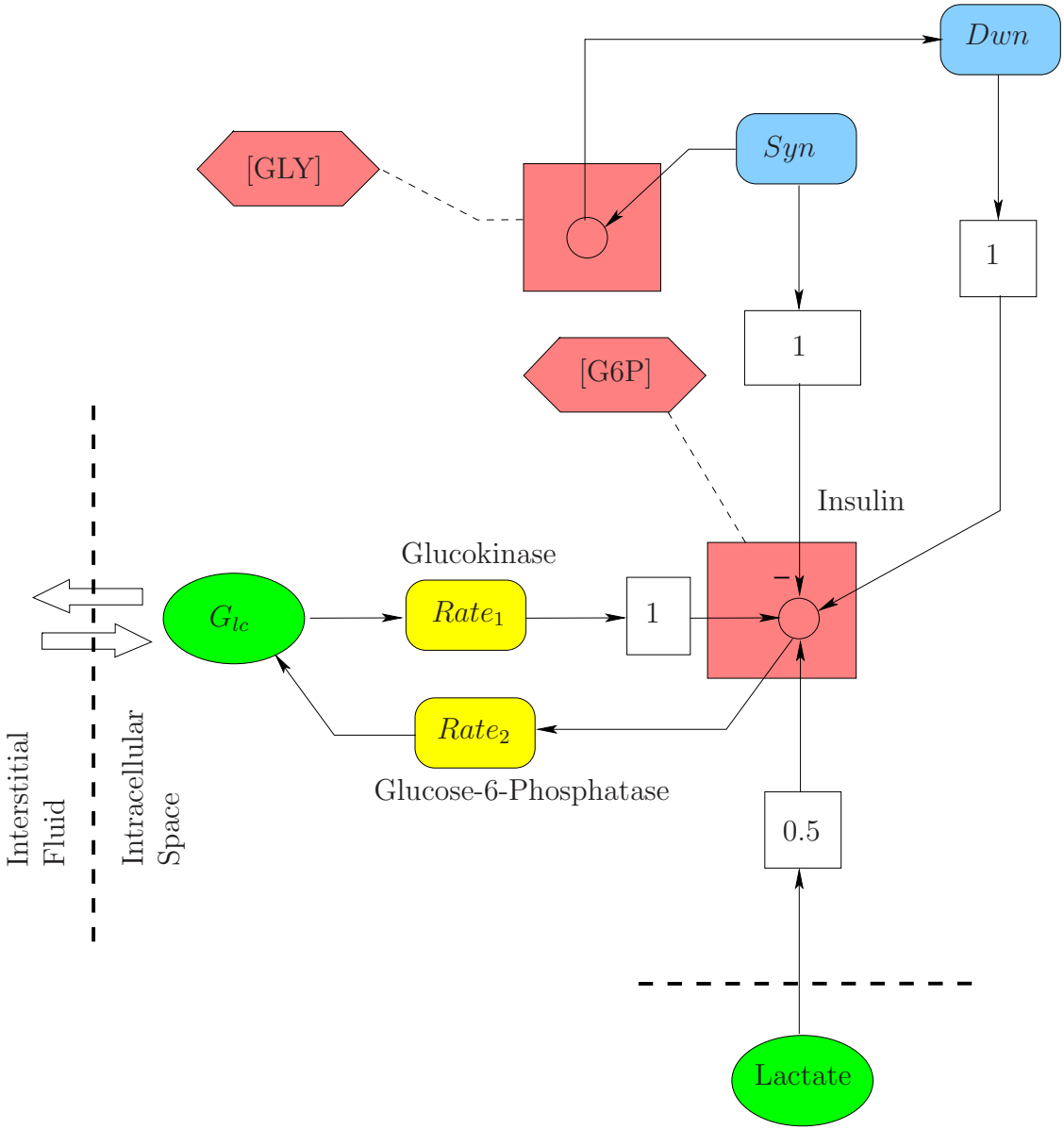

Figure 2.16. Glucose metabolism in the liver.

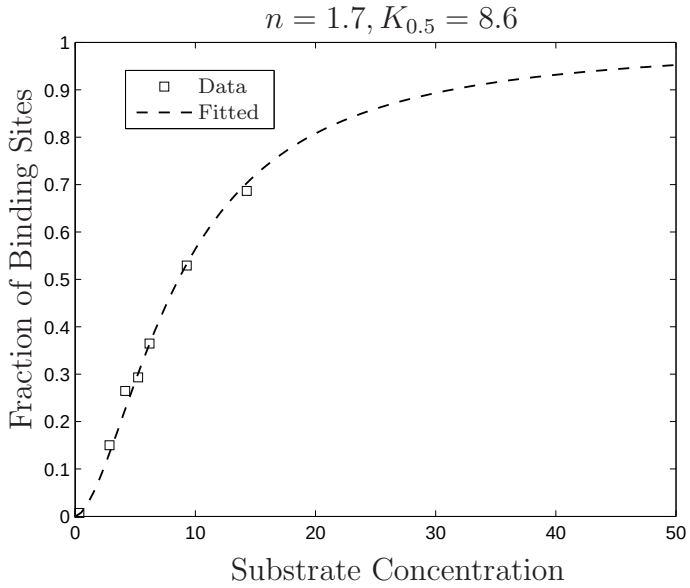

Figure 2.17. Data fitted from (Grimsby et al., 2003).

a form as below

$$\theta = \frac{[L]^n}{K_{0.5}^n + [L]^n}, \tag{2.44}$$

where θ represents the fraction of glucose binding sites filled in the reaction; n is the Hill index; $K_{0.5}$ represent the substrate concentration when $\theta = 0.5$; and $[L]$ represents the substrate concentration. In an experiment of GK, the maximal activity rate of a combinant GK is determined as $V_{\max Rate_1} =$ 15000 mmol·kg-protein^{-1}·min^{-1}. The parameters in the Hill equation are $n \approx 1.7$ and $K_{0.5} = 8.6$ mM (Grimsby et al., 2003). A plot of Hill equation is illustrated in Figure 2.17.

Thus, the rate of converting glucose to G6P is represented by $Rate_1$

(mmol·min^{-1}) which may be represented by

$$Rate_1(t) = V_{\max Rate_1} m_{lp} \frac{G_{lc}^n(t)}{K_{0.5lgk}^n + G_{lc}^n(t)}, \tag{2.45}$$

where m_{lp} (Kg) represents the weight of proteins in the liver; G_{lc} (mM) represents the intracellular glucose concentration; and the parameters of Hill equation are $n = 1.7, K_{0.5lgk} = 8.6$ mM. This process in the liver is not inhibited by its product G6P (Frayn, 2003).

2. In the liver, glucose can be produced from G6P and delivered to the other organs as a source of energy. This process makes the liver play a very important role in glucose metabolism because it provides glucose during the time without a meal. The reaction is mediated by the enzyme Glucose-6-Phosphatase, whose activity follows the Michaelis-Menten dynamics. The Michaelis-Menten parameters are $V_{\max Rate_2} = 340$ mmol·kg-protein^{-1}·min^{-1} and $K_{mlg6p} = 0.8$ mM (Hume et al., 2000). The reaction is not affected by either insulin or its product glucose (Frayn, 2003). Therefore the rate of glucose production from G6P in the liver ($Rate_2$, mmol·min^{-1}) may be represented by

$$Rate_2(t) = V_{\max Rate_2} m_{lp} \frac{G6P_l(t)}{K_{mlg6p} + G6P_l(t)}, \tag{2.46}$$

where m_{lp} (Kg) represents the weight of proteins in the liver; and $G6P_l$ (mM) represents the G6P concentration in the ICS.

3. G6P can be converted into glycogen and stored for future use in the process of glycogenesis. The rate of glycogenesis in the liver, Syn (mmol·min^{-1}), is affected by the concentrations of insulin, G6P and glycogen. The mathe-

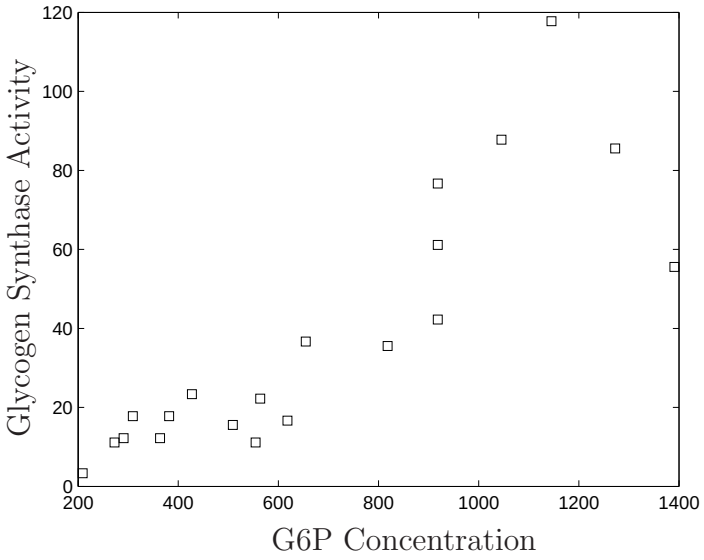

Figure 2.18. G6P effect on glycogenesis. Data fitted from (Cadefau et al., 1997).

matical relationships may be represented as follows.

(a) From experiments on rats, the degree of activation of glycogen synthase in hepatocytes is proportional to the G6P concentration (Cadefau et al., 1997; Villar-Palasí and Guinovart, 1997). The data are illustrated in Figure 2.18. Therefore the G6P effect on glycogenesis ($G6P_{Syn}$, mmol·min^{-1}) may be represented by

$$G6P_{Syn}(t) = 0.3G6P_l(t), \tag{2.47}$$

where $G6P_l$ (mM) represents the G6P concentration in the liver. The parameter is determined by trail and error.

(b) Insulin may stimulate the activity of glycogen synthase and increase the glycogenesis rate as a result. This effect will be saturated as the

insulin concentration increases, which is similar with the kinetics in skeletal muscle expressed in Equation 2.23 and illustrated in Figure 2.10. Thus, the insulin effect (I_{Syn}, unitless) may be represented by

$$I_{Syn}(t) = \frac{2}{1 + e^{(-I(t)+16)/3}}, \tag{2.48}$$

where I (mU·l^{-1}) represents the insulin concentration in the plasma. The parameters were determined by trail and error.

(c) Because the capacity of glycogen may be saturated, it is assumed that the glycogenesis rate is also a sigmoid function of glycogen concentration. The effect of glycogen on glycogenesis ($GLY_{Syn}(t)$, unitless) may be represented by

$$GLY_{Syn}(t) = \frac{2}{1 + e^{(GLY_l(t)-0.95GLY_{l\,\max})/3}}, \tag{2.49}$$

where GLY_l (mM) is the glycogen concentration in the liver and $GLY_{l\,\max}$ (mM) is the maximal glycogen concentration in the liver. The parameters were determined by trail and error.

(d) The basal glycogenesis rate is denoted by $Syn_0(t)$ (mmol·min^{-1}). It can be estimated from the data of a mouse liver perfusion, which is equal to 0.84 mmol glycosyl units·kg-liver^{-1}· min^{-1} (Seoane et al., 1996). Therefore the basal synthesis rate may be represented by

$$Syn_0(t) = 0.84m_l, \tag{2.50}$$

where m_l (Kg) represent the mass of the liver.

Therefore the rate of glycogenesis ($Syn(t)$, mmol·min^{-1}) may be represented by

$$Syn(t) = Syn_0(t) I_{Syn}(t) G6P_{Syn}(t) GLY_{Syn}(t). \tag{2.51}$$

4. The rate of the glycogen breakdown (also called glycogenolysis) is denoted by Dwn (mmol·min^{-1}). It is mediated by the enzyme of glycogen phosphorylase. The glycogenolysis rate is affected by the concentrations of insulin, G6P and glycogen.

   (a) Glycogen is broken down to supply G6P for energy generation (Frayn, 2003). Glycogenolysis is inhibited by the product G6P. Thus, the inhibition may be represented as a sigmoid function with respect to the G6P concentration which is illustrated in Figure 2.11. It may be represented by

   $$G6P_{Dwn}(t) = \frac{2}{1 + e^{G6P_l(t) - 1.5}}, \tag{2.52}$$

   where $G6P_l$ (mM) represents the G6P concentration in the liver. The parameters were determined by trial and error.

   (b) Glycogenolysis is also inhibited by insulin (Frayn, 2003). The effect of insulin on the rate of glycogenolysis (I_{Dwn}) is fitted from the data of dogs (Pagliassotti et al., 1994) which is illustrated in Figure 2.19.

   $$I_{Dwn}(t) = \frac{6.287}{1 + e^{(I(t) - 17.7)/7.824}} m_l, \tag{2.53}$$

   where $I(t)$ (mU·l^{-1}) represents the insulin concentration; and m_l (Kg) represents the weight of the liver. The parameters were determined using Matlab *fit()* function.

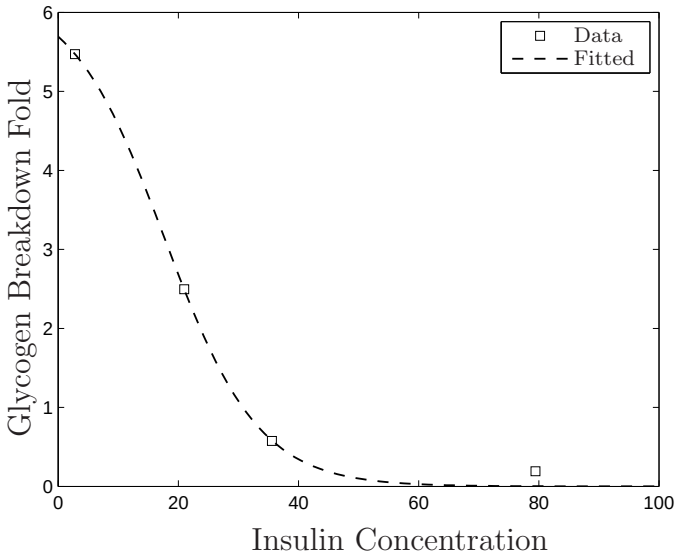

Figure 2.19. Insulin effect on glycogen breakdown. Data fitted from (Pagliassotti et al., 1994).

(c) Glycogenolysis is positively related with glycogen concentration, which is illustrated in Figure 2.13. The effect of glycogen on glycogenolysis (GLY_{Dwn}) may be represented by

$$GLY_{Dwn}(t) = \frac{2}{1 + e^{-GLY_l(t)+0.2GLY_{lmax}}}, \tag{2.54}$$

where $GLY_l(t)$ represents the glycogen concentration in the liver and $GLY_{l\,\max}$ (mM) represents the maximal glycogen concentration in the liver. The parameters were determined by trail and error.

Therefore the rate of glycogen breakdown ($Dwn(t)$, mmol·min^{-1}) may be represented by

$$Dwn(t) = Dwn_0 I_{Dwn}(t) G6P_{Dwn}(t) GLY_{Dwn}(t). \tag{2.55}$$

where $Dwn_0 = 5$ mmol·min^{-1} was determined from trial and error.

5. The process of gluconeogenesis produces G6P from other precursors, such as lactate. It is assumed that lactate entering the liver may be converted into G6P completely. Therefore with the chemical reaction

$$2 \text{ Lactate} \rightarrow 1 \text{ G6P}.$$

the rate of G6P production from lactate ($G6P_{Lac}$, mmol·min^{-1}) may be represented by

$$G6P_{Lac}(t) = 0.5 Lac_l(t), \tag{2.56}$$

where $Lac_l(t)$ (mmol·min^{-1}) represents the rate of lactate delivered to the liver.

Therefore the dynamics of G6P and glycogen concentrations are represented by

$$\frac{dG6P_l}{dt}(t) = \frac{1}{V_{lc}} \left(Rate_1(t) - Syn(t) + Dwn(t) + G6P_{Lac}(t) \right) \tag{2.57}$$

$$\frac{dGLY_l}{dt}(t) = \frac{1}{V_{lc}} \left(Syn(t) - Dwn(t) \right) \tag{2.58}$$

where V_{lc} (l) represents the volume of the ICS of the liver defined in Equation 2.40; $G6P_l(t)$ (mM) and $GLY_l(t)$ (mM) represent the concentrations of G6P and glycogen respectively. As a whole, glucose metabolism in the liver may be modeled

by Equation 2.41 through Equation 2.56 as below

$$
\begin{aligned}
f_{gl1}(t) &= 10.0(G(t) - G_{li}(t)) \\
f_{gl2}(t) &= 8.82\frac{G_{li}(t)}{K_{ml2} + G_{li}(t)} - 61.7\frac{G_{lc}(t)}{K_{ml2} + G_{lc}(t)} \\
Rate_1(t) &= V_{\max Rate_1} m_{lp} \frac{G_{lc}^n(t)}{K_{0.5lgk}^n + G_{lc}^n(t)} \\
Rate_2(t) &= V_{\max Rate_2} m_{lp} \frac{G6P_l(t)}{K_{mlg6p} + G6P_l(t)} \\
G6P_{Syn}(t) &= 0.3G6P_l(t) \\
I_{Syn}(t) &= \frac{2}{1 + e^{(-I(t)+16)/3}} \\
GLY_{Syn}(t) &= \frac{2}{1 + e^{(GLY_l(t) - 0.95GLY_{l\max})/3}} \\
Syn(t) &= Syn_0(t) I_{Syn}(t) G6P_{Syn}(t) GLY_{Syn}(t) \\
G6P_{Dwn}(t) &= \frac{2}{1 + e^{G6P_l(t) - 1.5}} \\
I_{Dwn}(t) &= \frac{6.287}{1 + e^{(I(t) - 17.7)/7.824}} m_l \\
GLY_{Dwn}(t) &= \frac{2}{1 + e^{-GLY_l(t) + 0.2GLY_{lmax}}} \\
Dwn(t) &= I_{Dwn}(t) G6P_{Dwn}(t) GLY_{Dwn}(t) \\
\frac{dG6P_l}{dt}(t) &= \frac{1}{V_{lc}} \left(Rate_1(t) - Syn(t) + Dwn(t) + G6P_{Lac}(t)\right) \\
\frac{dGLY_l}{dt}(t) &= \frac{1}{V_{lc}} \left(Syn(t) - Dwn(t)\right).
\end{aligned}
$$

2.5 Other Energy Consumption

The model also takes into account other cells, tissues or organs which consume energy. For example, in the post-absorptive state, the glucose consumption rate by red blood cells ($G_o(t)$, mmol·min^{-1}) is about 0.1388 mmol·min^{-1} (Frayn, 2003),

which is given by

$$\frac{dG_o}{dt}(t) = 0.1388. \tag{2.59}$$

As a whole, these metabolic equations determine the dynamics of glucose concentration in the model of human body.

2.6 Simulation Results

The whole metabolic equations are given as following. Among them, there are 22 equations receiving the forms from the literature; 15 equations receiving the forms from data fit of experimental data; and 3 equations receiving the forms from the reasoning of the physiological understanding of the chemical process. As for the values of the 109 parameters in the equations, there are 33 of them obtained from chemical reactions and the literature; 12 of them obtained from data fit of experimental data; 3 of them obtained from ranges of the normal values of healthy subjects in the literature; and 61 of them obtained from tuning in simulations.

$$\begin{aligned}
G_b(t) &= V_{maxb1} m_b \frac{G(t)}{K_{mb1} + G(t)} \\
\frac{dI_1}{dt}(t) &= \left(\frac{79.21}{1 + e^{-1.934G(t)+10.52}} + 29.84 \right) \frac{0.7n}{60V_p} \\
\frac{dI_2}{dt}(t) &= I(t)e^{-20t} \\
\frac{dI}{dt}(t) &= \frac{dI_1}{dt}(t) + \frac{dI_2}{dt}(t) \\
f_{gs}(t) &= 3.0(G(t) - G_{si}(t)) \\
y_{in} &= \frac{1.433}{1 + e^{-0.2473 \log_{10} I(t) - 3.271}} \\
y_{exe} &= \frac{4.453}{1 + e^{0.2(-198.5\mathrm{FO(t)}+60.95)}} + 1 \\
f_{gsi}(t) &= V_{maxs-basal} \frac{G_{si}(t)}{K_m + G_{si}(t)} y_{in} y_{exe}
\end{aligned}$$

$$\frac{dG_{si}}{dt}(t) = \frac{1}{V_{sc}}\left(f_{gs}(t) - f_{gsi}(t)\right)$$
$$ATP_{aerobic}(t) = \left(\frac{1429}{32} \times \frac{1}{6}\right) \mathrm{FO}(t)\dot{V}_{O_2\,\max}$$
$$G6P_{aerobic}(t) = \left(\frac{1429}{32} \times 130\right) \mathrm{FO}(t)\dot{V}_{O_2\,\max}$$
$$Rate_0(t) = 8.9 m_s \frac{G_{sc}(t)}{0.07 + G_{sc}(t)}$$
$$I_R(t) = \frac{2}{1 + e^{(-I(t)+40.0)/20}}$$
$$G6P_R(t) = \frac{2}{1 + e^{(G6P_s(t) - 0.12 m_s/V_{sc})/10}}$$
$$Rate_1(t) = Rate_0(t) I_R(t) G6P_R(t)$$
$$G6P_{Syn}(t) = 0.15 e^{\log_{10}\left(\frac{G6P_s(t)}{0.133}\right)}$$
$$I_{Syn}(t) = \frac{1.625}{1 + e^{-(I(t)-3.24)/38.2}}$$
$$GLY_{Syn}(t) = \frac{2}{1 + e^{GLY_s(t) - 0.95 GLY_{smax}}}$$
$$Syn(t) = Syn_0(t) I_{Syn}(t) G6P_{Syn}(t) GLY_{Syn}(t)$$
$$G6P_{Dwn}(t) = \frac{2}{1 + e^{(G6P_s(t)-1.8)/3}}$$
$$In_{Dwn}(t) = \frac{2}{1 + e^{(I(t)-12)/3}}$$
$$GLY_{Dwn}(t) = \frac{1}{1 + e^{(-GLY_s(t) + 0.1 GLY_{\max\, s})/3}}$$
$$Dwn_0(t) = 2.232 \frac{m_s}{35} e^{3.881 \mathrm{FO}(t)}$$
$$Dwn(t) = Dwn_0(t) G6P_{Dwn}(t) I_{Dwn}(t) GLY_{Dwn}(t)$$
$$K_{RC}Work(t) = ATP_a(t) + ATP_{an}(t) - ATP_{Rate_1}(t) - ATP_{Syn}(t)$$
$$ATP_{Rate_1}(t) = Rate_1(t)$$
$$ATP_{Syn}(t) = 2Syn(t)$$
$$\frac{dG6P_s}{dt}(t) = \frac{1}{V_{sc}}\left(Rate_1(t) - Syn(t) + Dwn(t) - G6P_a(t) - G6P_{an}(t)\right)$$
$$\frac{dGLY_s}{dt}(t) = \frac{1}{V_{sc}}\left(Syn(t) - Dwn(t)\right)$$

$$
\begin{aligned}
G6P_{an}(t) &= \frac{1}{3} ATP_{an(t)} \\
\frac{dLac_s}{dt}(t) &= 2G6P_{an}(t) \\
f_{gl1}(t) &= 10.0(G(t) - G_{li}(t)) \\
f_{gl2}(t) &= 8.82\frac{G_{li}(t)}{K_{ml2} + G_{li}(t)} - 61.7\frac{G_{lc}(t)}{K_{ml2} + G_{lc}(t)} \\
Rate_1(t) &= V_{\max Rate_1} m_{lp} \frac{G^n_{lc}(t)}{K^n_{0.5lgk} + G^n_{lc}(t)} \\
Rate_2(t) &= V_{\max Rate_2} m_{lp} \frac{G6P_l(t)}{K_{mlg6p} + G6P_l(t)} \\
G6P_{Syn}(t) &= 0.3G6P_l(t) \\
I_{Syn}(t) &= \frac{2}{1 + e^{(-I(t)+16)/3}} \\
GLY_{Syn}(t) &= \frac{2}{1 + e^{(GLY_l(t) - 0.95GLY_{l\max})/3}} \\
Syn_0(t) &= 0.84m_l \\
Syn(t) &= Syn_0(t) I_{Syn}(t) G6P_{Syn}(t) GLY_{Syn}(t) \\
G6P_{Dwn}(t) &= \frac{2}{1 + e^{G6P_l(t) - 1.5}} \\
I_{Dwn}(t) &= \frac{6.287}{1 + e^{(I(t) - 17.7)/7.824}} m_l \\
GLY_{Dwn}(t) &= \frac{2}{1 + e^{-GLY_l(t) + 0.2GLY_{lmax}}} \\
Dwn(t) &= I_{Dwn}(t) G6P_{Dwn}(t) GLY_{Dwn}(t) \\
\frac{dG6P_l}{dt}(t) &= \frac{1}{V_{lc}} \left(Rate_1(t) - Syn(t) + Dwn(t) + G6P_{Lac}(t)\right) \\
\frac{dGLY_l}{dt}(t) &= \frac{1}{V_{lc}} \left(Syn(t) - Dwn(t)\right) \\
\frac{dG_o}{dt}(t) &= 0.1388.
\end{aligned}
$$

Integrating all the models stated as above, a physiological model of body may be established, which includes the models of the brain, the liver and skeletal

muscle. This model is a set of ordinary differential equations which are solved numerically. The input variables of the model are the glucose uptake from meals and the oxygen consumption ratio (FO, percentage of $\dot{V}_{O2\,\max}$). The coefficients are from data fitted in the literature or from assumptions. The first protocol of simulation is designed as a four-hour activity

1. 1 hour of rest, followed by a 10 minutes of meal (with an input rate of glucose: 12 mmol·min^{-1}), then 30 minutes of exercise and finally 20 minutes of rest.

The implemented numerical method was Euler's method with Δt =1E-3 minute. Convergence of the numerical solution was verified by running the simulations with Δt =1E-4 minute and comparing the results. The simulation results of glucose, insulin, glycogen and G6P concentrations are illustrated in Figure 2.20, 2.21 and 2.23. It is illustrated that the glucose concentrations increases after taking meals and decreases during exercise due to the consumption for energy supply. Insulin concentration is changing according to the dynamics of glucose concentration which demonstrates the regulating effects of insulin. The glucose concentration in the plasma is maintained at a basal level with the help of the liver because the liver releases glucose to the plasma *via* gluconeogenesis. Glycogen in skeletal muscle may accumulate during rest and meals and be utilized during exercise. Glycogen in the liver decreases after the meal because the process of glycogenolysis in the liver metabolizes glycogen to maintain the reaction in the direction of supplying glucose.

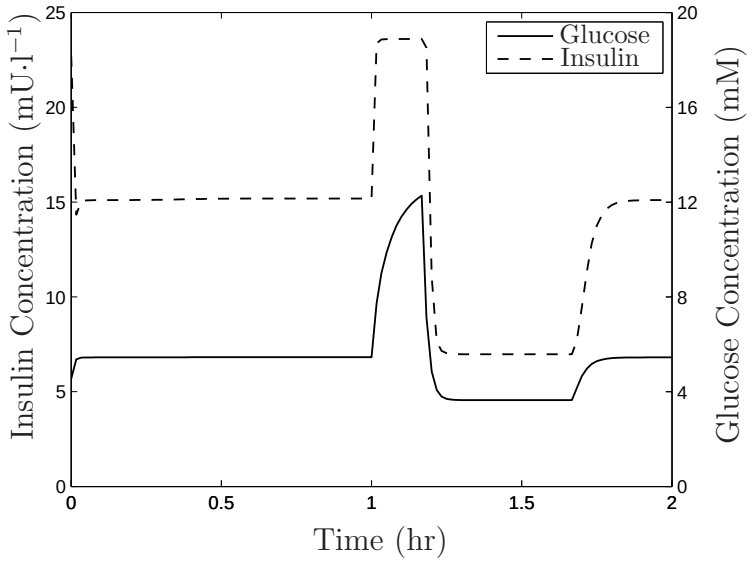

Figure 2.20. Simulation 1: Metabolites in the plasma.

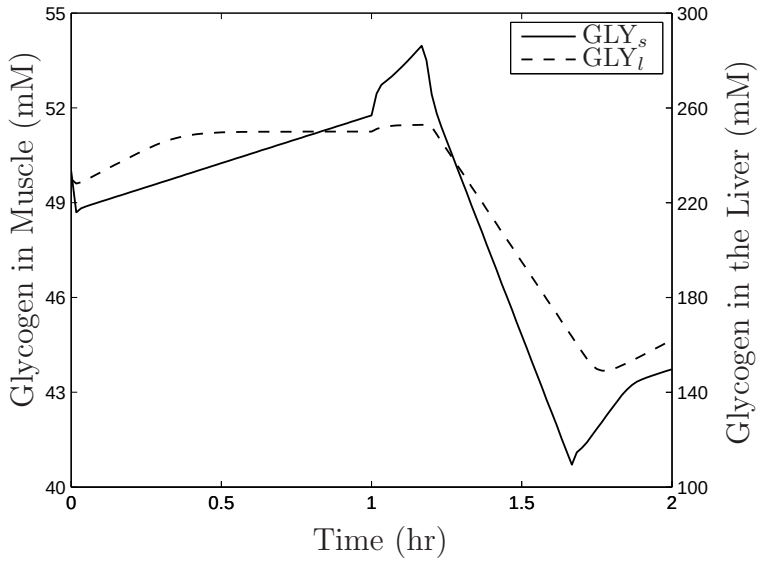

Figure 2.21. Simulation 1: Glycogen concentrations.

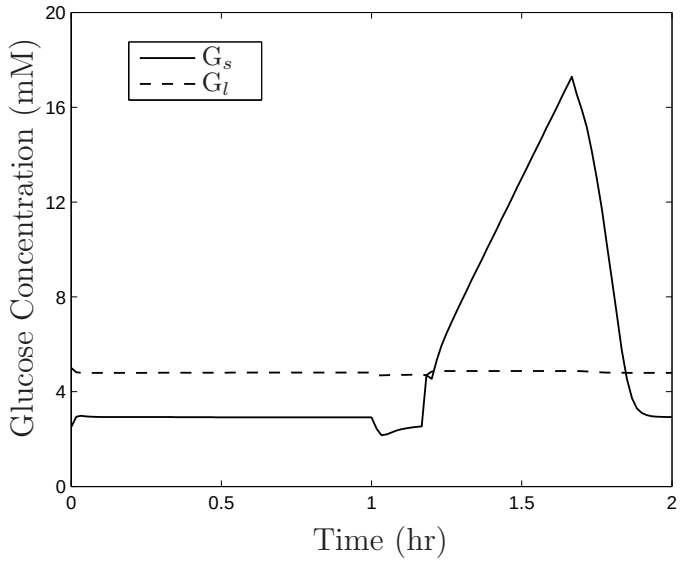

Figure 2.22. Simulation 1: Intracellular glucose concentrations.

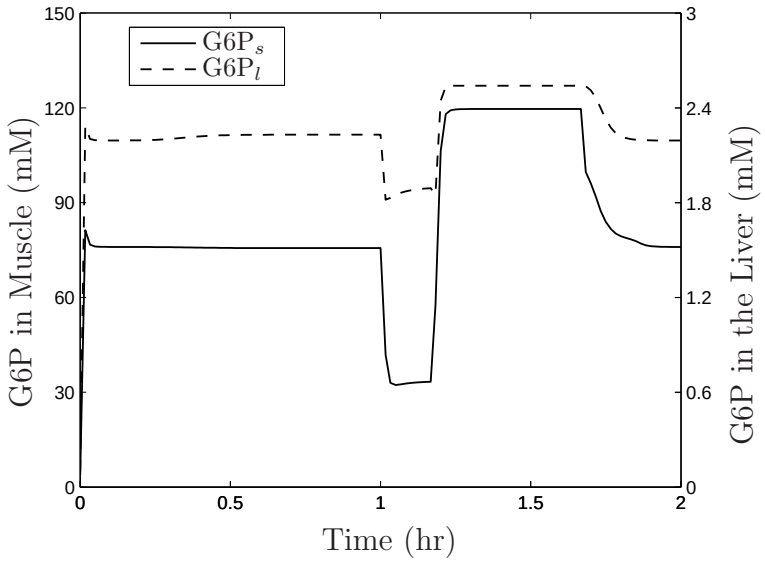

Figure 2.23. Simulation 1: G6P concentrations.

From the simulations, the ranges of metabolites are such as the concentration of glucose in the plasma: 3∼12 mM; the concentration of insulin: 6∼25 $\text{mU}\cdot\text{l}^{-1}$; the flag of oxygen consumption rate (FO): 0.1∼0.7; the glycogen concentrations GLY_s: 40∼55 mM, GLY_l: 140∼260 mM; the intracellular glucose concentrations G_s: 0∼20 mM, G_l: 4∼6 mM; and the intracellular G6P concentrations $G6P_s$: 30∼120 mM, $G6P_l$: 1.2∼3 mM. These ranges of simulations data locate inside the data from the literature which are illustrated in Figure 2.2, 2.4, 2.5, 2.7, 2.10, 2.12, 2.13, 2.14, 2.17, 2.18 and 2.19; while some may locate at the extrapolation of the data from the literature as illustrated in Figure 2.8, 2.9 and 2.11.

The glucose metabolism in skeletal muscle is also investigated under a constant glucose concentration which is set at $G = 4.55$ mM. There are three protocols of simulation stated as follows:

1. 1 hours rest;

2. 30min rest + 20min light housework + 10min rest;

3. 30min rest + 20min swimming + 10min rest.

The corresponding simulation results of glycogen and G6P concentrations in skeletal muscle are illustrated in Figure 2.24 and 2.26. In protocol 1, glycogen in muscle keeps increasing due to the continuous glucose uptake and low consumption. In protocol 2, glycogen decreases slightly due to the light housework and then increase because of glucose uptake. In protocol 3, glycogen in muscle is consumed rapidly to generate enough energy as requested by exercise, which is faster than that in the protocol 2, and be restored after that. The concentrations of G6P in the different protocols can maintain at a certain level during rest and decrease according to various activities. In the protocol 3, since the activity requires more

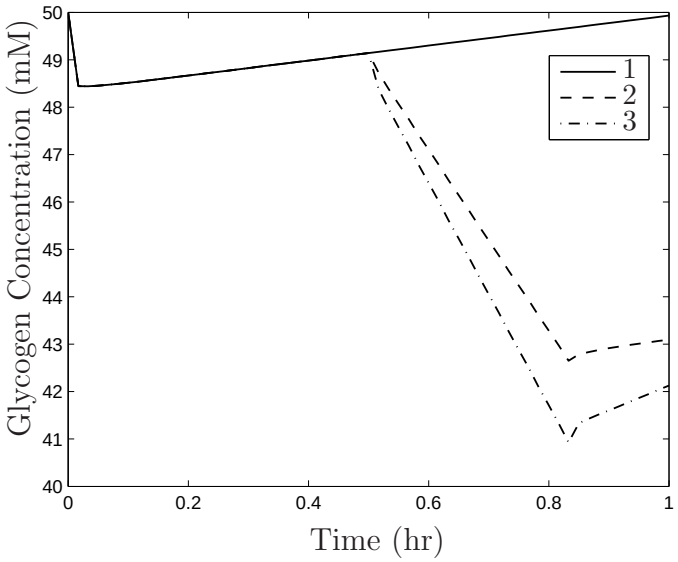

Figure 2.24. Simulation 2: Glycogen concentrations in muscle.

energy than the other protocols, the G6P concentration drops the most during the exercise.

From the simulations, the ranges of metabolites are such as the concentration of insulin: 9∼25 mU·l^{-1}; the flag of oxygen consumption rate (FO): 0.1∼0.7; the intracellular glucose concentrations G_s: 2∼18 mM; and the intracellular G6P concentrations $G6P_s$: 80∼120 mM. Same as the previous simulation, these ranges of simulations data locate inside the data from the literature which are illustrated in Figure 2.2, 2.4, 2.5, 2.7, 2.10, 2.12, 2.13, 2.14, 2.17, 2.18 and 2.19; while some may locate at the extrapolation of the data from the literature as illustrated in Figure 2.8, 2.9 and 2.11.

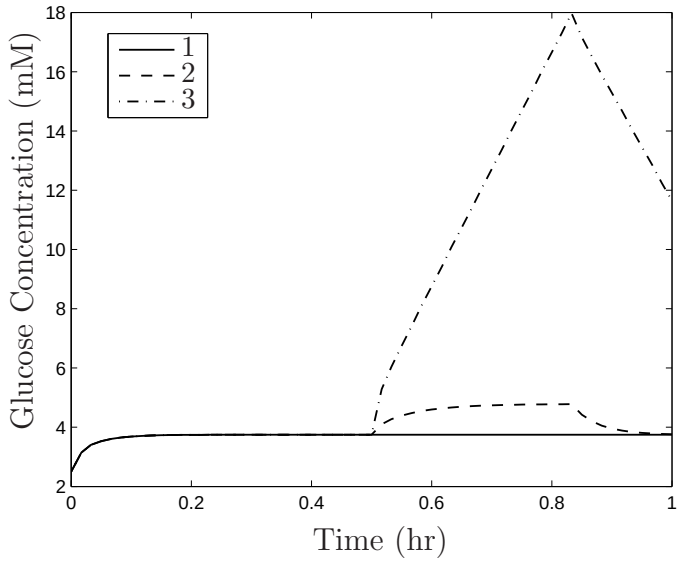

Figure 2.25. Simulation 2: Glucose concentrations in muscle.

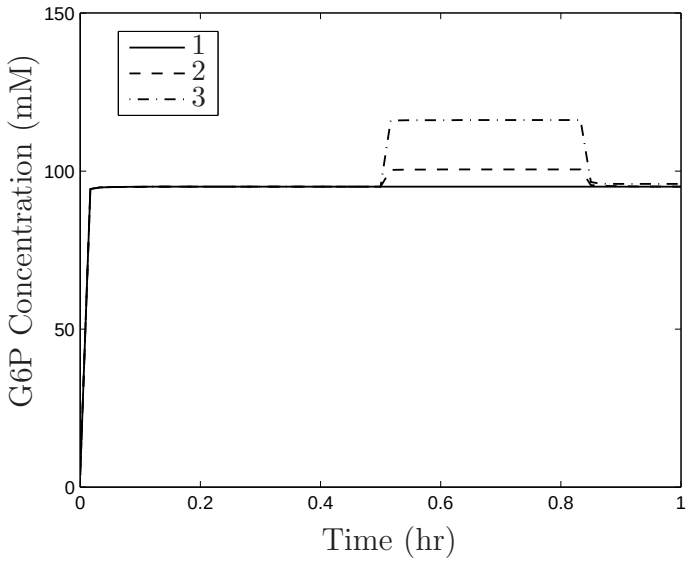

Figure 2.26. Simulation 2: G6P concentrations in muscle.

CHAPTER 3

REFINED MODELS

The framework of glucose metabolism model is established in Chapter 2. The model represents general dynamics of glucose and insulin in human body. However, the model parameters may come from animal experiments or from assumption. To improve the physiological model for human, the models of various organs are going to be refined to incorporate physiological data of experiments on humans and to obtain the model parameters through optimization. In this chapter, the models of the pancreas and glucose transport in skeletal muscle are investigated. The adopted optimization method is called DIRECT (DIviding RECTangles) which search globally in the space.

3.1 The Pancreas

The pancreas produces important hormones including insulin, glucagon and somatostatin, which have important regulatory roles in metabolism. Insulin and glucagon are closely related to glucose metabolism. The effect of glucagon is opposite that of insulin. When glucose concentration in plasma is high, insulin release is increased to activate glucose uptake in organs while glucagon secretion is inhibited. When glucose concentration drops, insulin release is reduced and glucagon secretion increases to stimulate the liver to release glucose. Therefore

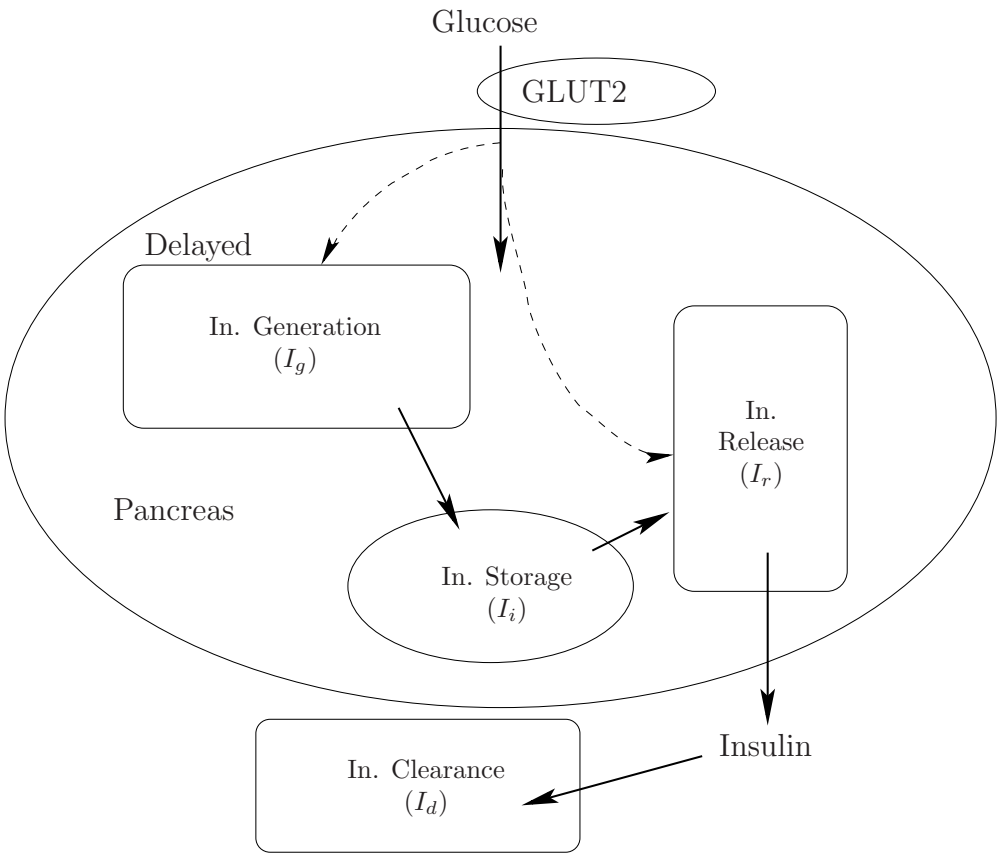

Figure 3.1. Proposed pancreas model.

only insulin is considered in this thesis. The structure of the pancreas model is illustrated in Figure 3.1. It includes three compartments: insulin generation (I_g), release (I_r) and removal (I_d).

The isoform of the glucose transporters expressed in the pancreas is glucose transporter type 2 (GLUT2), whose activity is not influenced by insulin. In the compartment of insulin generation (I_g), glucose is carried from plasma into β-cells by GLUT2. Glucose transport follows the Michaelis-Menten kinetics (Frayn, 2003). The amount of glucose transport into the pancreas in a fixed time interval is defined by $G_p(t)$ (mmol·min^{-1}). The mathematical relationship between $G_p(t)$

and the glucose concentration (G, mM) is represented by

$$\frac{dG_p}{dt}(t) = V_{\max p2}\frac{G(t)}{K_{p1} + G(t)}, \tag{3.1}$$

where $V_{\max p2}$ (mmol·min^{-1}) represents the maximal glucose removal rate from plasma; and K_{p1} (mM) is the Michaelis constant, which represents the sensitivity of β-cells to glucose. Since $V_{\max p2}$ can be combined with other parameters, as described subsequently, it is not included in the parameters space which is going to be obtained through an optimization method. The searching domain of K_{p1} is restricted to the interval of $[3, 30]$ for normal subjects because typically $K_{p1} \in [7, 20]$ (Frayn, 2003).

The production of insulin is stimulated by glucose. Intracellularly, insulin is stored in vesicle granules. Proinsulin is the precursor of insulin production. It follows a sigmoid relation with respect to the glucose concentration (Ashcroft et al., 1978; Schuit et al., 1988; Weiss et al., 2005). The clinical data are illustrated in Figure 3.2.

Therefore the mathematical relationship between the insulin generation rate (I_g, mU·min^{-1}) and $G_p(t)$, which is defined previously, may be represented by

$$I_g(t) = \frac{K_{p2}}{1 + e^{-K_{p3}(G_p(t) - K_{p4})}} + K_{p5}, \tag{3.2}$$

where K_{p2} (mU·min^{-1}) represents the maximal insulin synthesis rate; K_{p3} (mmol^{-1}) represents the changing slope of insulin synthesis rate; K_{p4} (mmol) represents the glucose amount when the synthesis rate reaches half of its maximal value; and K_{p5} (mU·min^{-1}) represents the basal insulin synthesis rate.

According to the clinical data of intravenous glucose tolerance tests (IVGTT)

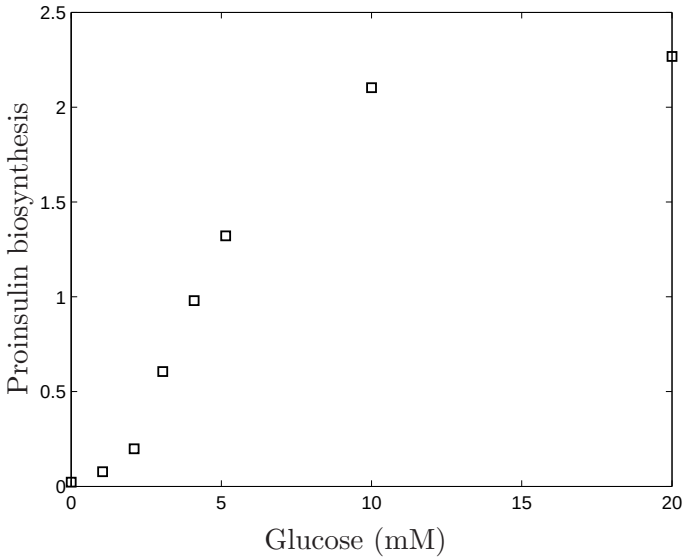

Figure 3.2. Glucose stimulates the synthesis of proinsulin. Data from (Schuit et al., 1988).

in diabetics, there are two phases of insulin release especially in the moderate diabetics (Fujita et al., 1975), which is illustrated in Figure 3.3.

The first phase of insulin release performs similarly as normal subjects for insulin increases when glucose concentration increases and decays after the peak. But there is a significant shift of the second phase of insulin release causing insulin concentration rising again. Therefore we propose that the shift of insulin release in the plasma is due to the signal delay in the pathways of insulin generation which cannot fulfill the demand in time. And the insulin storage rate, I_s (mU·min^{-1}), is defined as

$$\frac{dI_s}{dt}(t) = K_{p6}\left(I_g(t) - I_s(t)\right), \tag{3.3}$$

where K_{p6} (min^{-1}) is the delay parameter.

In the compartment I_r, insulin release is also stimulated by glucose (Frayn,

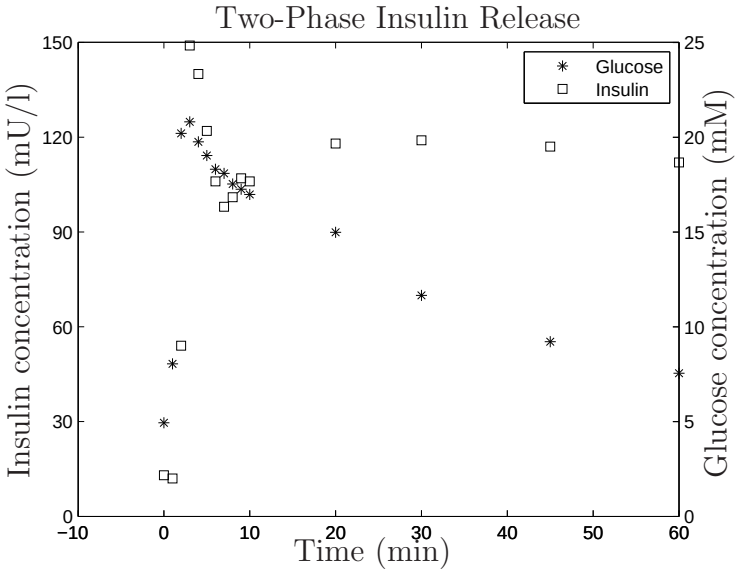

Figure 3.3. IVGTT results of a group of diabetics. Data from (Fujita et al., 1975).

2003; Rorsman and Renström, 2003). Glucose is metabolized intracellularly to generate ATP, which blocks K^+-ATP-dependent channels to cause the depolarization of cell membranes. As a consequence, calcium channels are activated. The inward calcium ions stimulate the insulin release (Cobelli et al., 2007; Wilcox, 2005). The experimental data are illustrated in Figure 3.4.

The mathematical relationship between the release rate (I_r, mU·min^{-1}) and G_p follows a sigmoid function (Frayn, 2003; Harrison et al., 1985). It may be represented by

$$I_r(t) = \frac{K_{p7}}{1 + e^{-K_{p8}(G_p(t) - K_{p9})}} + K_{p10}, \tag{3.4}$$

where G_1 (mmol) represents the amount of glucose entering the pancreas; K_{p7} (mU·min^{-1}) represents the maximal insulin release rate; K_{p8} (mmol^{-1}) represents the changing slope of insulin release rate; K_{p9} (mmol) represents the glu-

cose amount when the release rate reaches half of its maximal value; and K_{p10} ($\mathrm{mU{\cdot}min^{-1}}$) represents the basal insulin release rate. If the release request is larger than the storage, the pancreas will release all the insulin in the granules. This is may be another cause of the delay of insulin release.

The storage of insulin in granules is denoted by I_i ($\mathrm{mU{\cdot}min^{-1}}$). The initial value of I_i is adopted as another parameter in the model of the pancreas, $I_{i0} = K_{p11}$ (mU). The mathematical relationship of insulin storage and release may be represented by

$$\frac{dI_i}{dt}(t) = I_s(t) - I_r(t). \tag{3.5}$$

The definition states that although there may be an expectation of high insulin release rate, the granules may not have sufficient insulin storage. Therefore the insulin release is dependent on both the stimulation and the storage.

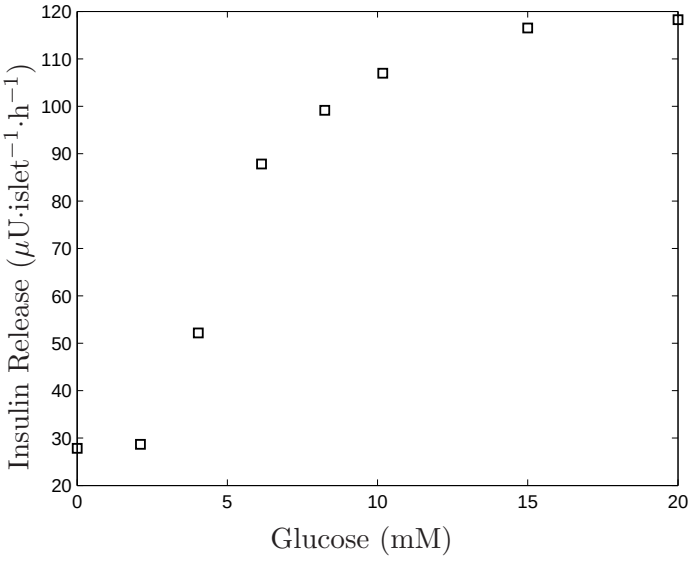

Figure 3.4. Glucose stimulates the release of insulin. Data from (Frayn, 2003).

In the compartment of insulin removal (I_d), insulin enters the plasma *via* the portal vein. About 60% of insulin is immediately removed by the liver. After entering circulation, approximately 50% of peripheral insulin is removed by the kidneys (Duckworth et al., 1998; Wilcox, 2005). Insulin is degraded by enzymes intracellularly. The mathematical relationship between the clearance rate (I_d, $\text{mU}\cdot\text{l}^{-1}\cdot\text{min}^{-1}$) and the insulin concentration in the plasma ($\text{mU}\cdot\text{l}^{-1}$) follows a Michaelis-Menten function (Chase et al., 2005; Thorsteinsson, 1990).

Thus, the clearance rate I_d may be represented by

$$I_d(t) = -K_{p12}\frac{I(t)}{I(t) + K_{p13}}, \tag{3.6}$$

where K_{p12} and K_{p13} represent the maximal rate ($\text{mU}\cdot\text{l}^{-1}\cdot\text{min}^{-1}$) and Michaelis constant ($\text{mU}\cdot\text{l}^{-1}$) respectively.

The output of the pancreas model is the insulin concentration in the plasma (I, $\text{mU}\cdot\text{l}^{-1}$). It is defined as

$$\frac{dI}{dt}(t) = I_d(t) + \frac{I_r(t)}{V_p}, \tag{3.7}$$

where V_p represents the plasma volume (l). The volume is assumed to be linearly correlated with a subject's mass (Levitt, 2003). If the mass was not provided in an experiment, it is assumed to be 70 Kg.

Thus, Equations 3.1 through 3.7 determine the dynamics of insulin. There are 13 parameters ($K_{p1}, \cdots, K_{p13}$) in the pancreas model. These parameters will be obtained by a deterministic optimization method called DIRECT (DIviding RECTangles), which is going to be introduced subsequently.

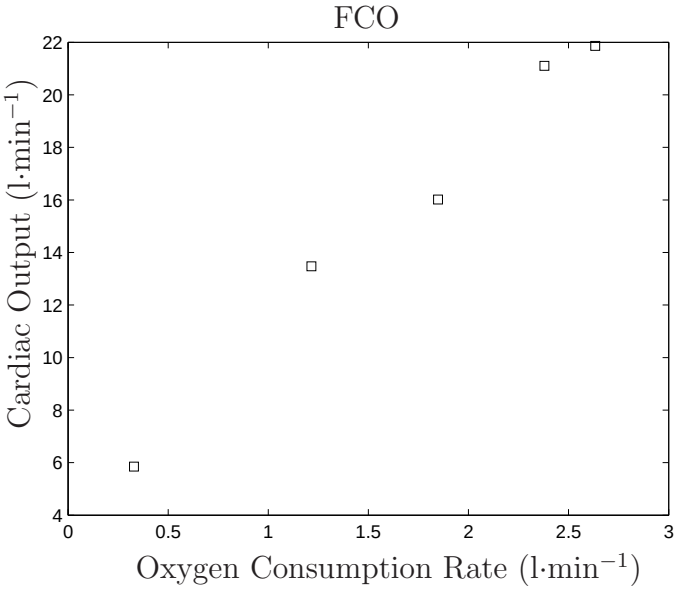

Figure 3.5. Exercise stimulates the output of the heart. Data from (Johnson et al., 1994).

3.2 Glucose Transport in Skeletal Muscle

The model of glucose transport in muscle is divided into three compartments: the plasma, the interstitial fluid space (IFS) and the intracellular space (ICS) as illustrated in Figure 2.3. In this refined model, blood distribution is taken into account. Blood is carried to skeletal muscle by the heart, the output of which determines blood distribution. The delivery of blood to muscle is increased as exercise intensity increases because more substrates and oxygen are needed for energy production. The cardiac output is about five l·min^{-1} at rest and may reach about 25 l·min^{-1} in heavy work (Frayn, 2003). The cardiac output(FCO, called the flag of cardiac output, l·min^{-1}) becomes saturated as exercise intensity increases due to the limit of the heart. The data of cardiac output are illustrated in Figure 3.5.

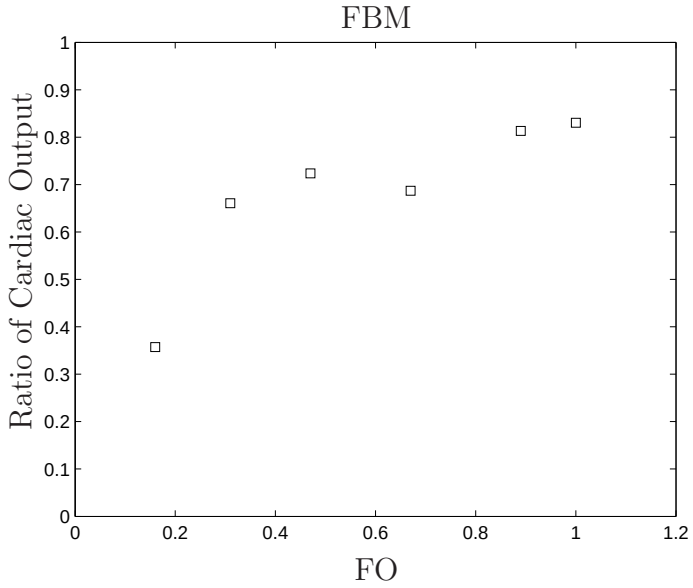

Figure 3.6. Exercise stimulates blood distribution to skeletal muscle. Data from (Armstrong et al., 1987).

Thus, the mathematical relationship between FCO and the oxygen consumption ratio (FO, called the flag of oxygen consumption rate, which is equal to the ratio of the maximal oxygen consumption rate $\dot{\mathrm{V}}_{\mathrm{O2\,max}}$) may be represented by

$$\mathrm{FCO}(t) = 5 + \frac{20}{1 + e^{-K_{s1}(\mathrm{FO}(t) - K_{s2})}}, \tag{3.8}$$

where K_{s1} represents the steepness of cardiac output; K_{s2} represents the shift of oxygen consumption ratio when the cardiac output is half-maximal.

The portion of blood arriving at skeletal muscle is also stimulated by exercise because muscle is the main site of energy production. In the basal state, the percentage of blood delivered to muscle is about 15%-20% while in heavy work, it will be increased to 80%-85% (Frayn, 2003). The distribution of cardiac output to skeletal muscle in swine is illustrated in Figure 3.6.

Thus, the mathematical relationship between the potion of blood delivered to muscle (FBM, called the flag of blood distribution in muscle, unitless) and the oxygen consumption ration (FO) may be represented by

$$\mathrm{FBM}(t) = 0.15 + \frac{0.7}{1 + e^{-K_{s3}(\mathrm{FO}(t) - K_{s4})}}, \tag{3.9}$$

where K_{s3} represents the steepness of blood distribution; K_{s4} represents the shift of oxygen consumption ratio when the blood delivered to the skeletal muscle is half-maximal.

The rate of glucose uptake from the plasma ($G_{s1}(t)$, mmol·min^{-1}), which is dependent on the difference of glucose concentrations in the plasma ($G(t)$) and the IFS ($G_{si}(t)$). Therefore the glucose transport rate from the plasma to the IFS ($G_{s1}(t)$, mmol·min^{-1}) may be represented by

$$G_{s1}(t) = K_{s5}(G(t) - G_{si}(t))\mathrm{FCO}(t)\mathrm{FBM}(t), \tag{3.10}$$

where K_{s5} represents the percentage of exchanged blood volume between plasma and IFS. A positive value of G_{s1} represents glucose transport from the plasma to the IFS.

Glucose in the IFS is carried into the ICS across cell membranes mainly by GLUT4. At the basal state, GLUT4 is stored intracellularly. It is translocated to cell membranes by the stimulation of insulin and exercise. The dynamics of GLUT4 follow a Michaelis-Menten relation with respect to glucose concentration in the IFS ($G_{si}(t)$) (Frayn, 2003). The volumes of the IFS (V_{si}) and the ICS (V_{sc}) are determined in Equation 3.11 and 3.12 respectively (Levitt, 2003) which are

given by

$$V_{si} = 0.117 m_s \tag{3.11}$$

$$V_{sc} = 0.663 m_s, \tag{3.12}$$

where m_s (Kg) represents the mass of skeletal muscle.

Therefore with the facilitation of GLUT4, the rate of glucose entering the ICS ($G_{s2}(t)$, mmol·min^{-1}) may be represented by

$$G_{s2}(t) = v_{s\,\max}(t) \frac{G_{si}(t)}{G_{si}(t) + K_{m4}} v_{sexe}(t), \tag{3.13}$$

where $v_{s\,\max}(t)$ (mmol·min^{-1}) represents the maximal glucose transport rate by GLUT4; K_{m4} (mmol·l^{-1}) represents the Michaelis constant of GLUT4; and $v_{sexe}(t)$ is a unitless scale representing the influence ratio of exercise on GLUT4 activity.

The effects of insulin stimulation on GLUT4 translocation are increasing the maximal glucose transport rate ($v_{smax}(t)$) and the Michaelis constant ($K_{m4}(t)$) (Sarabia et al., 1992; Yki-Järvinen et al., 1987). These two variables have a Michaelis-Menten relation with insulin concentration respectively which are illustrated in Figure 3.7 and 3.8.

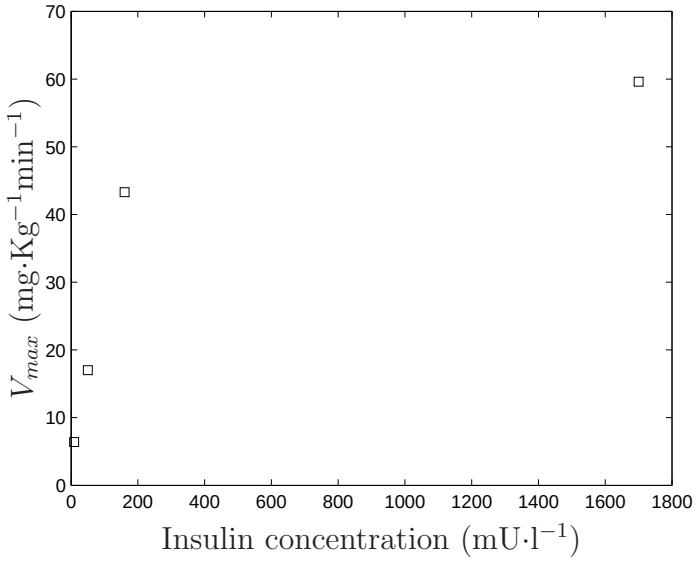

Figure 3.7. Insulin stimulates the maximal rate of GLUT4 transport activity. Data from (Yki-Järvinen et al., 1987).

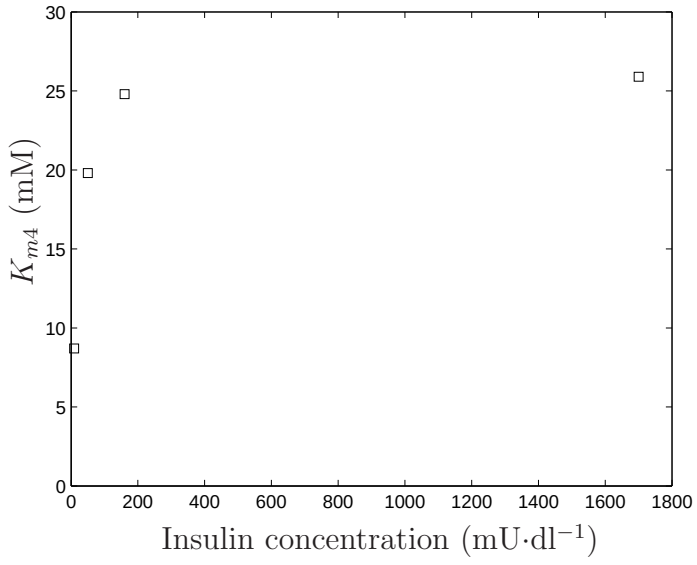

Figure 3.8. Insulin stimulates the Michaelis constant of GLUT4 transport activity. Data from (Yki-Järvinen et al., 1987).

Thus the mathematical representations are given by

$$v_{smax}(t) = K_{s6} m_s \frac{I(t)}{I(t) + K_{s7}} \tag{3.14}$$

$$K_{m4}(t) = K_{s8} \frac{I(t)}{I(t) + K_{s9}}, \tag{3.15}$$

where K_{s6} (mmol·min^{-1}·kg-muscle^{-1}) and K_{s8} (mmol·l^{-1}) represent the maximal values respectively; K_{s7} (mU·l^{-1}) and K_{s9} (mU·l^{-1}) represent the Michaelis constants; and wts (Kg) represents the weight of skeletal muscle.

GLUT4 translocation can also be triggered by exercise. During exercise, ions concentrations such as calcium concentration may be changed intracellularly, which can stimulate the translocation of GLUT4 to cell membranes (Fujimoto et al., 2003; Hayashi et al., 1997; Holloszy et al., 1986). As a consequence of exercise, the maximal glucose transport rate is increased while the Michaelis constant K_m stays unaffected (King et al., 1989; Sternlicht et al., 1989; Zinker et al., 1993). The data are illustrated in Figure 2.5. The stimulation of exercise on glucose transport is defined as above ($v_{sexe}(t)$, unitless). The mathematical relationship between v_{sexe} and the oxygen consumption ratio (FO, percentage of $\dot{\mathrm{V}}_{\mathrm{O2\,max}}$) may be represented by

$$v_{sexe}(t) = 1 + \frac{K_{s10}}{1 + e^{-K_{s11}(\mathrm{FO}(t) - K_{s12})}}, \tag{3.16}$$

where K_{s10} represents the maximal rate stimulated by exercise; K_{s11} represents the changing rate of v_{sexe}; and K_{s12} represents the oxygen consumption ratio of $\dot{\mathrm{V}}_{\mathrm{O2\,max}}$ when $v_{sexe}(t)$ is half-maximal. At the basal state, $v_{sexe} = 1$ which means that there is no stimulation of GLUT4 from exercise. The value of v_{sexe} increases until getting saturated as the intensity of exercise increases.

Together, Equations 3.8 through 3.16 determine the glucose uptake of skeletal

muscle. There are 12 parameters to be determined subsequently using the optimization method called DIRECT. The rate of glucose removal from the plasma to muscle is defined as G_{s1} (mmol·min^{-1}) in Equation 3.10.

3.3 Optimization

The simulation results above demonstrate the general information of glucose metabolism in the body. In this research, not only an empirical modeling is investigated, but also the parameters of models are achieved by an optimization method. A deterministic optimization method called DIRECT (DIviding RECTangles) is adopted to determine the models' parameters (He et al., 2002; Jones et al., 1993). One of the advantages of DIRECT is that it searches optima globally in a simple boundary space. The model parameters of the pancreas and glucose transport in skeletal muscle are obtained by this method.

3.3.1 The Optimization Method: DIRECT

At first, a unit hyper-cube is defined based on the domain of parameters. Each side is denoted as $\hat{K}_i \in [0,1]$ ($i = 1, 2, \cdots, n$ where n represents the amount of model parameters). $\hat{K}_i$ represents the normalized domain of each model parameter satisfying

$$\overrightarrow{K} = \mathrm{A}\overrightarrow{\hat{K}} + \mathrm{B}, \tag{3.17}$$

where $\overrightarrow{K}$ represents the domain of the parameter; $\overrightarrow{\hat{K}}$ represents the normalized domain of the parameter (both $\overrightarrow{K}$ and $\overrightarrow{\hat{K}}$ are vectors with size $n\times1$); A and B are constant vectors with sizes of $1\times n$ and $n\times1$ respectively. Each point in the hyper-cube represents a set of model parameters values which are determined from its coordinates in the parameters space, i.e. the hyper-cube. The objective functions

are defined respectively in the models which is going to be stated subsequently. The objective function values are obtained at the center of the initial hyper-cube and its adjacent points, which have a distance of one third of the side length of the edge of the hyper-cube in each direction.

The hyper-cube is divided to search the optimal results. The rule of dividing is to keep the points with smaller objective function values in the larger hyper-rectangles. This will keep the dividing progress around these points with smaller objective function values since the larger hyper-rectangles are more likely to be divided in the next step. At first, the parameters space is divided into three equal parts along the direction, in which the smallest objective function values is located, while keeping the sides in the other directions unchanged. Then the parameters space is divided along the side in the direction of the next smallest objective function value while keeping the sides in the other directions unchanged until all directions of the parameter space are divided.

As illustrated in Figure 3.9, the sizes of hyper-rectangles and the objective function values at their centers are collected to determine the candidate rectangles, which are the hyper-rectangles or hyper-cubes to be divided in the next step of searching. Among all the minimal values on centers of the boxes with various sizes, a lower convex hull is determined by an algorithm called Gift Wrapping which is also illustrated in Figure 3.9. The corners of the convex hull are recognized as the candidate rectangles. The algorithm of Gift Wrapping starts from the point residing in the box with the largest size (the most right). It compares the slopes with every point to its left and choses the point which achieves the greatest slope. Starting from the chosen point, the same process continues until the algorithm travels all the minimal value points.

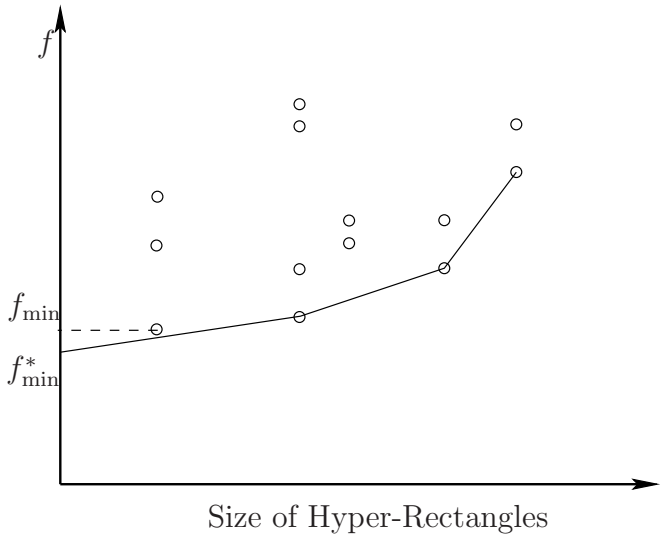

Figure 3.9. The determination of candidate hyper-rectangles.

The largest size of hyper-rectangle with the smallest objective function value is always chosen as the candidate rectangle. That is the reason that the smaller function values are kept in the larger hyper-rectangles. Also, this algorithm not only divides around the smaller function values, but also search the other places globally. There is a modification of the minimal objective function value which is given as

$$f^*_{\min} = f_{\min} - \epsilon|f_{\min}|, \tag{3.18}$$

where $f_{\min}$ and $f^*_{\min}$ represent the minimal objective function value and its modified one respectively; $\epsilon > 0$ represents a controlling factor to adjust the search globally rather than locally, which is equal to 0.001 in the optimization in the research. A larger ϵ represents a larger scale of global searching. This process divides the parameters space globally and converges to optimal values which are adopted as the optimal parameters.

3.3.2 A Mathematical Example

A two dimensional example of DIRECT implementation, the Branin optimal function, is illustrated in Figure 3.10. The Branin function is defined as

$$f = \left(x_2 - \frac{5.1}{4\pi^2} x_1^2 + \frac{5}{\pi} x_1 - 6 \right)^2 + 10 \left(1 - \frac{1}{8\pi} \right) \cos(x_1) + 10, \tag{3.19}$$

where $x_1 \in [-5, 10]$ and $x_2 \in [0, 15]$. So the parameters and normalized ones of Branin function $(K_1, K_2, \hat{K}_1, \hat{K}_2)$ are given as

$$\begin{bmatrix} K_1 \\ K_2 \end{bmatrix} = \begin{bmatrix} 15 \\ 15 \end{bmatrix} \begin{bmatrix} \hat{K}_1 \\ \hat{K}_2 \end{bmatrix} + \begin{bmatrix} \text{-5} \\ 0 \end{bmatrix}. \tag{3.20}$$

Adopting ϵ=0.001, the algorithm converges to the three optima: $[-\pi, 12.275]$, $[\pi, 2.275]$, $[9.42478, 2.475]$.

As illustrated in Figure 3.10(a), in step 1, Branin function values are obtained at the center and adjacent points in the 2-D parameters space, which are 2.4051, 13.0031, 24.2781, 53.1758 and 96.1511. The space is first divided horizontally, and then vertically across the middle, because DIRECT first keeps the smallest objective function value (2.4051) in the largest rectangles as stated above and continue dividing in the direction of the next smallest value (13.0031). After step 1, the candidate rectangles to be divided is determined by Gift Wrapping. In this example, the bottom rectangle, which contains the smallest objective function value (2.4051), is chosen as the candidate illustrated in Figure 3.11, which is divided in step 2. Again, by Gift Wrapping, the current candidate rectangles are the upper rectangle (96.1511) and the bottom-center square (2.4051) illustrated in Figure 3.12, which are divided in step 3 following the same rule. Continuing

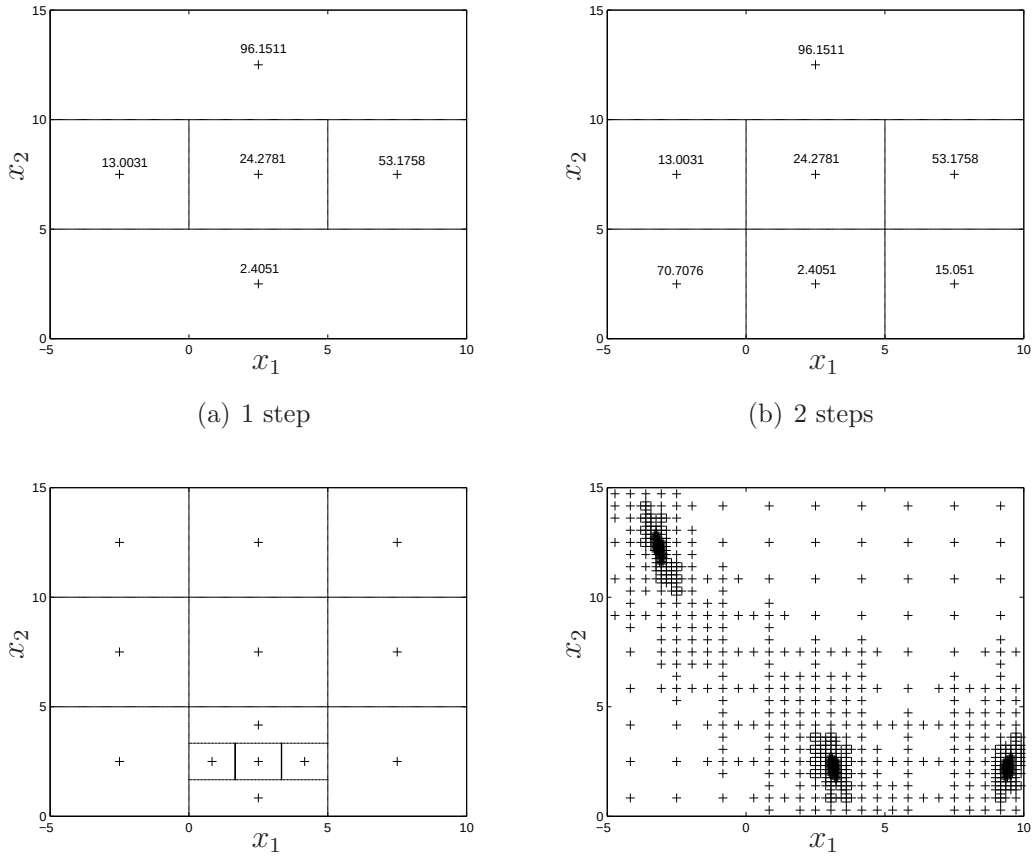

(a) 1 step

(b) 2 steps

(c) 3 steps

(d) 50 steps

Figure 3.10: Demonstration of using DIRECT for the Branin optimal function. The crosses represent the centers of hyper-rectangles. The numbers are the objective function values at the center points. The dash lines represent dividing hyper-rectangles.

this process, the algorithm converges to the clusters of crosses illustrated in Figure 3.10(d) where the optima are located.

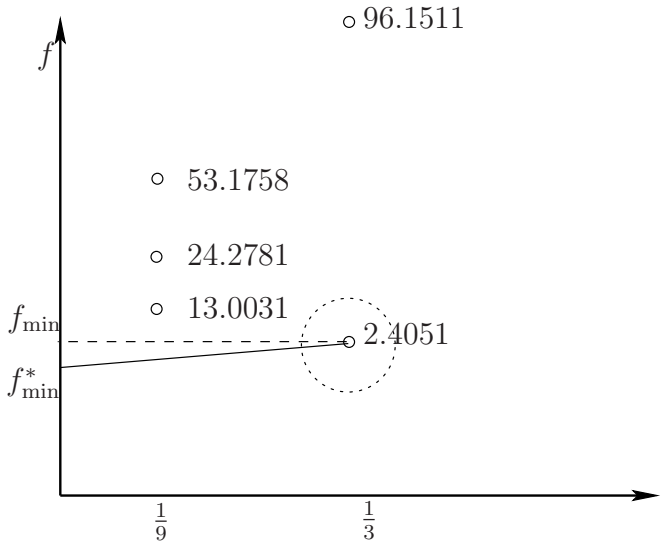

Figure 3.11. Candidate rectangles: Step 1.

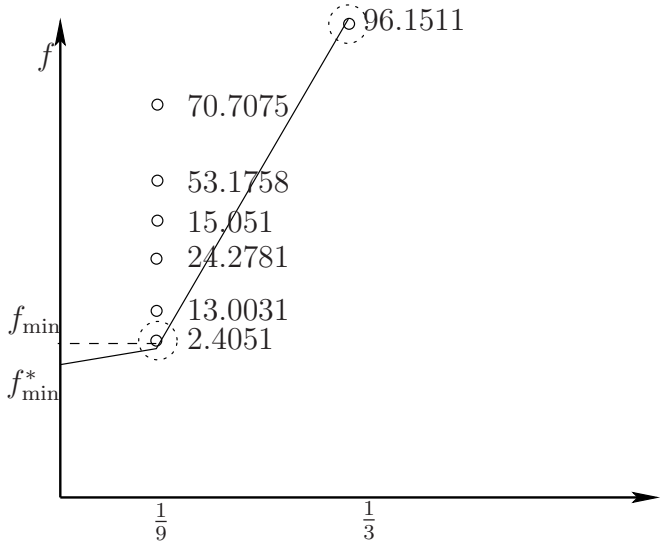

Figure 3.12. Candidate rectangles: Step 2.

3.4 Proof of Lipschitz Continuity

Since DIRECT is one of the Lipschitzian optimization methods (He et al., 2002; Jones et al., 1993), the objective function needs to be Lipschitz continuous on the parameters space. The proofs are given in the models of the pancreas and glucose transport in muscle respectively.

3.4.1 The Model of the Pancreas

The definition of the objective function is

$$f(\tilde{\hat{I}}; \tilde{I}_0) = \sqrt{\left(\frac{\hat{I}_1 - I_{0,1}}{I_{0,1}}\right)^2 + \left(\frac{\hat{I}_2 - I_{0,2}}{I_{0,2}}\right)^2 + \cdots + \left(\frac{\hat{I}_n - I_{0,n}}{I_{0,n}}\right)^2} \tag{3.21}$$

where $i = 1, 2, \ldots, n$ represent the sample points; $\tilde{\hat{I}} = \hat{I}_i = \left(\hat{I}_1, \cdots, \hat{I}_n\right)$ represents the simulation results of insulin concentrations at the sample point i; and $\tilde{I}_0 = I_{0,i} = (I_{0,1}, \cdots, I_{0,n})$ represents the insulin concentrations at the sampled point i in the clinical data, which are constant. The ideal minimal value of $f(\tilde{\hat{I}}; \tilde{I}_0)$ will be 0, which means the complete match of simulation results and the clinical data at the sampled points, which is

$$f_{\min} = 0. \tag{3.22}$$

The next step is to find the possible maximal value of $f(\tilde{\hat{I}}; \tilde{I}_0)$. Given a profile of simulation results of insulin concentration, $\tilde{\hat{I}}(p) = \left(\hat{I}_{p,1}, \hat{I}_{p,2}, \cdots, \hat{I}_{p,n}\right)$, the

objective function satisfies

$$
\begin{aligned}
f(\tilde{\hat{I}}(p);\tilde{I}_0) &= \sqrt{\left(\frac{\hat{I}_{p,1}-I_{0,1}}{I_{0,1}}\right)^2+\left(\frac{\hat{I}_{p,2}-I_{0,2}}{I_{0,2}}\right)^2+\cdots+\left(\frac{\hat{I}_{p,n}-I_{0,n}}{I_{0,n}}\right)^2} \\
&\leqslant \sqrt{n\max_i\left(\frac{\hat{I}_{p,i}-I_{0,i}}{I_{0,i}}\right)^2} \\
&= \sqrt{n\left(\frac{\max_i\|\hat{I}_{p,i}-I_{0,i}\|}{\min_i I_{0,i}}\right)^2} \\
&\leqslant \sqrt{n}\frac{\max_i|\hat{I}_{p,i}|+\max_i I_{0,i}}{\min_i I_{0,i}}.
\end{aligned}
\tag{3.23}
$$

Therefore, for any two given profiles of simulation results of insulin concentration, $\tilde{\hat{I}}(p)=\left(\hat{I}_{p,1},\hat{I}_{p,2},\cdots,\hat{I}_{p,n}\right)$ and $\tilde{\hat{I}}(q)=\left(\hat{I}_{q,1},\hat{I}_{q,2},\cdots,\hat{I}_{q,n}\right)$, we have

$$
\begin{aligned}
\left\|f(\tilde{\hat{I}}(p);\tilde{I}_0)-f(\tilde{\hat{I}}(q);\tilde{I}_0)\right\| &\leqslant \sqrt{n}\max_{r=p,q}\left(\frac{\max_i|\hat{I}_{r,i}|+\max_i I_{0,i}}{\min_i I_{0,i}}\right)-0 \\
&\leqslant \sqrt{n}\frac{\max_{r=p,q}\left(\max_i|\hat{I}_{r,i}|\right)+\max_i I_{0,i}}{\min_i I_{0,i}}.
\end{aligned}
\tag{3.24}
$$

From the definition of insulin release in the model,

$$
\begin{aligned}
\frac{dI}{dt} &= -I_d+I_r \\
&= -\frac{K_{12}}{I+K_{13}}+\frac{1}{V}\left(\frac{K_7}{1+e^{-K_8(G_1-K_9)}}+K_{10}\right) \\
&\leqslant \frac{1}{V}(K_7+K_{10}),
\end{aligned}
\tag{3.25}
$$

where V represents the volume of the plasma; K_7 and K_{10} represent the parameters in the pancreas model. Thus, the maximal simulation result of insulin

concentration in the time interval $t = [t_0, t_1]$ is

$$\begin{aligned}\max_i |\hat{I}_{r,i}| &= I_{ini} + \int_{t_0}^{t_1} \frac{dI}{dt} dt \\ &\leqslant I_{ini} + \frac{t_1 - t_0}{V}(\max K_7 + \max K_{10}),\end{aligned} \tag{3.26}$$

where I_{ini} represents the initial insulin concentration in the clinical data; $\max K_7$ and $\max K_{10}$ represent the upper bounds of the ranges of K_7 and K_{10} which are constants chosen in the optimization.

In the parameters space of optimization, the minimal distance between any two grid is

$$d_{p,q} \geqslant \left(\frac{1}{3}\right)^{\alpha}, \tag{3.27}$$

where $d_{p,q}$ represents the distance between any two sets of parameters in the parameters space; and α represents the number of dividing procedures. Therefore, we have

$$\begin{aligned}\frac{\left\| f(\tilde{\hat{I}}(p); \tilde{I}_0) - f(\tilde{\hat{I}}(q); \tilde{I}_0) \right\|}{d_{p,q}} &\leqslant 3^{\alpha} \frac{\max_{r=p,q}\left(\max_i |\hat{I}_{r,i}|\right) + \max_i I_{0,i}}{\min_i I_{0,i}} \\ &\leqslant 3^{\alpha} \frac{I_{ini} + \frac{t_1 - t_0}{V}(\max K_7 + \max K_{10}) + \max_i I_{0,i}}{\min_i I_{0,i}}.\end{aligned} \tag{3.28}$$

Since the profiles of simulation result of insulin concentration $(\tilde{\hat{I}}(p), \tilde{\hat{I}}(q))$ are determined by the coordinates in the parameters space respectively $(\tilde{x}_p, \tilde{x}_q)$, the objective function may be written as $f(\tilde{x}, \tilde{I}_0)$. The distance between two grids in the parameters space is determined by

$$d_{p,q} = \|\tilde{x}_p - \tilde{x}_q\|.$$

Let

$$\gamma_1 = 3^{\alpha} \frac{I_{ini} + \frac{t_1 - t_0}{V}(\max K_7 + \max K_{10}) + \max_i I_{0,i}}{\min_i I_{0,i}}, \tag{3.29}$$

the values of $I_{ini}, V, t_0, t_1, \max_i I_{0,i}$ and $\min_i I_{0,i}$ are constants from the clinical data; and $\max K_7, \max K_{10}$ and α are constants chosen for optimization. Therefore the inequality formula may be written as

$$\left\| f(\tilde{x}_p; \tilde{I}_0) - f(\tilde{x}_q; \tilde{I}_0) \right\| \leqslant \gamma_1 \|\tilde{x}_p - \tilde{x}_q\|, \tag{3.30}$$

where γ_1 is determined from the equation 3.29. Thus, the objective function $f(\tilde{x}; \tilde{I}_0)$ is Lipschitz continuous in the parameters space and the Lipschitz constant is defined as γ in the equation 3.29.

3.4.2 The Model of Glucose Transport in Skeletal Muscle

Similarly, the definition of the objective function is

$$g(\tilde{\hat{G}}; \tilde{G}_0) = \sqrt{\left(\frac{\hat{G}_1 - G_{0,1}}{G_{0,1}}\right)^2 + \left(\frac{\hat{G}_2 - G_{0,2}}{G_{0,2}}\right)^2 + \cdots + \left(\frac{\hat{G}_n - G_{0,n}}{G_{0,n}}\right)^2}, \tag{3.31}$$

where $i = 1, 2, \ldots, n$ represent the sample points; $\tilde{\hat{G}} = \hat{G}_i = \left(\hat{G}_1, \cdots, \hat{G}_n\right)$ represents the simulation results of glucose amount disappearance rates from the plasma at the sample point i; and $\tilde{G}_0 = G_{0,i} = (G_{0,1}, \cdots, G_{0,n})$ represents the amount of glucose disappearance rates from the plasma at the sampled point i in the clinical data, which are constant. The ideal minimal value of $g(\tilde{\hat{G}}; \tilde{G}_0)$ will be 0, which means the complete match of simulation results and the clinical data at the sampled points, such as

$$g_{\min} = 0. \tag{3.32}$$

The next step is to find the possible maximal value of $g(\tilde{\hat{G}}_s; \tilde{G}_{s0})$. Given a profile of simulation results of insulin concentration, $\tilde{\hat{G}}(p) = \left(\hat{G}_{p,1}, \hat{G}_{p,2}, \cdots, \hat{G}_{p,n}\right)$, the objective function satisfies

$$\begin{aligned} g(\tilde{\hat{G}}(p); \tilde{G}_0) &= \sqrt{\left(\frac{\hat{G}_{p,1} - G_{0,1}}{G_{0,1}}\right)^2 + \left(\frac{\hat{G}_{p,2} - G_{0,2}}{G_{0,2}}\right)^2 + \cdots + \left(\frac{\hat{G}_{p,n} - G_{0,n}}{I_{0,n}}\right)^2} \\ &\leqslant \sqrt{n \max_i \left(\frac{\hat{G}_{p,i} - G_{0,i}}{G_{0,i}}\right)^2} \\ &= \sqrt{n \left(\frac{\max_i \|\hat{G}_{p,i} - G_{0,i}\|}{\min_i G_{0,i}}\right)^2} \\ &= \sqrt{n} \frac{\max_i \|\hat{G}_{p,i} - G_{0,i}\|}{\min_i G_{0,i}} \\ &\leqslant \sqrt{n} \frac{\max_i |\hat{G}_{p,i}| + \max_i G_{0,i}}{\min_i G_{0,i}}. \end{aligned} \tag{3.33}$$

Therefore, for any two given profiles of simulation results of insulin concentration, $\tilde{\hat{G}}(p) = \left(\hat{G}_{p,1}, \hat{G}_{p,2}, \cdots, \hat{G}_{p,n}\right)$ and $\tilde{\hat{G}}(q) = \left(\hat{G}_{q,1}, \hat{G}_{q,2}, \cdots, \hat{G}_{q,n}\right)$, we have

$$\begin{aligned} \left\| g(\tilde{\hat{G}}(p); \tilde{G}_0) - g(\tilde{\hat{G}}(q); \tilde{G}_0) \right\| &\leqslant \sqrt{n} \max_{r=p,q} \left(\frac{\max_i |\hat{G}_{r,i}| + \max_i G_{0,i}}{\min_i G_{0,i}} \right) - 0 \\ &\leqslant \sqrt{n} \frac{\max_{r=p,q} \left(\max_i |\hat{G}_{r,i}| \right) + \max_i G_{0,i}}{\min_i G_{0,i}}. \end{aligned} \tag{3.34}$$

From the definition of glucose disappearance rate in the model,

$$\begin{aligned} G &= (FCO)(FBM)K_5\left(G_p - G_i\right) \\ &= \left(5 + \frac{20}{1+e^{-K_1(FO-K_2)}}\right)\left(0.15 + \frac{0.7}{1+e^{-K_3(FO-K_4)}}\right)K_5\left(G_p - G_i\right) \\ &\leqslant (25)(0.85)(\max K_5)(\max G_p) \\ &= 21.25(\max K_5)(\max G_p), \end{aligned} \tag{3.35}$$

where FCO represents the flag of cardiac output; FBM represents the flag of blood distribution in muscle; and G_p, G_i represents the glucose concentrations in the plasma and the IFS respectively. Thus, the maximal simulation result of glucose disappearance rate from the plasma in the time interval $t = [t_0, t_1]$ is

$$\max_i |\hat{G}_{r,i}| = 21.25(\max K_5)(\max G_p), \tag{3.36}$$

where $\max K_5$ represent the upper bound of the parameter K_5; and $\max G_p$ represent the maximal glucose concentration in the plasma in the clinical data.

In the parameters space of optimization, the minimal distance between any two grid is

$$d_{p,q} \geqslant \left(\frac{1}{3}\right)^{\alpha}, \tag{3.37}$$

where $d_{p,q}$ represents the distance between any two sets of parameters in the parameters space; and α represents the number of dividing procedures. Therefore,

we have

$$\frac{\left\|g(\tilde{\hat{G}}(p);\tilde{G}_0)-g(\tilde{\hat{G}}(q);\tilde{G}_0)\right\|}{d_{p,q}} \leqslant 3^{\alpha}\frac{\max_{r=p,q}\left(\max_i|\hat{G}_{r,i}|\right)+\max_i G_{0,i}}{\min_i G_{0,i}}$$
$$\leqslant 3^{\alpha}\frac{21.25(\max K_5)(\max G_p)+\max_i G_{0,i}}{\min_i G_{0,i}}. \quad (3.38)$$

Since the profiles of simulation result of insulin concentration $(\tilde{\hat{G}}(p), \tilde{\hat{G}}(q))$ are determined by the coordinates in the parameters space respectively $(\tilde{x}_p, \tilde{x}_q)$, the objective function may be written as $g(\tilde{x};\tilde{G}_0)$. The distance between two grids in the parameters space is determined by

$$d_{p,q} = \|\tilde{x}_p - \tilde{x}_q\|.$$

Let

$$\gamma_2 = 3^{\alpha}\frac{21.25(\max K_5)(\max G_p)+\max_i G_{0,i}}{\min_i G_{0,i}}, \quad (3.39)$$

the values of $\max_i G_{0,i}$ and $\min_i G_{0,i}$ are constants in the clinical data; and $\max K_5$ is defined for simulations. Therefore the inequality formula may be written as

$$\left\|g(\tilde{x}_p;\tilde{G}_0)-g(\tilde{x}_q;\tilde{G}_0)\right\| \leqslant \gamma_2\|\tilde{x}_p-\tilde{x}_q\|, \quad (3.40)$$

where γ_2 is determined from the equation 3.39. Thus, the objective function $g(\tilde{x};\tilde{G}_0)$ is Lipschitz continuous in the parameters space and the Lipschitz constant is defined as γ_2 in the equation 3.39.

3.5 Simulation Results

There are 13 parameters in the model $(K_{p1}, \cdots, K_{p13})$ stated in Session 3.1. The deterministic optimization method DIRECT is used to obtain their values by searching globally in the parameters space. There are seven intravenous glucose tolerance tests (IVGTT) data sets for optimization and validation from the literature (Avogaro et al., 1989; Bergman et al., 1981; Henriksen et al., 1994; Hovorka et al., 2002; Pacini et al., 1998; Vicini et al., 1997). The time span of each experiment is at least 180 minutes. In each data set, the sample values are the average of the experiments on a group of subjects with the count w_i $\{w_1$=14, w_2=5, w_3=3, w_4=20, w_5=6, w_6=6, w_7=16$\}$ respectively. We first divide the data sets into two groups for optimization (4 data sets: w_1, w_2, w_3, and w_4) and validation (3 data sets: w_5, w_6, and w_7). Then we derive the pooled samples of data sets for simulations (Dunn, 2005). In the groups of optimization and validation, the pooled weighted mean $(\bar{x}_w)$, the pooled weighted standard deviation $(\{S_x\}_w)$, and the pooled weighted standard deviation of the means $(\{S_{\bar{x}}\}_w)$ at a specific sample time point j are given by

$$\bar{x}_{wj} = \frac{\sum_{i=1}^{n_i} w_i x_j}{\sum_{i=1}^{n_i} w_i} \tag{3.41}$$

$$\{S_x\}_{wj} = \sqrt{\frac{v_1 S^2_{x(1,j)} + \cdots + v_{n_i} S^2_{x(n_i,j)}}{v}} \tag{3.42}$$

$$v = \sum_{i=1}^{n_i} v_i = \sum_{i=1}^{n_i} (w_i - 1) \tag{3.43}$$

$$\{S_{\bar{x}}\}_{wj} = \frac{\{S_x\}_{wj}}{\sqrt{\sum_{i=1}^{n_i} w_i}}, \tag{3.44}$$

where x_j (mU$\cdot$l^{-1}) represent the insulin concentration in plasma at the sample time point j; n_i represents the count of data sets for pooling (n_i=4 in optimization;

n_i=3 in validation); $S_{x(1,j)}, \cdots, S_{x(n_i,j)}$ represent the standard deviation in each data set at the sample time point j. Because the sample time points might be different, the rule was given that if there is no data available at a specific sample time point in a data set, the value is obtained *via* interpolation. The objective function is defined as

$$f = \sqrt{\sum_{j=1}^{\hat{n}_j} \left(\frac{x_j - \bar{x}_{wj}}{\bar{x}_{wj}} \right)^2}, \tag{3.45}$$

where $\hat{n}_j$ represents the sample size of the pooled data; and x_j (mU·l^{-1}) represents the insulin concentration in plasma at the sample time point j during simulations. The weight factor $w_i = 1$.

The IVGTT data of groups of healthy subjects for optimization (Group ID1∼ID4) and validation (Group ID5∼ID7) are cited from the literature (Avogaro et al., 1989; Bergman et al., 1981; Henriksen et al., 1994; Hovorka et al., 2002; Pacini et al., 1998; Vicini et al., 1997). The standard glucose tests last at least 180 minutes. There are three sample points at $Time = -5, -2, -1$ minute added to totally 28 sample points. Since the characteristics of the pancreas in healthy subjects are similar, we use the pooled samples of data sets for simulations (Dunn, 2005; Lv and Goodwine, 2009). The results are illustrated in Figure 3.13. In the plot, the symbols of stars represent the sampled data of glucose concentration; the empty squares represent the sampled data of insulin concentration; and the dashed lines represent the simulation results of insulin concentration. It shows that the proposed pancreas model is able to capture not only the transient response of insulin increasing peak, but also the decay of insulin. The obtained parameters of healthy subjects are K_{p1}=9.39 mM, K_{p2}=32.11 mU·min^{-1}, K_{p3}=3112.55 mmol^{-1}, K_{p4}=4.85×10^{-3} mmol, K_{p5}=32.82 mU·min^{-1}, K_{p6}=1.13 min^{-1}, K_{p7}=111.10 mU·min^{-1}, K_{p8}=2327.77 mmol^{-1}, K_{p9}=4.52×10^{-3} mmol,

K_{p10}=12.33 mU·min^{-1}, K_{p11}=304.68 mU, K_{p12}=77.79 mU·l^{-1}·min^{-1} and K_{p13}=92.55 mU·l^{-1}. After the pancreas model is established from these parameters, the model is used to validate the data sets in the validation group (Group ID5∼ID7). The validation results are illustrated in Figure 3.14, 3.15 and 3.16. The validation is also performed on two subjects individually (ID8 and ID9) (Caumo and Cobelli, 1993; Pacini and Bergman, 1986). The results are illustrated in Figure 3.17 and 3.18. The numerical method used was Euler method with $\Delta t = 0.01$ minute and the convergence was verified with $\Delta t = 0.001$ minute.

Our proposed model can describe the insulin dynamics better especially in the initial and peak insulin values. In contrast, given a fixed glucose profile in time and the determined parameters (Pacini and Bergman, 1986), the simulation results of the minimal model are illustrated in Figure 3.19. As stated in Chapter 1, the mathematical representation of the minimal model is given by

$$\frac{dG}{dt}(t) = -(p_1 + X(t))G(t) + p_1 G_b \tag{3.46}$$

$$\frac{dX}{dt}(t) = -p_2 X(t) + p_3(I(t) - I_b) \tag{3.47}$$

$$\frac{dI}{dt}(t) = -nI(t) + \gamma(G(t) - h)t, \tag{3.48}$$

with $G(0)$=G_0, $X(0)$=0 and $I(0)$=I_0 where $G(t), X(t)$ and $I(t)$ represent the concentrations of glucose in the plasma, the remote insulin and insulin in the plasma respectively and $p_1, p_2, p_3, G_0, n, \gamma, h$ and I_0 are parameters. The given parameters are p_1=0.03082, p_2=0.02093, p_3=1.062 $\times 10^{-4}$, G_0=287.0, n=0.3, γ=3.349$\times 10^{-3}$, h=89.5 and I_0=403.4.

It is illustrated that the minimal model fails to capture the insulin transient response to the increase of glucose concentration which is very important for the

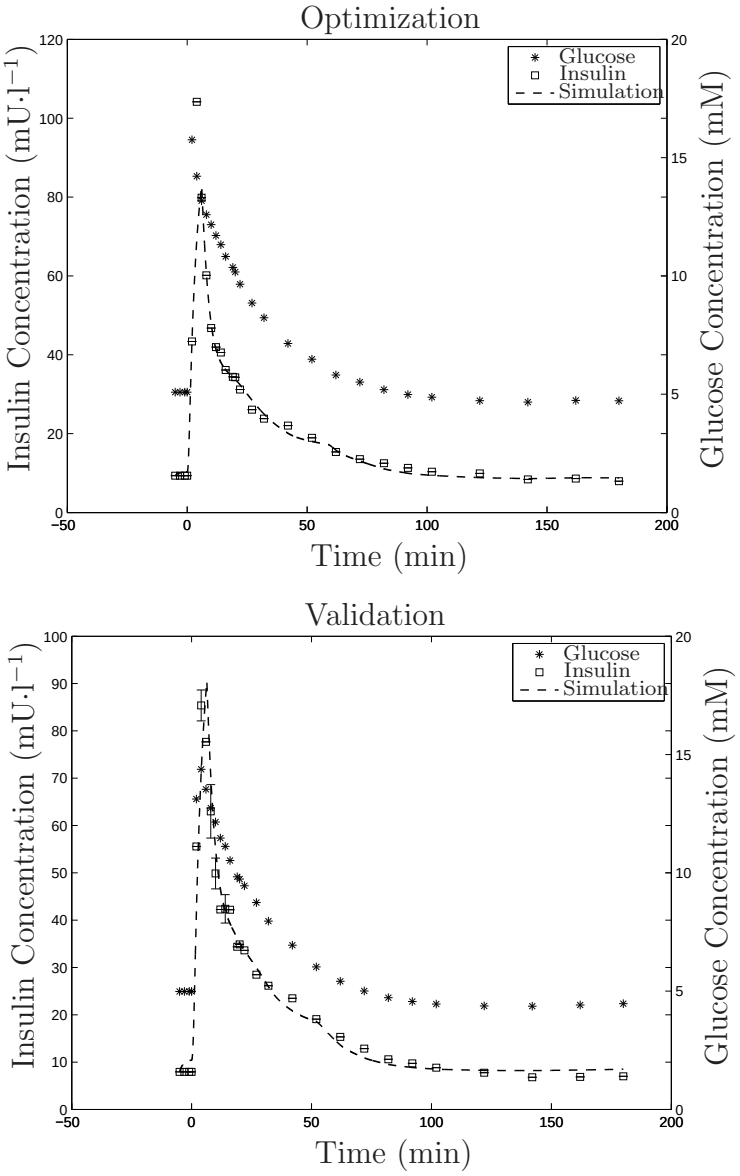

Figure 3.13. Optimization and validation results of healthy subjects (Optimization: Group ID1∼ID4; Validation: Group ID5∼ID7).

assessment of health. Furthermore, our model can represent long term time scale of insulin response. Another advantage of our model is that its parameters contain more physiological information since it is constructed in a mechanistic way.

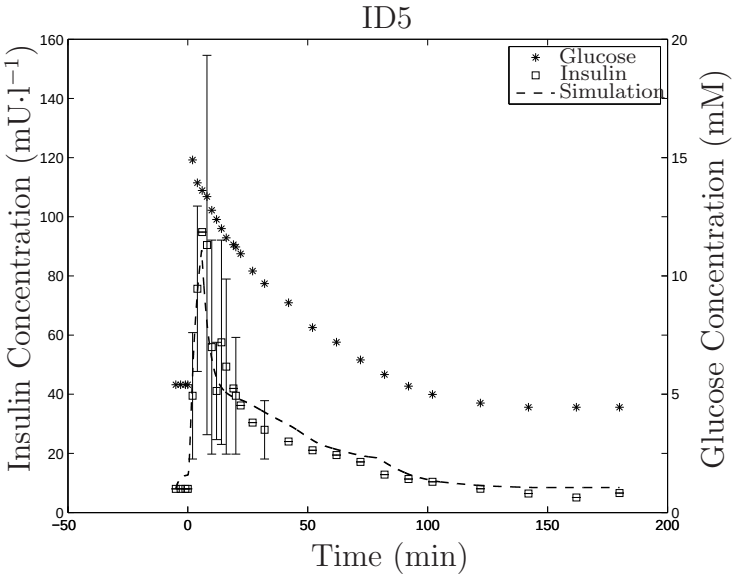

Figure 3.14. Validation on group ID5.

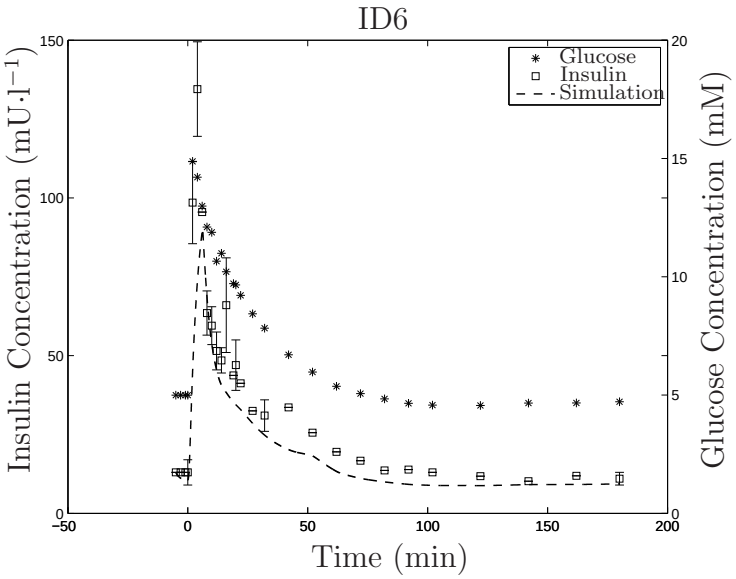

Figure 3.15. Validation on group ID6.

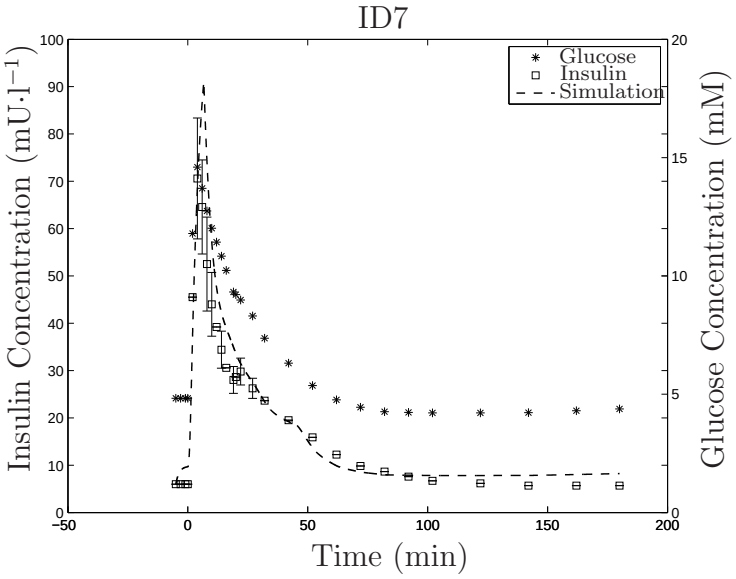

Figure 3.16. Validation on group ID7.

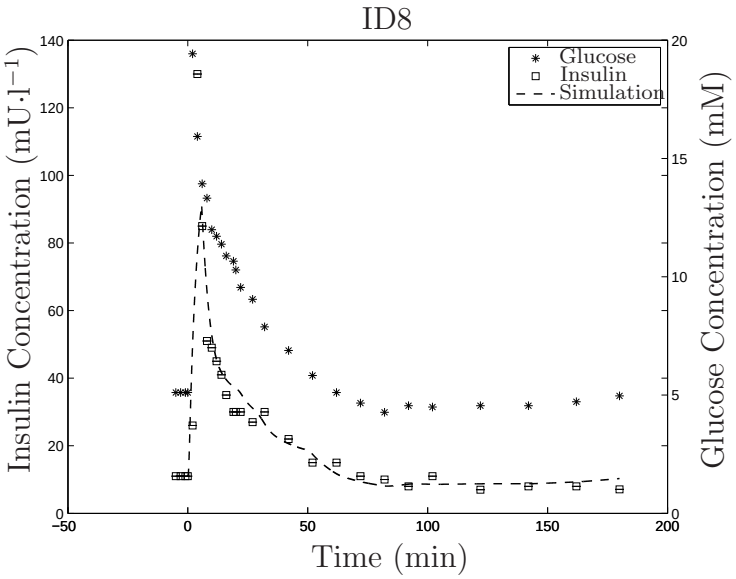

Figure 3.17. Validation on subject ID8.

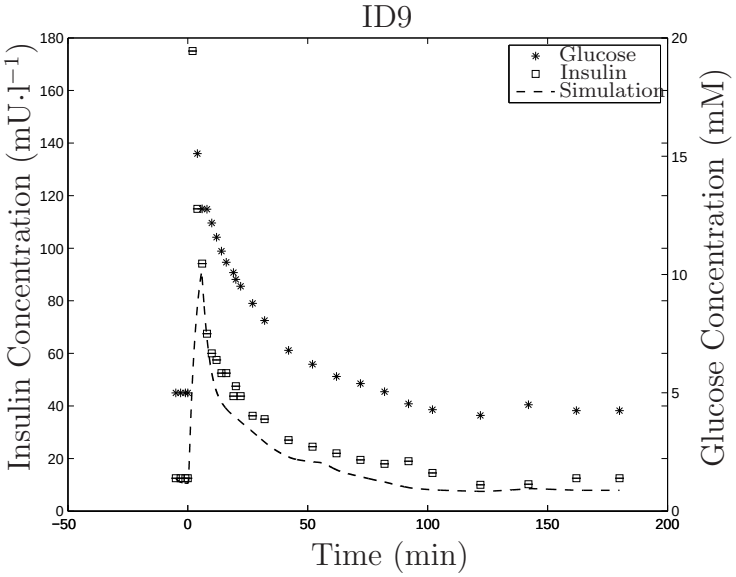

Figure 3.18. Validation on subject ID9.

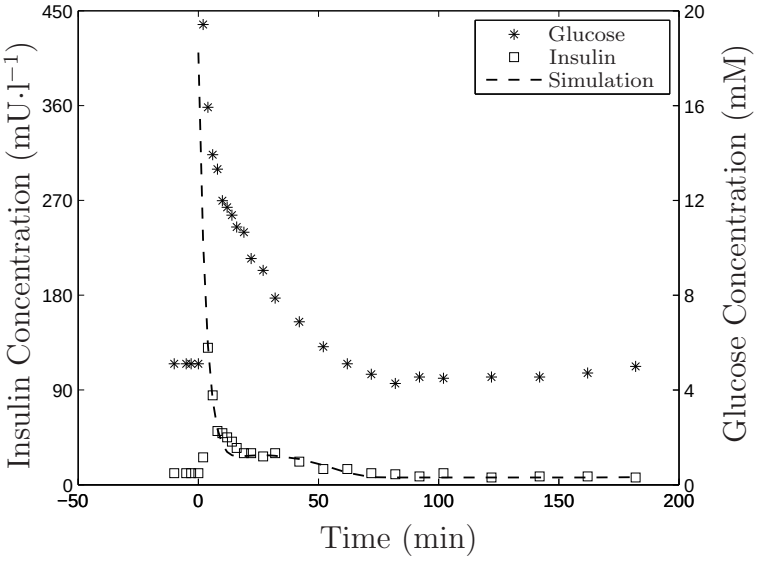

Figure 3.19. Experimental data and simulation results of insulin response to IVGTT from the minimal model (Pacini and Bergman, 1986). Data before time $t = 0$ are extended from the basal states.

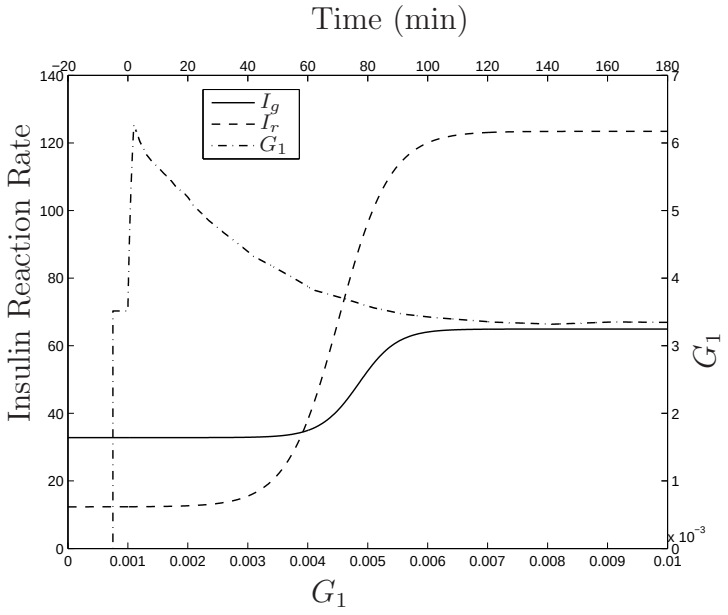

Figure 3.20. Component functions in group of optimization.

Also the functions of insulin generation and release and the states of G_1 are illustrated in Figure 3.20 through 3.26. It is illustrated that the range of G_1 covers the overall domain of insulin production and release in normal subjects and diabetics subjects, the concentrations of G_1 is higher than that in normal ones which covers the upper domain of insulin production and release. This also reflects the difference between normal subjects and diabetics.

The pancreas model is also implemented for diabetics. The data of diabetics are cited from the literature (Fujita et al., 1975). There are two sets of mild diabetic subjects (Group ID10 and ID11) and one set of moderate diabetic ones (Group ID12). Each set of subjects has two separate IVGTTs. The optimization results of mild diabetic subjects are illustrated in Figure 3.27 and 3.28.

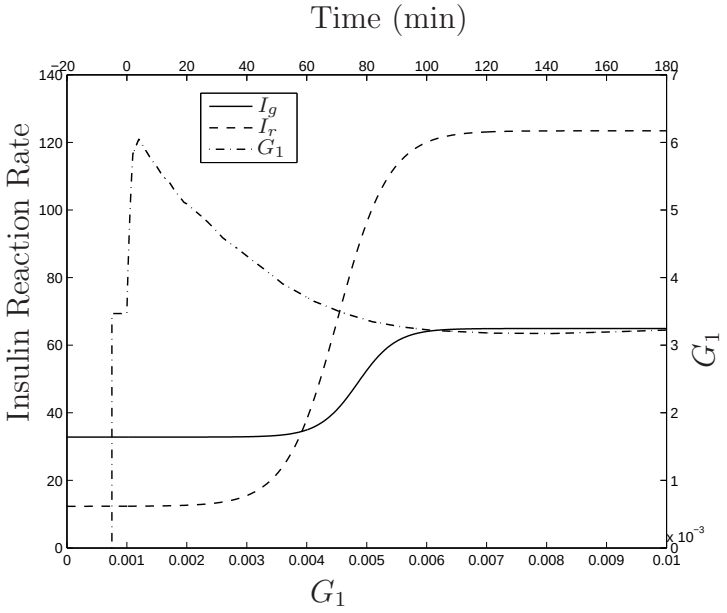

Figure 3.21. Component functions in group of validation.

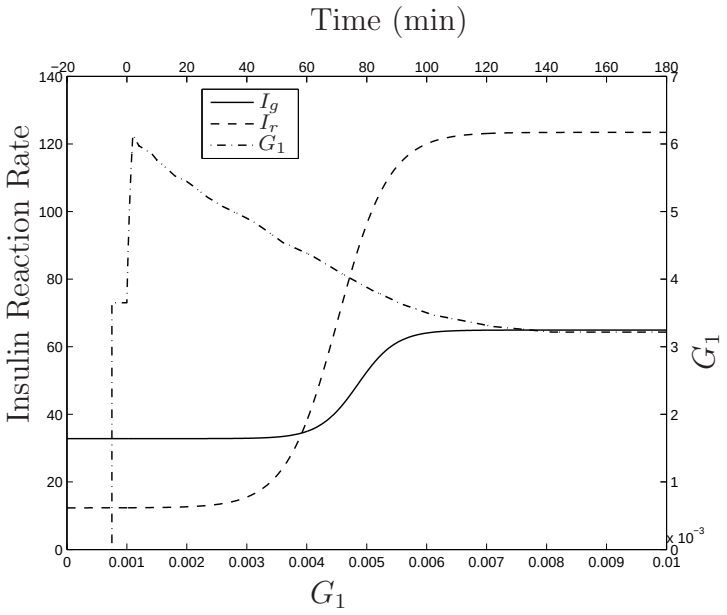

Figure 3.22. Component functions in group ID5.

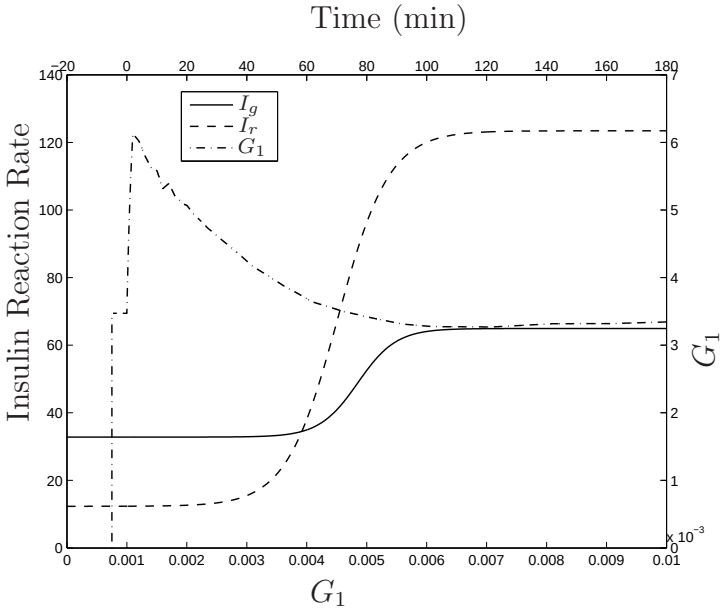

Figure 3.23. Component functions in group ID6.

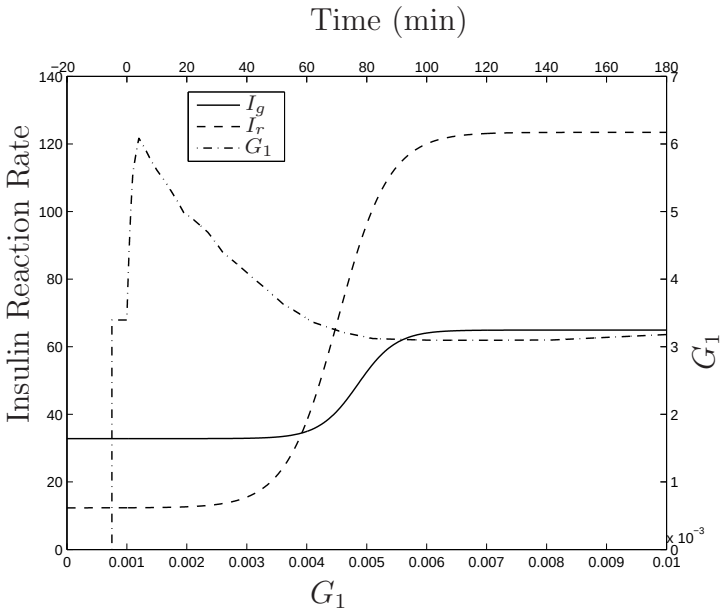

Figure 3.24. Component functions in group ID7.

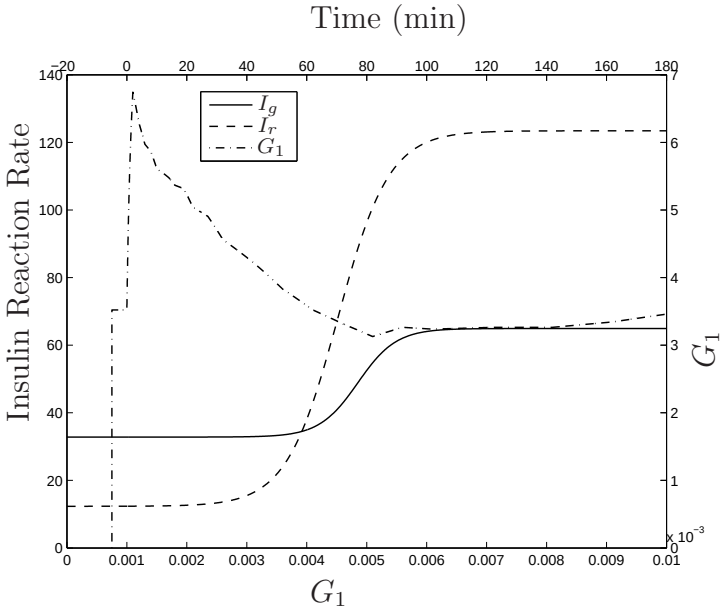

Figure 3.25. Component functions in group ID8.

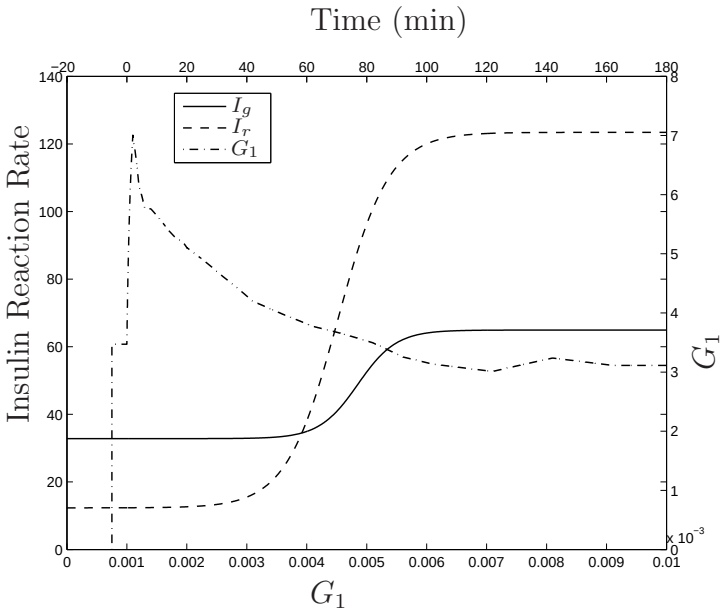

Figure 3.26. Component functions in group ID9.

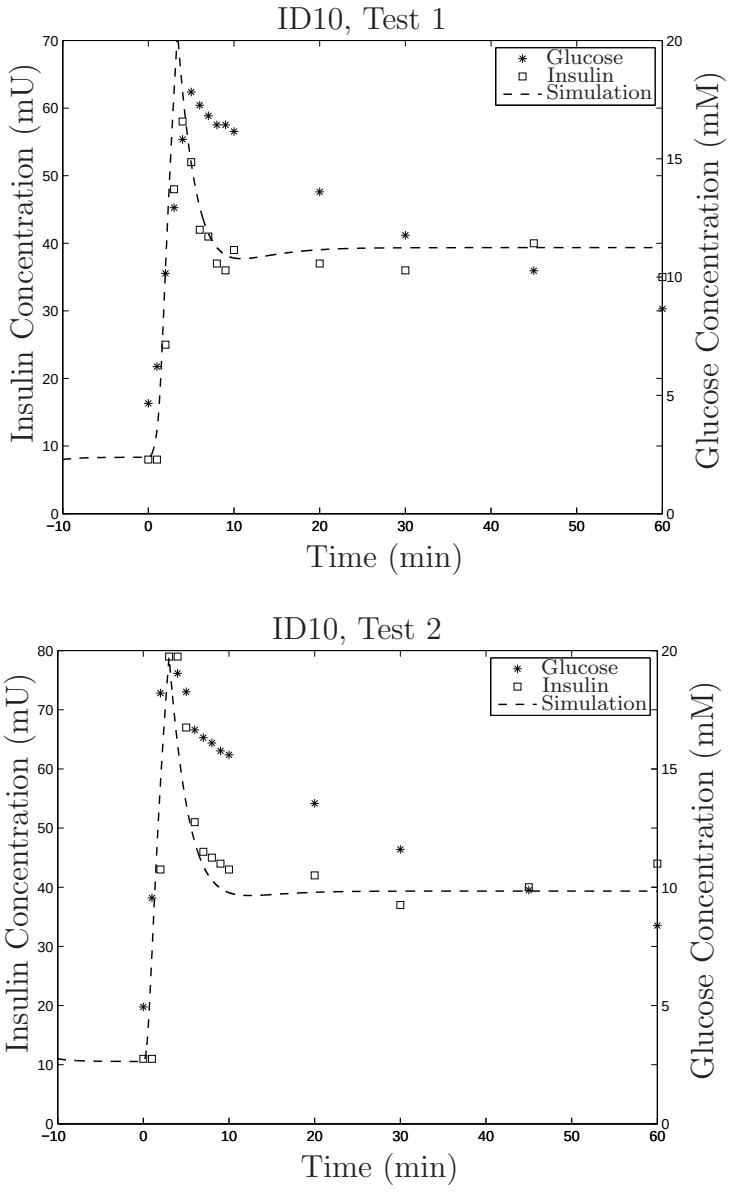

Figure 3.27. Simulation results of mild diabetic subjects group 1.

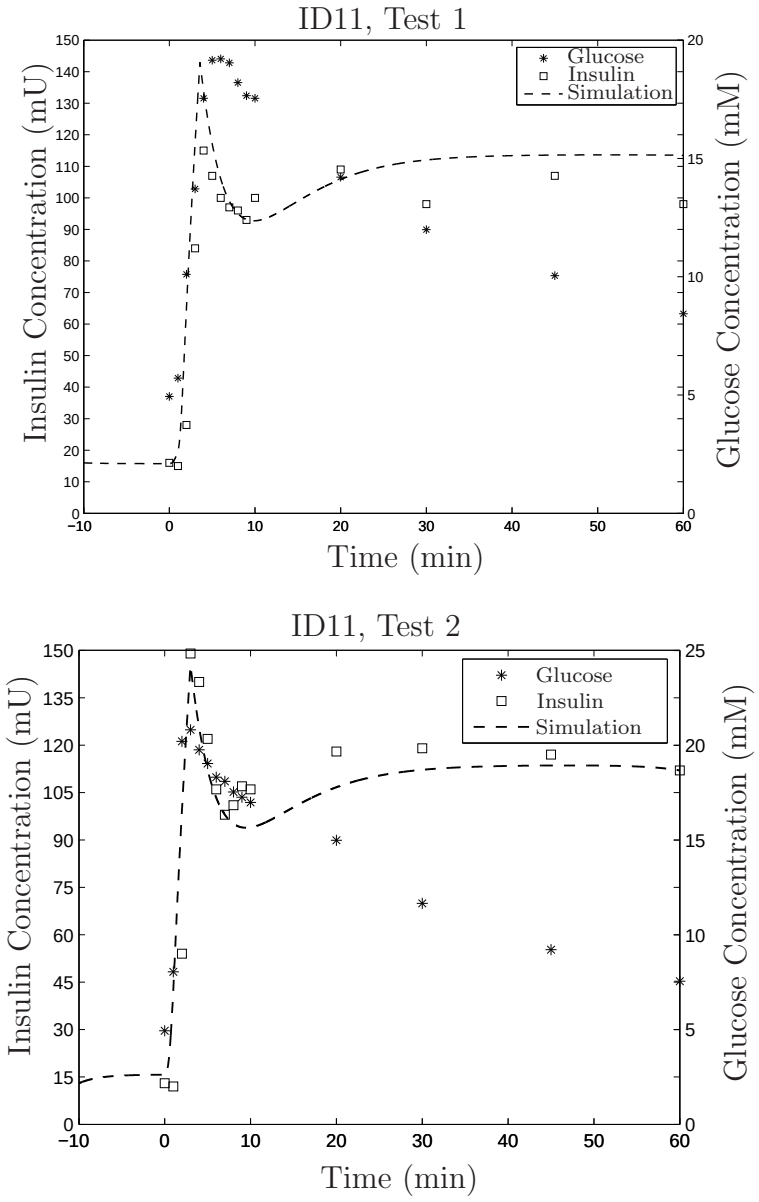

Figure 3.28. Simulation results of mild diabetic subjects group 2.

There are 10 subjects in Group ID10 and the achieved optimal parameters are K_{p1}=13.05 mM, K_{p2}=66.67 mU·min^{-1}, K_{p3}=8518.49 mmol^{-1}, K_{p4}=2.83×10^{-3} mmol, K_{p5}=3.14 mU·min^{-1}, K_{p6}=0.30 min^{-1}, K_{p7}=181.48 mU·min^{-1}, K_{p8}=3178.85 mmol^{-1}, K_{p9}=3.5×10^{-3}, K_{p10}=6.53 mU·min^{-1}, K_{p11}=407.64 mU, K_{p12}=98.42 mU·l^{-1}·min^{-1} and K_{p13}=171.24 mU·l^{-1}. There are 5 subjects in ID11 and the achieved optimal parameters set is: K_{p1}=20.0 mM, K_{p2}=188.89 mU·min^{-1}, K_{p3}=9937.59 mmol^{-1}, K_{p4}=2.45×10^{-3} mmol, K_{p5}=18.61 mU·min^{-1}, K_{p6}=0.23 min^{-1}, K_{p7}=479.77 mU·min^{-1}, K_{p8}=4936.21 mmol^{-1}, K_{p9}=2.5×10^{-3}, K_{p10}=9.85 mU·min^{-1}, K_{p11}=1344.03 mU, K_{p12}=86.67 mU·l^{-1}·min^{-1} and K_{p13}=166.67 mU·l^{-1}.

There are also clinical data of the moderate diabetics (Group ID12, 5 subjects) for the pancreas model. Since the experimental data (Test 1 and Test 2) are significantly different in these two tests such as the basal and the peak insulin concentrations, it is proposed that the discrepancy of data, which represents different characteristics of the pancreas, may be due to some changes in the bodies during the days between the two tests. Simulation results are illustrated in Figure 3.29. The optimal parameters of Test 1 are K_{p1}=20.96 mM, K_{p2}=15.55 mU·min^{-1}, K_{p3}=4975.3 mmol^{-1}, K_{p4}=3.8×10^{-3} mmol, K_{p5}=6.78 mU·min^{-1}, K_{p6}=0.04 min^{-1}, K_{p7}=138.78 mU·min^{-1}, K_{p8}=2271.32 mmol^{-1}, K_{p9}=4.72×10^{-3}, K_{p10}=4.13 mU·min^{-1}, K_{p11}=88.89 mU, K_{p12}=32.96 mU·l^{-1}·min^{-1} and K_{p13}=144.64 mU·l^{-1}. Test 2 is performed on the same 5 subjects after a few days. The optimal parameters are K_{p1}=16.11 mM, K_{p2}=69.0 mU·min^{-1}, K_{p3}=4823.1 mmol^{-1}, K_{p4}=3.67×10^{-3} mmol, K_{p5}=20.50 mU·min^{-1}, K_{p6}=0.033 min^{-1}, K_{p7}=45.47 mU·min^{-1}, K_{p8}=2387.31 mmol^{-1}, K_{p9}=4.17×10^{-3}, K_{p10}=19.65 mU·min^{-1}, K_{p11}=333.33 mU, K_{p12}=60 mU·l^{-1}·min^{-1} and K_{p13}=100 mU·l^{-1}.

The characteristics of parameters are also investigated in another group of 8

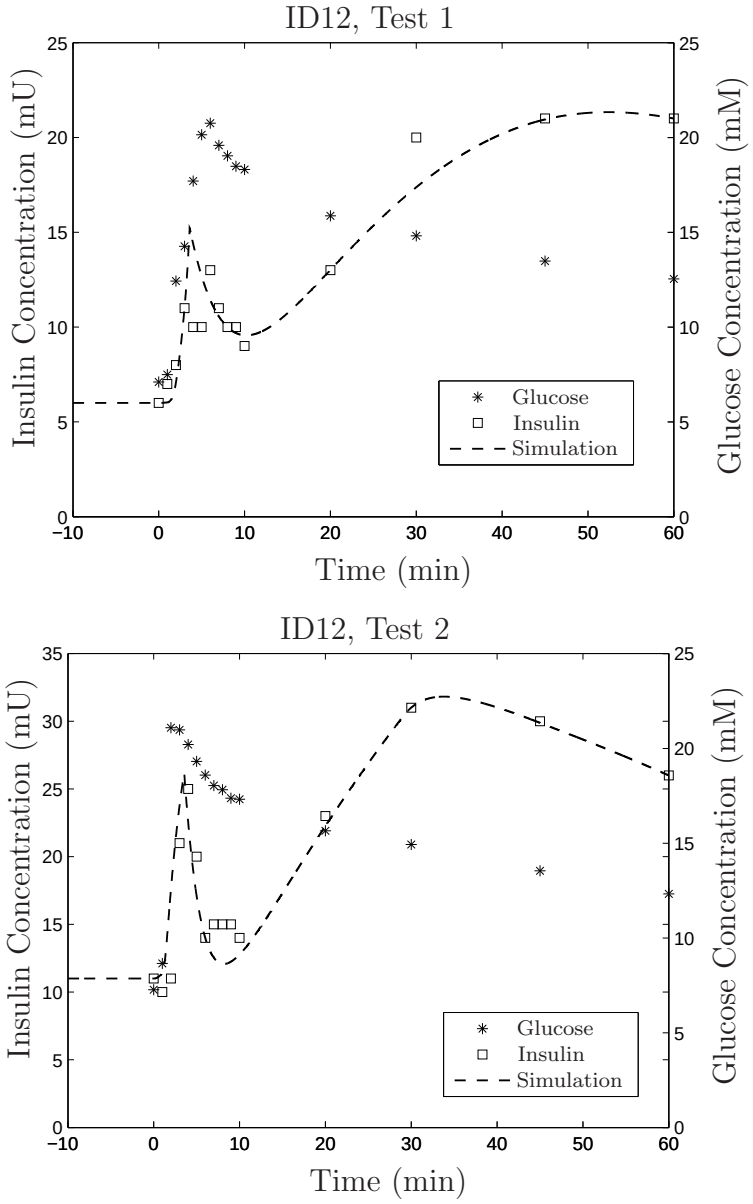

Figure 3.29. Simulation results of moderate diabetic subjects.

diabetics (Group ID13) who are treated with tolbutamide (Kjems et al., 2001), which is a K^+-channel blocker with the ability of stimulating insulin release. The regular IVGTT begins at 0 min, then the tolbutamide is added at 20 min. Simu-

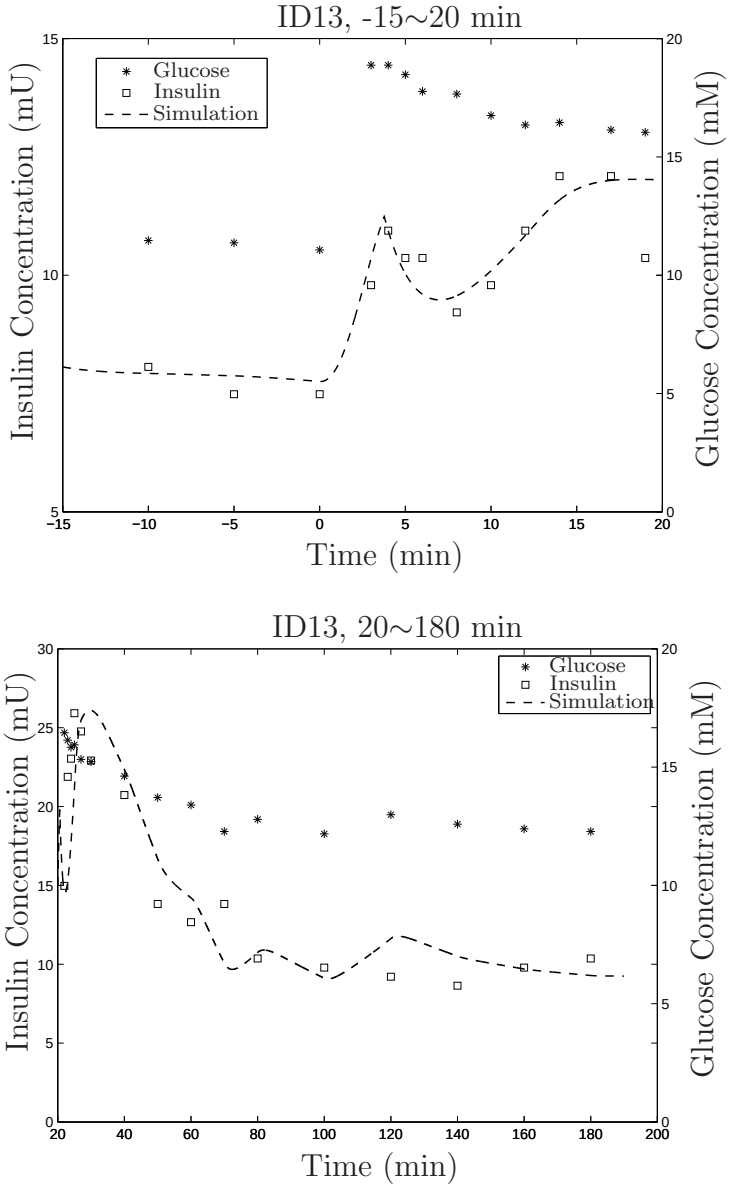

Figure 3.30. Simulation results of diabetic subjects treated with tolbutamide.

lation results are illustrated in Figure 3.30.

The achieved parameters in the test of $-15 \sim 20$ min are K_{p1}=16.52 mM, K_{p2}=37.53 mU·min^{-1}, K_{p3}=2113.17 mmol^{-1}, K_{p4}=3.81×10^{-3} mmol, K_{p5}=6.06

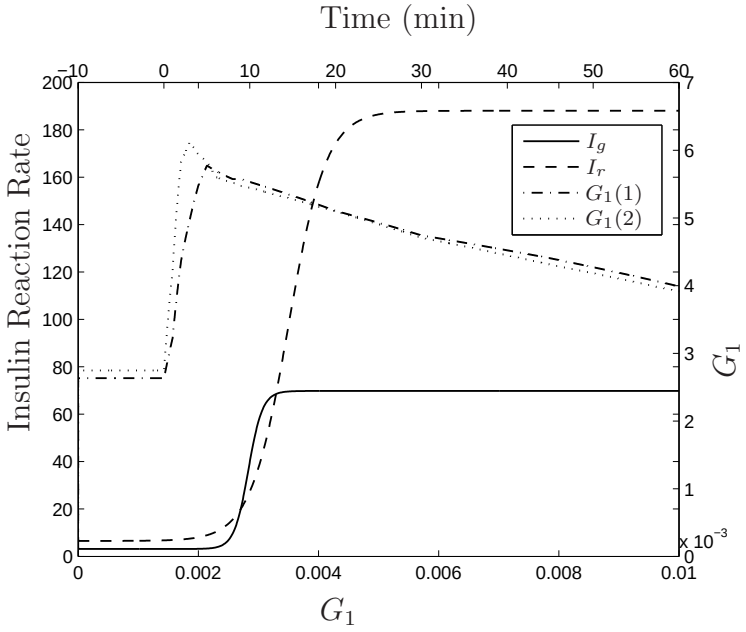

Figure 3.31. Component functions in group ID10.

mU·min^{-1}, K_{p6}=0.025 min^{-1}, K_{p7}=11.11 mU·min^{-1}, K_{p8}=2813.44 mmol^{-1}, K_{p9}= 4.72×10^{-3}, K_{p10}=10.5 mU·min^{-1}, K_{p11}=129.63 mU, K_{p12}=40.06 mU·l^{-1}·min^{-1} and K_{p13}=79.94 mU·l^{-1}.

In the other test of 20 $\sim$ 180 min, the achieved optimal parameters are K_{p1}=26.67 mM, K_{p2}=68.67 mU·min^{-1}, K_{p3}=3777.18 mmol^{-1}, K_{p4}=3.23×10^{-3} mmol, K_{p5}=33.48 mU·min^{-1}, K_{p6}=0.20 min^{-1}, K_{p7}=177.77 mU·min^{-1}, K_{p8}=2991.74 mmol^{-1}, K_{p9}=4.17×10^{-3}, K_{p10}=9.44 mU·min^{-1}, K_{p11}=22.22 mU, K_{p12}=59.96 mU·l^{-1}·min^{-1} and K_{p13}=100 mU·l^{-1}.

Also, the dynamics of G_1, insulin generation (I_g) and release (I_r) are illustrated from Figure 3.33 through 3.36.

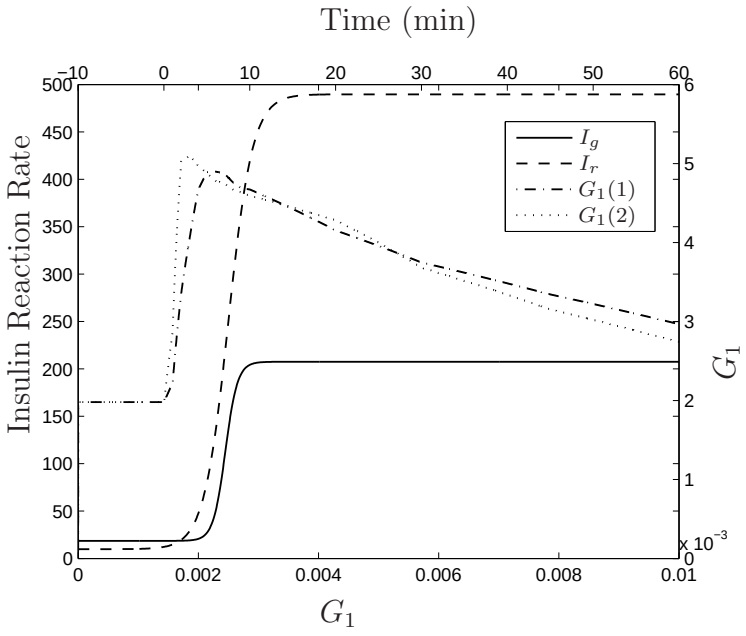

Figure 3.32. Component functions in group ID11.

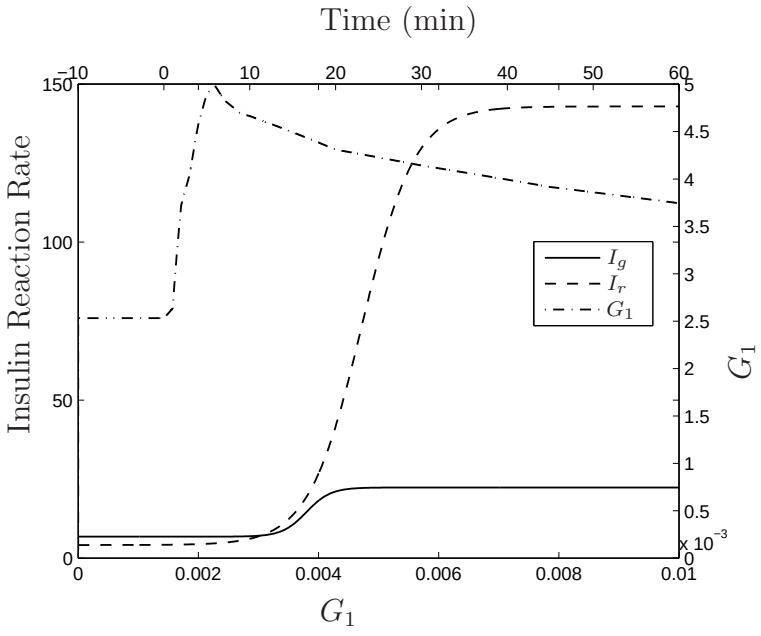

Figure 3.33. Component functions in group ID12, Test 1.

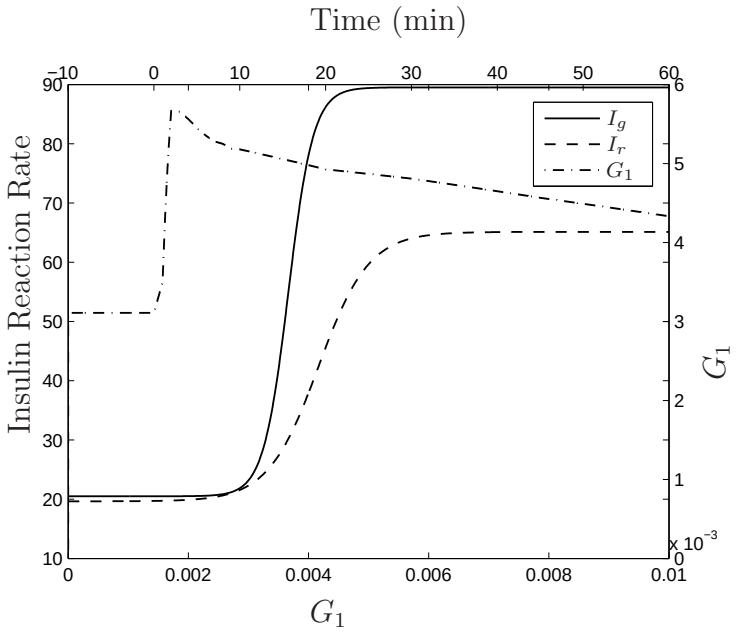

Figure 3.34. Component functions in group ID12, Test 2.

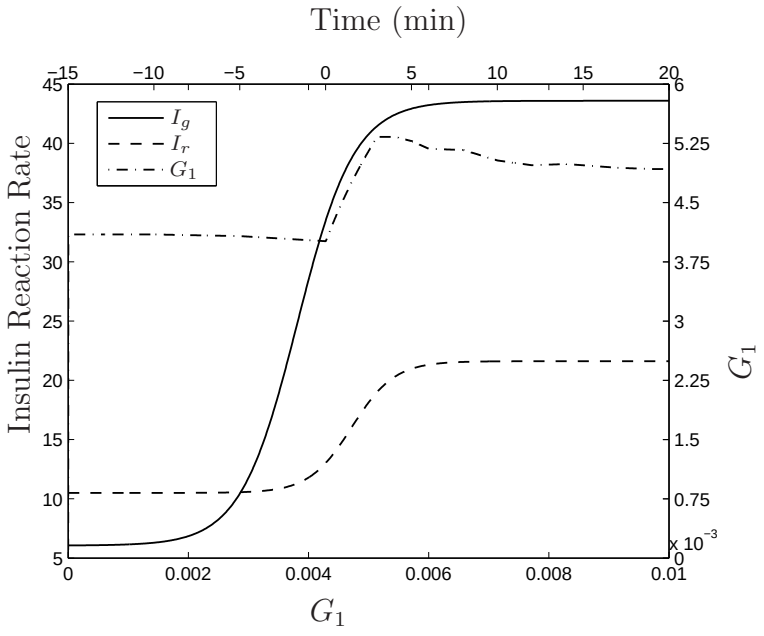

Figure 3.35. Component functions in group ID13, -15∼20min.

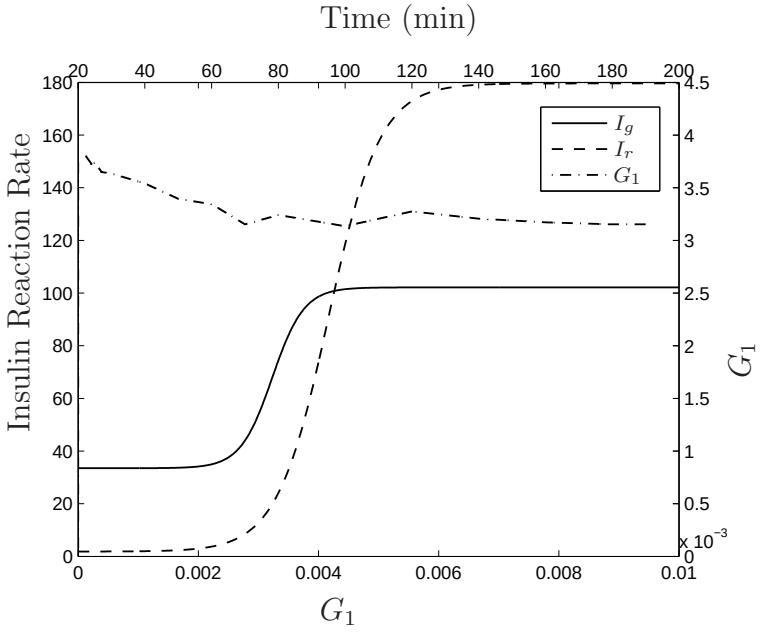

Figure 3.36. Component functions in group ID13, 20∼180min.

In summary, the parameters of the pancreas model in various groups of subjects (normal subjects and diabetics) are illustrated in the Table 3.1. These values represent the characteristics of the pancreas in various subjects. For example in the compartment of I_g, K_1 represents the ability of glucose transport by GLUT2. In healthy subjects, K_1 has a smaller value (9.39) than that in diabetics which represents that GLUT2 may reach the maximal transport rate earlier in health subjects than in diabetics.

In the compartment of I_g, K_2 (the maximal insulin production rate) increased from 37.53 to 68.67 In the group of treated diabetics after the treatment. As for the basal insulin generation rate (K_5) is greater in normal subjects (32.82) than that in diabetic subjects This may indicate a smaller basal insulin production in diabetic subjects. In the treated diabetics group, it is illustrated that K_5 was increased from 6.06 to 33.48 after treatment.

TABLE 3.1

THE PARAMETERS OF THE PANCREAS (MIL.D.: MILD DIABETICS; MOD.D.: MODERATE DIABETICS; TRT.D.: TREATED DIABETICS).

K_i	Normal	Mil.D.1	Mil.D.2	Mod.D.1	Mod.D.2	Trt.D.1	Trt.D.2
K_1	9.39	13.05	20.0	20.96	16.11	16.52	26.67
K_2	32.11	66.67	188.89	15.55	69.0	37.53	68.67
K_3	3112.55	8518.49	9937.59	4975.3	4823.1	2113.17	3777.18
K_4	4.85E-3	2.83E-3	2.45E-3	3.8E-3	3.67E-3	3.81E-3	3.23E-3
K_5	32.82	3.14	18.61	6.78	20.50	6.06	33.48
K_6	1.13	0.30	0.23	0.04	0.033	0.025	0.20
K_7	111.10	181.48	479.77	138.78	45.47	11.11	177.77
K_8	2327.77	3178.85	4936.21	2271.32	2387.31	2813.44	2991.74
K_9	4.52E-3	3.5E-3	2.5E-3	4.72E-3	4.17E-3	4.72E-3	4.17E-3
K_{10}	12.33	6.53	9.85	4.13	19.65	10.5	9.44
K_{11}	304.68	407.64	1344.03	88.89	333.33	129.63	22.22
K_{12}	77.79	98.42	86.67	32.96	60	40.06	59.96
K_{13}	92.55	171.24	166.67	144.64	100	79.94	100

As the indicator of insulin generation delay, K_6 has a greater value in healthy subjects (1.13) which represents a smaller delay comparing the corresponding values in the mild diabetic subjects (0.30 and 0.23) and the moderate diabetic subjects (0.04 and 0.033). In the group of treated diabetics, K_6 is small before treatment (0.025) and increases after tolbutamide injection (0.20). It is concluded that a more severe diabetic subject may have a smaller K_6 which represents a larger delay. K_{11} represents the initial insulin storage in granules. It varies in different subjects. In ID13, the storage decreases after the first phase of inulin release (from 129.63 to 22.22).

In the compartment of insulin release (I_r), K_7 is generally smaller in moderate diabetic subjects (moderate diabetics group 2, treated diabetics) which represents a weak insulin release. In the group of treated diabetics, K_7 increased after treatment (from 11.11 to 177.77) because of the stimulation of tolbutamide. The dynamics of insulin release in various groups are illustrated in Figure 3.37.

In the compartment of insulin clearance (I_d), the maximal insulin clearance rate (K_{12}) is smaller in diabetic subjects, which represents less insulin removal of organs. The Michaelis constant of insulin clearance (K_{13}) is smaller in healthy ones which represents a faster insulin clearance. In the group of treated diabetics, K_{12} increased after the treatment (from 40.06 to 59.96) and K_{13} increased after treatment (from 79.94 to 100) which improved the insulin clearance. The insulin removal dynamics in various groups are illustrated in Figure 3.38.

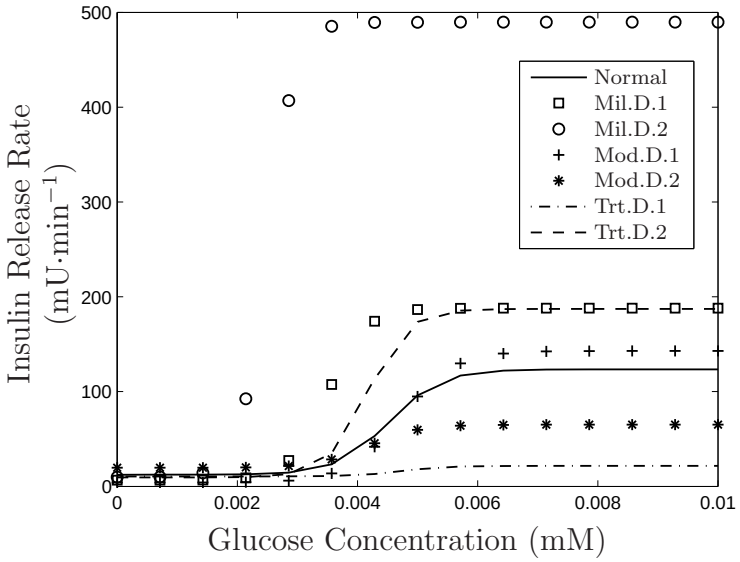

Figure 3.37. Insulin release in various groups.

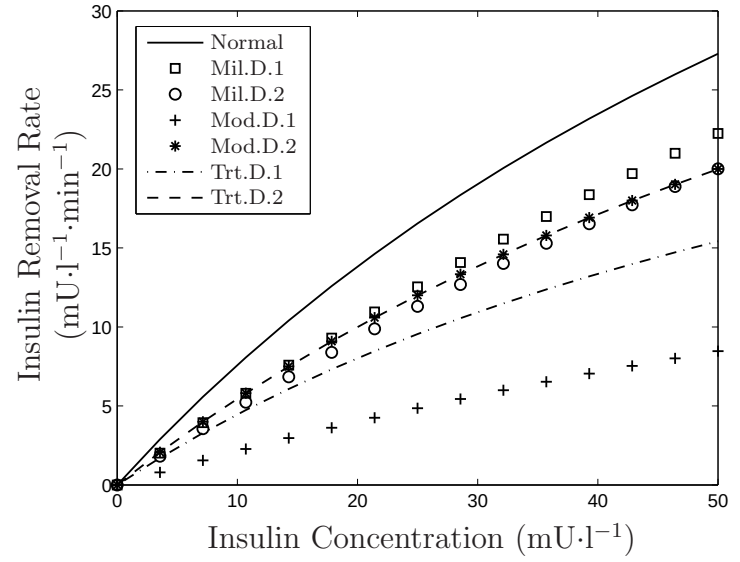

Figure 3.38. Insulin removal in various groups.

The normal subjects (solid lines) have the normal levels of insulin release and clearance. While in the group of mild diabetes (symbols of open square and open circle), the ability of insulin response is decreased which is represented by the impaired ability of insulin removal. Therefore the rate of insulin release is increased as a compensation for glucose uptake. When the status of diabetes gets worse (moderate diabetes, e.g., symbols of plus and asterisk), the ability of maintaining a high insulin release rate fails. The release of insulin can not catch up the demand. Thus, the release of insulin decreases and the ability of insulin removal is still impaired. In the group of treated diabetes (dash-dot and dashed lines), the abilities of both insulin release and removal are improved after the treatment of tolbutamide, which is one type of potassium channel blockers with the ability of stimulating insulin release as described in the compartment of insulin release previously. These results accord with the development of insulin resistance and diabetes (Frayn, 2003) which may make this model an important tool to investigate insulin dynamics in normal subjects and diabetics.

3.6 The Glucose Transport Model in Skeletal Muscle

In the model of glucose transport in skeletal muscle, there are 12 parameters $(K_{s1}, \cdots, K_{s12})$ to be determined. The objective function for optimization is defined as the sum of squares of glucose uptake rate difference (mmol·min^{-1}) at sampled times in skeletal muscle between data from the model simulation and data from the clinical experiments. The experimental data (8 healthy males) are cited from the literature (Katz et al., 1986). The designed experimental protocol is given by

1. Rest + Cycle at 50% $\dot{\mathrm{V}}_{\mathrm{O2\,max}}$ ($\approx$ 15 min) + 100% $\dot{\mathrm{V}}_{\mathrm{O2\,max}}$ until fatigue ($\approx$ 5

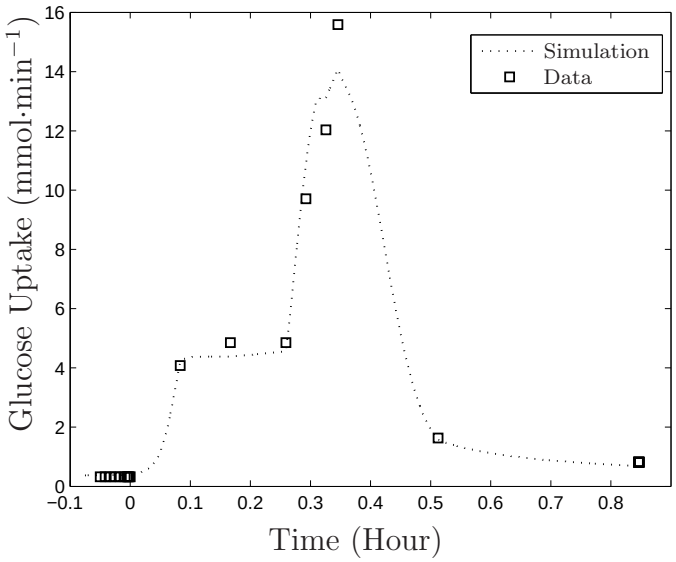

Figure 3.39. Glucose uptake in skeletal muscle.

min).

Glucose concentration in plasma is monitored and sampled. Insulin concentration is determined by the mechanistic pancreas sub-model defined in Section 3.1. The sampled data are leg glucose uptake rates which are converted to glucose uptake in skeletal muscle based on the weight distribution of skeletal muscle (Janssen et al., 2000). There are 18 data points added to the sampled data (9 points at the beginning; 9 other points at the end). With a profile of glucose concentrations and different oxygen consumption ratios of $\dot{\mathrm{V}}_{\mathrm{O2\,max}}$, the determined optimal parameters values for this set of subjects are: $K_{s1} = 5.02$, $K_{s2} = 0.61$, $K_{s3} = 5.0$, $K_{s4} = 0.69$, $K_{s5} = 0.25$, $K_{s6} = 1.15$ mmol·min^{-1}·kg-muscle^{-1}, $K_{s7} = 199.99$ mU·l^{-1}, $K_{s8} = 21.47$ mM, and $K_{s9} = 10.0$ mU·l^{-1}, $K_{s10} = 55.55$, $K_{s11} = 16.67$, $K_{s12} = 0.4$. The simulation result of glucose uptake is illustrated in Figure 3.39 which demonstrates a good match with the clinical data in a profile of various exercise intensities.

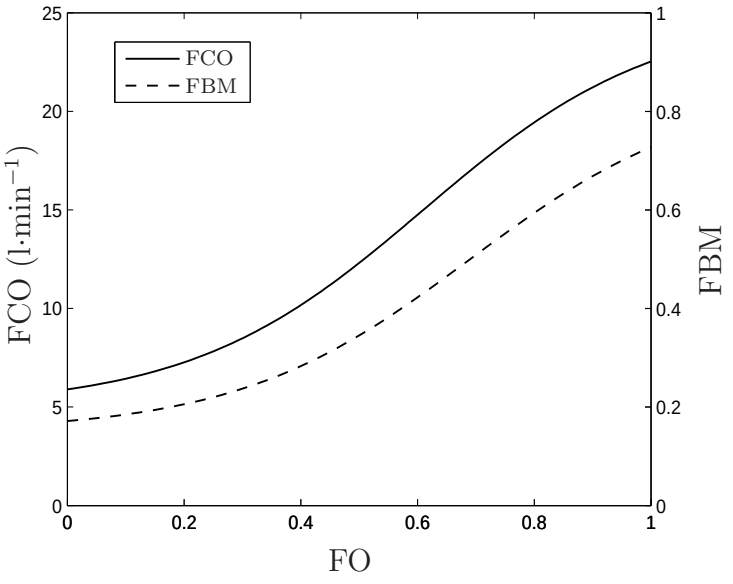

Figure 3.40. The cardiac output and blood distribution.

The cardiac output and the blood distribution in skeletal muscle are illustrated in Figure 3.40.

For this specific group of subjects, the average cardiac output has the basal rate of 6 l·min^{-1} and may reach 23 l·min^{-1} at maximal oxygen consumption rate. Also, the average blood distribution of skeletal muscle is about 17% at basal sate and 72% at maximal oxygen consumption ratio. These results are very close to the ranges of FCO and FBM stated previously. The GLUT4 dynamics stimulated by insulin and exercise respectively is illustrated in Figure 3.41. The Michaelis-Menten characteristics of GLUT4, $V_{\max}$ and K_m, are stimulated by insulin as insulin concentration increases. The domain of K_m in the simulation is about 3.5$\sim$5.0 mM in the insulin profile of experiment, which is close to the reference value (5.0 mM) (Frayn, 2003). The activity of GLUT4 is also stimulated by

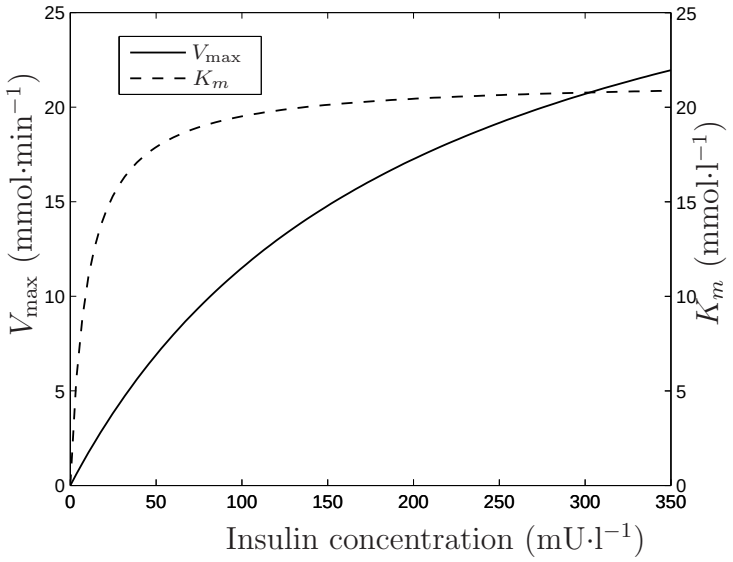

(a) Insulin effect

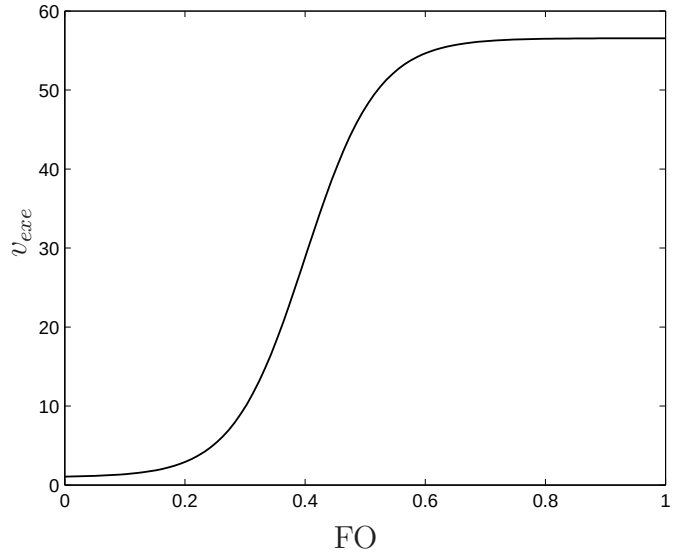

(b) Exercise effect

Figure 3.41: GLUT4 dynamics.

exercise, which brings more GLUT4 to cell membranes to carry glucose. As a consequence, the maximal rate of glucose transport, $V_{\max}$, is increased.

CHAPTER 4

CONCLUSIONS AND FUTURE WORK

4.1 Conclusions

This thesis proposed a mechanistic model of glucose metabolism in the human body, including the organs of the brain, the liver, skeletal muscle and the pancreas. The different properties of glucose transporters in various organs are incorporated into the model. The parameters in the model have physical meanings. In the protocols of meals and various exercise intensities, the dynamics of metabolites have a good qualitative match of glucose metabolism in healthy subjects.

The sub-models of the pancreas and glucose transport in skeletal muscle are also further refined to incorporate more physiological information. The parameters of these models are obtained by the global deterministic optimization method (DIRECT), which is implemented in a parallel computation framework. The simulation results demonstrate a good match with the experimental data of normal subjects, as well as mild and moderate diabetics and diabetics treated with medicine. The parameters of the pancreas model for the normal subjects are validated using different sets of experimental data. These parameters represent the characteristics of subjects. For example, in the model of the pancreas, the parameter of delay (K_6) is a strong candidate which can be used to categorize subjects. The smaller the value of K_6 is (representing a greater delay), the more severe of diabetes a subject may have.

This mechanistic model may provide some insights on the analysis of metabolic pathways especially in the research area of type 2 diabetes. It may be a great tool for *in silico* medical research.

4.2 Future Work

The proposed model may be improved in several aspects. One is to obtain more information such as glucose concentrations in the IFS and the ICS which may provide more information for optimization. Another concern is that in the model of glucose transport in skeletal muscle, the adopted data from the literature are glucose uptake in legs rather than that in skeletal muscle of the whole body. The intracellular glucose metabolism in skeletal muscle, glucose transport in the liver and intracellular glucose metabolism in the liver may be developed and validated and connected to represent glucose metabolism in the body. Plus, the model development of the adipose may provide insight into obesity, fat accumulation and distribution. The interaction of glucose metabolism and fatty acid metabolism may provide guidance on medical and human health research.

Similar to the discussion in Chapter 3, the parameters of models of the intracellular glucose metabolism in skeletal muscle, glucose transport in the liver and intracellular glucose metabolism in the liver may be determined from clinical data by the same optimization method DIRECT.

As stated above, the goal of this physiological metabolism system model is to investigate metabolic dynamics in a mechanistic way. Besides glucose metabolism, another important one, fatty acid metabolism, is going to be taken into account (Horowitz et al., 1999; Kissebah et al., 1982; Klein, 2004). The distorted fat accumulation and distribution may cause health problems (Bjorntorp et al.,

1990; Chan et al., 1994; Jensen et al., 1989; Nielsen et al., 2004). There are some connections between obesity and diabetes (Chan et al., 1994; Shadid et al., 2007). The relation between glucose metabolism and fatty acid metabolism is complicated (Boden and Chen, 1995; Boden et al., 1991; Colberg et al., 1995; Groop et al., 1989; Homko et al., 2003; Sidossis et al., 1996). Experiments on animals demonstrate some insights for fat acid metabolism (Basso and HaveL, 1970; Robertson et al., 1982). Insulin also has great influence in fatty acid metabolism (Green and Newsholme, 1979; Greenwood et al., 1966; Groop et al., 1991; Harrison et al., 1976; Roden et al., 1996).

Fatty acids may be bounded to other molecules such as esterified triglycerides (TAG) or they can move without attachment, known as *Free Fatty Acids* (FFA) or *Non-Esterified Fatty Acids* (NEFA). In the free state, fatty acids can be transported to other organs as fuel. They may be esterified into TAG and form fat cells (adipocytes) to store fat as energy. Fatty acids can also be released from TAG to meet the demand of energy by other organs. Besides, the adipose may secrete important substances to regulate the physiological system, such as some hormones (Frayn, 2003).

There are two types of adipose: brown adipose and white adipose. The brown adipose tissue is a main source of heat for animals. It may oxidize substrates *via* TCA cycle and release heat from an uncoupling process without combining the free energy in compounds (Frayn, 2003). But there is not a significant amount of the brown adipose in adult humans where adipose is mainly composed of the white adipose tissue. So in the sub-model of the adipose, only the white adipose is going to be investigated.

In the plasma, there are free fatty acids and the lipoprotein particles in the

form of the chylomicrons (CLM), Very Low Density Lipoprotein particles (VLDL), Low Density Lipoprotein particles (LDL), *etc.* Since we are more interested at he dynamics of TAG, the CLM and VLDL particles, which are rich in TAG, are taken into account in the model. The CLM comes from the meals. They are created in the gut and released through the lymphatic system, up the thoracic duct and then entering the circulating system. The VLDL particles are secreted by the liver, delivering the TAG from the liver to other tissues (Frayn, 2003).

The triglycerides in the lipoprotein particles will be released into the plasma and hydrolyzed to fatty acids by the lipoprotein lipase (LPL) located in endothelial cells lining the capillaries. The lipoprotein lipase is located at the adipose, skeletal muscle and heart muscle. In the adipose, the activity of LPL is stimulated by insulin while in skeletal muscle, it is slightly suppressed by insulin and stimulated by exercises (Frayn, 2003).

Released from lipoproteins, fatty acids will diffuse into IFS and enter ICS by a carrier, FAT/CD36. The uptake rate is largely determined by the delivery rate (*i.e.* the product of blood flow and concentration) where the blood flow may be reflected by the oxygen consumption rate, showing the connection with exercises (Frayn, 2003). After fatty acids are carried into cells, they enter the metabolism pathways and show different characteristics in different organs.

For the mechanistic model, the sub-models of skeletal muscle and the liver may be extended to include the metabolism of fatty acids locally. Also the sub-model of the adipose is to be established. The functions about the adipose are currently under investigation and the mathematical representations are from assumption which will be verified in further research.

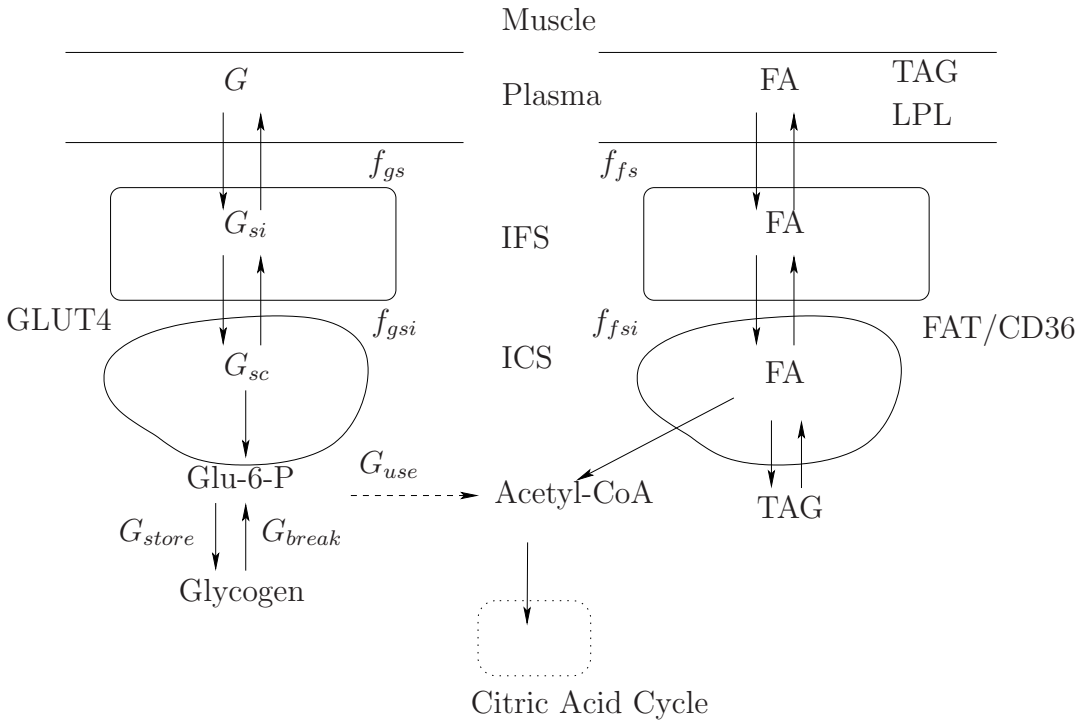

Figure 4.1. Glucose and fatty acids transported into muscle.

4.3 Skeletal Muscle

4.3.1 Glucose and Fatty Acids Transport

The model of glucose and fatty acids (FA) transport is illustrated in Figure 4.1. The left side represents the glucose transportation while the right side represents the fatty acids transportation. In the capillaries, LPL acts on TAG in the lipoproteins to release the fatty acids. By the concentration gradient, the fatty acids enter IFS. Then the fatty acids are taken up to the cells carried by FAT/CD36 (Frayn, 2003).

Now the transport of fatty acids may be added to the sub-model of skeletal muscle.

1. LPL acts on the lipoproteins (CLM and VLDL) in the capillaries which is slightly suppressed by insulin (Frayn, 2003). Plus, exercise may stimulate its activity (Frayn, 2003). The rate may also be saturated while increasing the concentrations of CLM and $VLDL$.

2. The fatty acids are transported between plasma and IFS *via* concentration gradient and taken up into cells by carriers involving FAT/CD36 (Frayn, 2003).

As illustrated in Figure 4.1, fatty acids may be stored as TAG or be converted into Acetyl-CoA (ACA) after entering the cells. TAG in skeletal muscle is mainly for local use. It should be noted that ACA is another important metabolite connecting the glucose metabolism and the fat metabolism as in the Citric Acid Cycle (also called TCA cycle).

4.3.2 Glucose and Fatty Acid Metabolism

The intracellular metabolism model of skeletal muscle incorporates more information concerning the fatty acid metabolism. Intracellularly, G6P may be converted to pyruvate (Pyr) during glycolysis given by the relation:

$$1\,\text{G6P} \rightarrow 2\,\text{Pyr}. \tag{4.1}$$

Afterward, pyruvate may be converted to Acetyl-CoA (ACA) and enter the TCA cycle in the pathway of aerobic respiration. Also, pyruvate is converted to lactate (Lac) in the pathway of anaerobic respiration as illustrated in Figure 4.2. The

relations are expressed as

$$1\,\text{Pyr} \rightarrow 1\,\text{ACA} \tag{4.2}$$

$$1\,\text{Pyr} \rightarrow 1\,\text{Lac.} \tag{4.3}$$

In skeletal muscle, fatty acids cannot be generated from ACA due to the lack of fatty acid synthase. But ACA here can result in an inhibition on the oxidation of fatty acids because ACA may be converted to malonyl-CoA which may suppress the β-oxidation of fatty acids (Frayn, 2003).

1. The dynamics of Acetyl-CoA (ACA) is determined by the aerobic respiration, pyruvate and fatty acids. Therefore its activity is related oxygen consumption rate, the cardiac output and the blood flow distribution. The rate of fatty acids converted into Acetyl-CoA through β-oxidation is inhibited by insulin. The generation of ATP is represented by

$$1\text{FADH}_2 \rightarrow 1.5\text{ATP} \tag{4.4}$$

$$1\text{NADH} \rightarrow 2.5\text{ATP} \tag{4.5}$$

$$1\text{Acetyl} - \text{CoA} \rightarrow \text{TCA.} \tag{4.6}$$

   One of the most common fatty acids is palmitic acid. It is even-number chained with $2n, n = 8$. Two extra units of ATP are consumed to activate the oxidation (Frayn, 2003). Hence,

$$\text{ATP}_{production} = (8-1) \times (1.5 + 2.5) = 28 \tag{4.7}$$

$$\text{ATP}_{consumption} = 2. \tag{4.8}$$

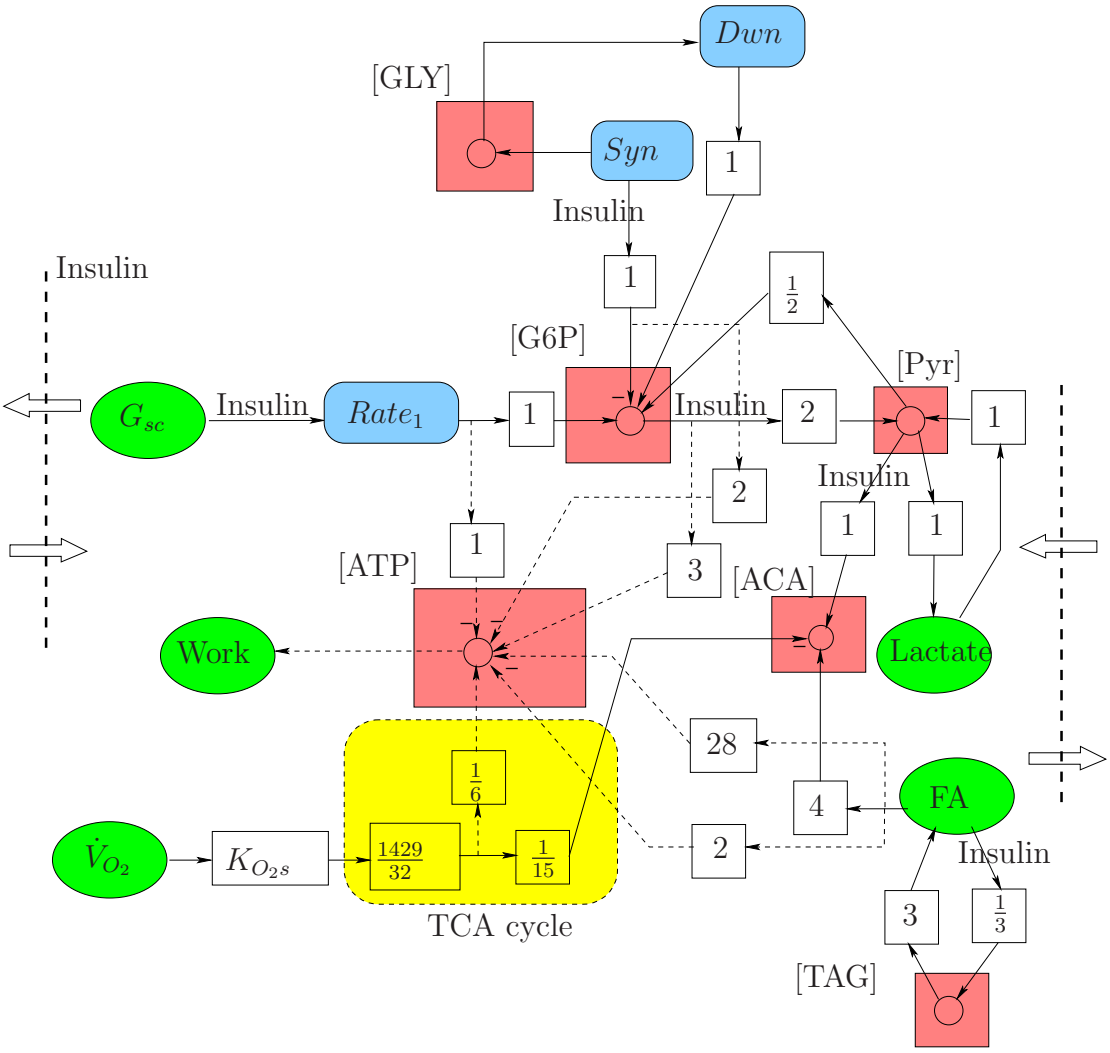

Figure 4.2. Glucose and fatty acid metabolism in skeletal muscle.

2. The dynamics of TAG may be esterified from fatty acids and release fatty acids for energy requirement. Insulin inhibits the conversion from TAG to fatty acids and stimulates the esterification of TAG from fatty acids (Frayn, 2003).

3. The dynamics of pyruvate is determined by its relations to G6P, ACA and lactate. Pyruvate may be generated from lactate through the process of gluconeogenesis; while pyruvate will produce lactate through anaerobic glycolysis (Frayn, 2003).

Therefore, the energy balance between demand and production is influenced by the concentrations of G6P, Pyr, ACA and lactate.

4.4 The Liver

4.4.1 Glucose and Fatty Acids Transport

The transport of glucose and fatty acids in the liver is illustrated in Figure 4.3. Compared with that in the skeletal muscle, the liver does not have the lipoprotein lipase (LPL) to utilize lipoprotein particles in the capillaries. Also, VLDL particles may be released to the circulation system by the liver. Additionally, inside the liver cells, there exists ketogenesis to release ketone bodies, which may be a fuel source for the heart, the brain, *etc.* (Frayn, 2003)

The transport of fatty acids are similar with that in skeletal muscle.

1. The VLDL particles may be released into the plasma. It is secreted by the liver and contains triacylglycerol, cholesteryl ester and apolipoproteins (Frayn, 2003).

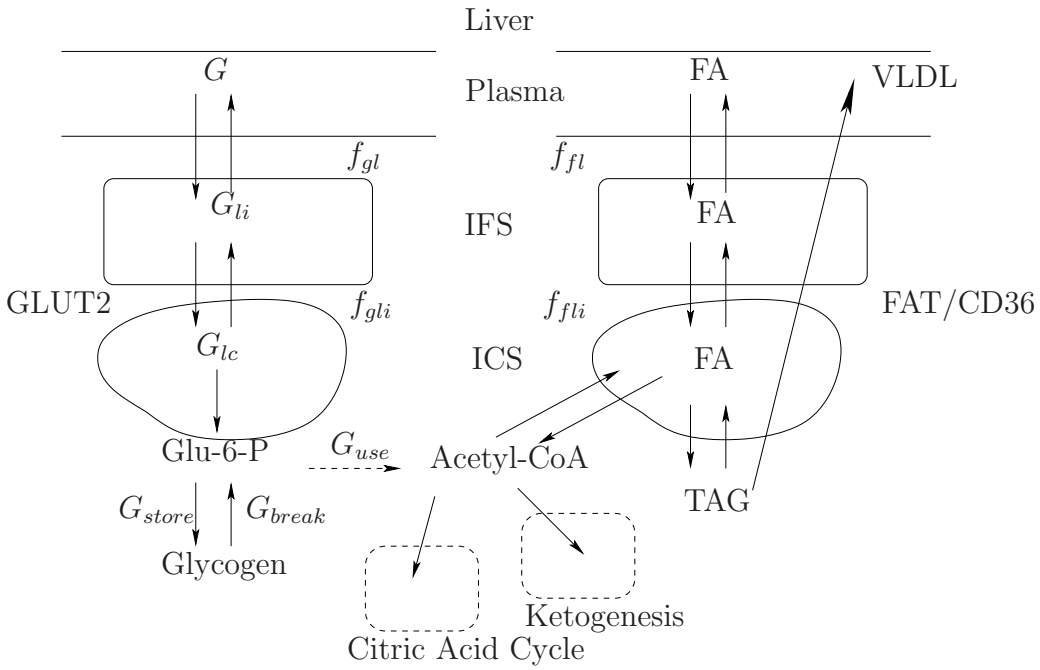

Figure 4.3. Glucose and fatty acids transport in the liver.

2. The fatty acids are transported between plasma and IFS *via* concentration gradient and taken up into cells by carriers involving FAT/CD36 which is influenced by the oxygen consumption rate (Frayn, 2003).

4.4.2 Glucose and Fatty Acid Metabolism

Similar with the intracellular glucose and fatty acid metabolism in skeletal muscle, more details are incorporated into the model of intracellular metabolism in the liver, such as pyruvate (Pyr), Acetyl-CoA (ACA), fatty acids (FA), *etc.* For fatty acid metabolism, there exists the fatty acid synthase in the liver. Hence, ACA may be converted to fatty acids. And ketone bodies (another form of fuel mainly used by the heart and the brain) may be produced in the liver through ketogenesis (Frayn, 2003). These are illustrated in Figure 4.4.

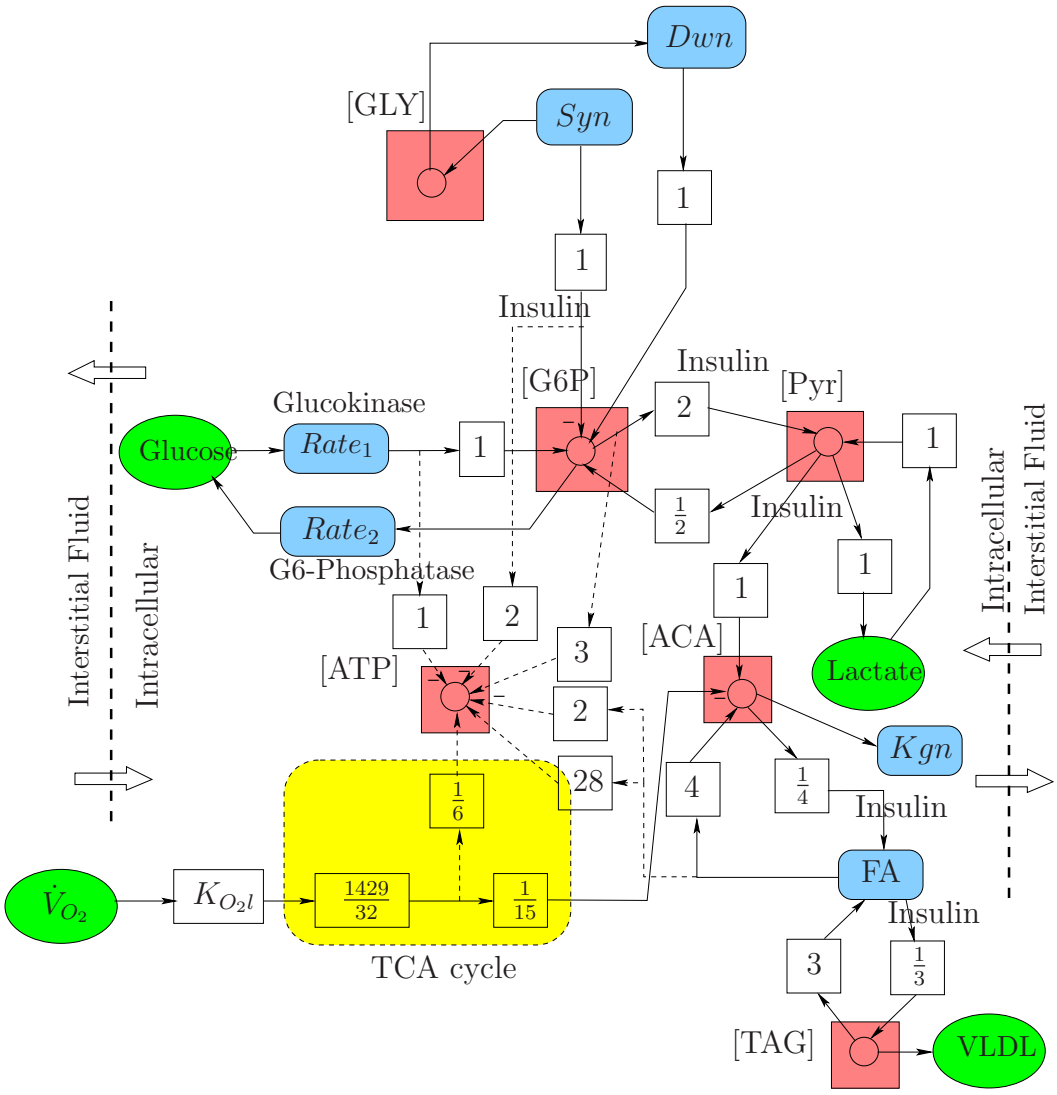

Figure 4.4. Glucose and fatty acid metabolism in the liver.

1. The concentration of Acetyl-CoA (ACA) is connected to the aerobic respiration, pyruvate and fatty acids. Therefore it is influenced by the oxygen consumption rate, the cardiac output and the blood distribution to the liver. The rate of converting Pyr into ACA is stimulated by insulin (Frayn, 2003).

2. Fatty acids may be broken down to generate ACA through β-oxidation as a source of TCA cycle while fatty acids may be produced from ACA in the process of *de novo* lipogenesis (Frayn, 2003). One of the productions of β-oxidation is ketone bodies which is another form of fuels (Frayn, 2003).

3. The process of breaking down TAG to fatty acids is inhibited by insulin while the counter process of esterifying fatty acids to TAG is stimulated by insulin (Frayn, 2003).

4. The liver may release lipoprotein particles in the form of VLDL to the plasma (Frayn, 2003).

5. Besides G6P and ACA, the dynamics of pyruvate is also influenced by lactate through the process of gluconeogenesis and anaerobic glycolysis.

4.5 Adipose Tissue

4.5.1 Glucose and Fatty Acids Transport

The transport of fatty acids in the adipose is illustrated in Figure 4.5. The lipoprotein lipase (LPL) may release fatty acids from lipoprotein particles in the capillaries.

1. The fatty acids are transported between plasma and IFS *via* concentration gradient and taken up into cells by carriers involving FAT/CD36 which is

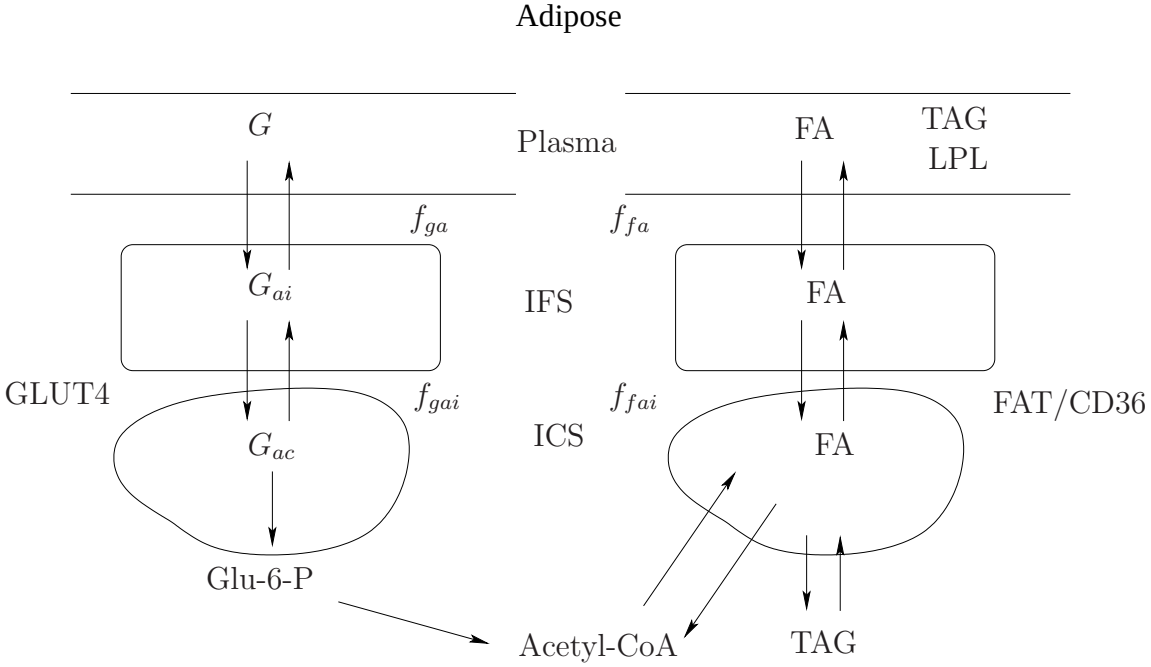

Figure 4.5. Glucose and fatty acids transported into the adipose.

influenced by the oxygen consumption rate (Frayn, 2003). The lipoprotein lipase (LPL) is also located at the adipose, which may release fatty acids from lipoprotein particles in the capillaries, such as CLM and VLDL particles.

2. The glucose transport between the IFS and the ICS is facilitated by glucose transporter type 4 (GLUT4), which follows the Michaelis-Menten movement (Frayn, 2003).

4.5.2 Glucose and Fatty Acid Metabolism

The intracellular glucose and fatty acid metabolism in the adipose tissue is illustrated in Figure 4.6.

1. Glucose is carried by GLUT4 into the adipocytes. It may be converted

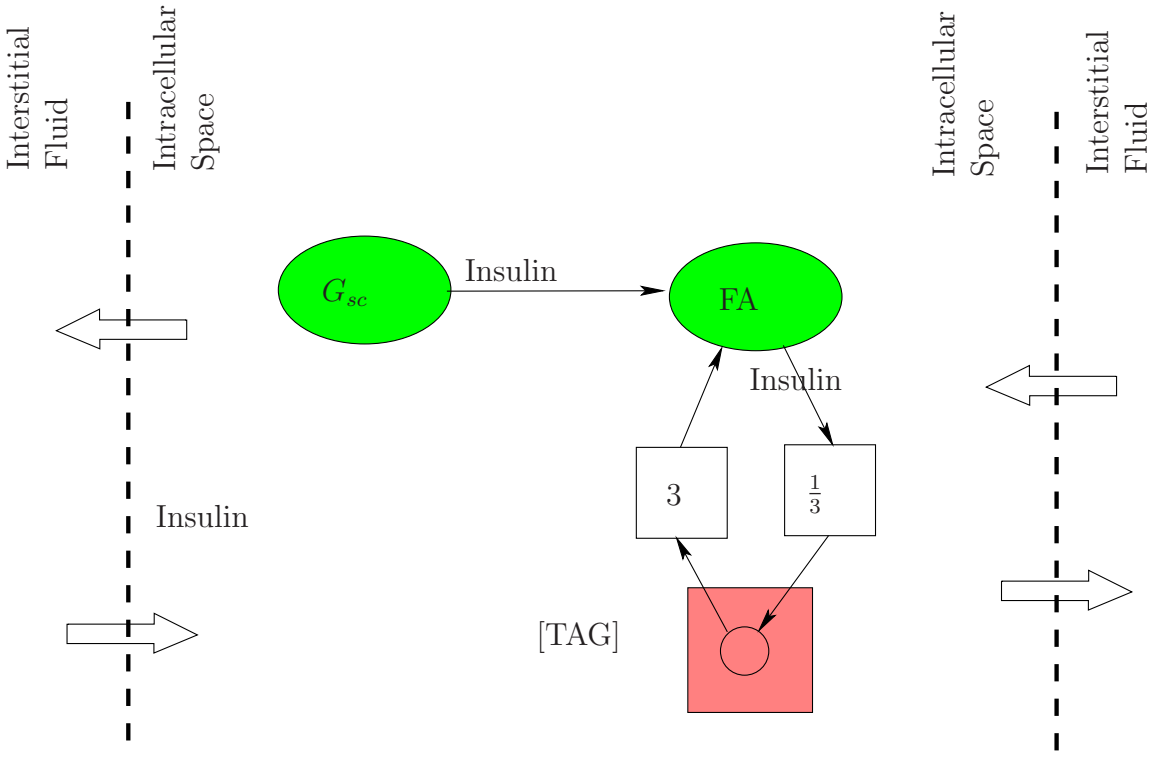

Figure 4.6. Glucose and fatty acid metabolism in the adipose tissue.

to fatty acids through the process of lipogenesis which is stimulated by insulin (Frayn, 2003).

2. The process of breaking down TAG to fatty acids is inhibited by insulin while fatty acids may be esterified to TAG which is stimulated by insulin (Frayn, 2003).

BIBLIOGRAPHY

A. Adrover et al. *Physica D*, 213:121–146, 2006.

S. Aiston et al. *Diabetes*, 52(6):1333–1339, 2003.

American Diabetes Association. http://www.diabetes.org/, 2007.

R. Armstrong et al. *J. Appl. Physiol.*, 62:1285–1298, 1987.

S. Ashcroft et al. *Biochem J.*, 174:517–526, 1978.

K. Aukland and R. Reed. *Physio. Reviews*, 73:1–78, 1993.

A. Avogaro et al. *Diabetes*, 38:1048–1055, 1989.

A. Bagust and S. Beale. *Q J Med.*, 96:281–288, 2003.

L. V. Basso and R. J. HaveL. *J. Clin. Invest.*, 49:537–547, 1970.

R. Bergman et al. *J. Clin. Invest.*, 68:1456–1467, 1981.

T. Binzoni et al. *J. Nucl. Med.*, 27:192–197, 1998.

P. Bjorntorp et al. *Arteriosclerosis*, 10:493–496, 1990.

G. Blomqvist et al. *European Journal of Nuclear Medicine and Molecular Imaging*, 18(10):834–837, 1991.

G. Boden and X. Chen. *J. Clin. Invest.*, 96:1261–1268, 1995.

G. Boden et al. *J. Clin. Invest.*, 88:960–966, 1991.

G. A. Brooks. *Comparative Biochem. and Physio.*, 120:89–107, 1998.

M. E. Cabrera et al. *Annals of Biomedical Engineering*, 26:1–27, 1998.

J. Cadefau et al. *Biochem. J.*, 322(3):745–750, 1997.

D. U. Campos-Delgado et al. *ABBI*, 2(2):61–71, 2005.

D. U. Campos-Delgado et al. *IEEE Transactions on Biomedical Engineering*, 53 (11):2201–2210, 2006.

M. L. Cárdenas. *Glucokinase: Its regulation and role in liver metabolism*. Springer-Verlag, 1995.

A. Caumo and C. Cobelli. *Am. J. Physiol.*, 264:E829–E841, 1993.

J. M. Chan et al. *J. Clin. Endocrinol. Metab.*, 17(9):961–969, 1994.

J. Chase et al. *Medical Engineering & Physics*, 27:1–11, 2005.

F. Chee et al. *IEEE Transctions on Biomedial Engineering*, 52(10):1625–1631, 2005.

C. Cobelli et al. *Am. J. Physiol. Endocrinol. Metab.*, 293:E1–15, 2007.

C. Cobelli et al. *Mathematical Biosciences*, 58:27–60, 1982.

S. R. Colberg et al. *J. Clin. Invest.*, 95:1846–1853, 1995.

F. Creta et al. *J. Phys. Chem. A*, 110:13447–13462, 2006.

R. Dash et al. *BioMedical Engineering OnLine*, 6(1):14, 2007.

W. C. Duckworth et al. *Endocrine Rev.*, 19:608–624, 1998.

P. Dunn. *Measurement and data analysis for engineering and science*. Boston: McGraw-Hill Higher Education, 2005.

D. T. Finegood and B. G. Topp. *Diabetes, Obesity and Metabolism*, 3(Suppl. 1): S20–S27, 2001.

K. N. Frayn. *Metabolic regulation: a human perspective*. Blackwell Publishing, 2003.

T. Fujimoto et al. *Med. Sci. Sports Exerc.*, 35:777–783, 2003.

Y. Fujita et al. *Diabetes*, 24:17–27, 1975.

M. Giona et al. *J. Phys. Chem. A*, 110:13463–13474, 2006.

R. Govers et al. *Ame. J. Physiol. Endocrinol Metab.*, 281:E72–80, 2001.

D. Gray. *Transplantation proceedings*, 17(1):381–382, 1985.

A. Green and E. A. Newsholme. *Biochem. J.*, 180:365–370, 1979.

F. C. Greenwood et al. *J. Clin. Invest.*, 45(4):429–436, 1966.

M. Gregoriou et al. *Eur. J. Biochem.*, 161:171–176, 1986.

J. Grimsby et al. *Science*, 301(5631):370–373, 2003.

L. C. Groop et al. *J. Clin. Invest.*, 84:205–213, 1989.

L. C. Groop et al. *J. Clin. Invest.*, 87:83–89, 1991.

M.-T. Guillam et al. *Proc. Natl. Acad. Sci. USA*, 95:12317–12321, 1998.

J. Guyton et al. *Diabetes*, 27:1027–1042, 1978.

D. Harrison et al. *Diabetologia*, 28:99–103, 1985.

L. C. Harrison et al. *J. Clin. Invest.*, 58:1435–1441, 1976.

T. Hayashi et al. *Am. J. Physiol. Endocrinol. Metab.*, 273(36):E1039–1051, 1997.

J. He et al. *Computational Optimization and Application*, 23:5–25, 2002.

J. Henriksen et al. *J. Clin. Invest.*, 94:1196–1204, 1994.

P. Hespel and E. Richter. *Biochem. J.*, 284:777–780, 1992.

J. Holloszy et al. *Diabetes Metab. Rev.*, 1:409–424, 1986.

C. J. Homko et al. *Diabetes*, 52:487–491, 2003.

J. F. Horowitz et al. *Am. J. Physiol.*, 276:E278–E284, 1999.

R. Hovorka et al. *Am. J. Physiol. Endocrinol. Metab.*, 282:E992–1007, 2002.

R. Hume et al. *J. Perinatology*, 20(5):301–306, 2000.

I. Janssen et al. *J. of Appl. Physiol.*, 89(1):81–88, 2000.

M. D. Jensen et al. *J. Clin. Invest.*, 83:1168–1173, 1989.

R. Johnson et al. *Cardiovascular Response to Exercise*, chapter Effects of high altitude and training on oxygen transport and exercise performance, pages 223–252. Futura Publishing Company, Inc. NY, 1994.

D. Jones et al. *J. of Optimization Theory and Application*, 79(1):157–181, 1993.

A. Katz et al. *Am. J. Physiol. Endocrinol. Metab.*, 251(1):E65–70, 1986.

D. E. Kelley and L. J. Mandarino. *J. Clin. Invest.*, 86:1999–2007, 1990.

P. King et al. *Am. J. Physiol. Cell Physiol..*, 257:C1128–1134, 1989.

A. H. Kissebah et al. *J. Clin. Endocrinol. Metab.*, 54:254–260, 1982.

L. Kjems et al. *Diabetologia*, 44:1339–1348, 2001.

S. Klein. *J. Clin. Invest.*, 113(11):1530–1532, 2004.

Y. T. Kruszynska et al. *DIABETES*, 47:1107–1113, 1998.

D. Levitt. *BMC Clinical Pharmacology*, 3:3, 2003.

D. Lv and B. Goodwine. Pancreas modeling from ivgtt data using a deterministic optimal search method. In *2009 IEEE International Conference on Bioinformatics and Biomedicine*, pages 303–308, 2009.

L. Mandarino et al. *J. Clin. Invest.*, 80(3):655–663, 1987.

J. Mellor. *Biochemistry*. Nabu Press, 2010.

S. Nielsen et al. *J. Clin. Invest.*, 113(11):1582–1588, 2004.

C. Owens et al. *IEEE Transactions on Biomedical Engineering*, 53(6):996–1005, 2006.

G. Pacini and R. Bergman. *Computer Methods and Programs in Biomedicine*, 23: 113–122, 1986.

G. Pacini et al. *Am. J. Physiol.*, 274:E592–E599, 1998.

M. J. Pagliassotti et al. *The role of the liver in maintaining glucose homeostasis*. R.G. Landes Company, 1994.

S. Panunzi et al. *Theoretical Biology and Medical Modelling*, 43:35, 2007.

R. S. Park et al. *IEEE Transactions on Biomedical Engineering*, 46(2):148–157, 1999.

R. Parker et al. *IEEE Engineering in Medicine and Biology*, pages 65–73, 2001.

R. S. Parker et al. *AIChE Journal*, 46(12):2537–2549, 2000.

R. E. Petrosyan. Developments of the intrinsic low dimensional manifold method and application of the method to a model of the glucose regulatory system. Master's thesis, University of Notre Dame, 2003.

R. Printz et al. *J. Biol. Chem*, 268(7):5209–5219, 1993.

D. Qian and J. T. Brosnan. *Biochem J.*, 313:479–486, 1996.

G. Quiroz and R. Femat. *Mathematical Biosciences*, 210:554–575, 2007.

J. P. Robertson et al. *Biochem. J.*, 206:577–586, 1982.

M. Roden et al. *J. Clin. Invest.*, 97(12):2859–2865, 1996.

P. Rorsman and E. Renström. *Diabetologia*, 46:1029–1045, 2003.

E. Ruiz-Velázquez et al. *Control Engineering Practice*, 12:1179–1195, 2004.

V. Sarabia et al. *J. Clin. Invest.*, 90:1386–1395, 1992.

E. V. Schaftingen and I. Gerint. *Biochem. J.*, 362:513–532, 2002.

F. Schuit et al. *Proc. Natl. Acad. Sci. USA*, 85:3865–3869, 1988.

J. Seoane et al. *J. Biol. Chem.*, 271(39):23756–23760, 1996.

S. Shadid et al. *Diabetes*, 56:1369–1375, 2007.

R. S. Sherwin et al. *J. Clin. Invest.*, 53:1481–1492, 1974.

L. S. Sidossis et al. *J. Clin. Invest.*, 98(10):2244–2250, 1996.

J. T. Sorensen. *A Physiologic Model of Glucose Metabolism in Man and its Use to Design and Assess Improved Insulin Therapies for Diabetes*. PhD thesis, MIT, 1985.

E. Sternlicht et al. *Am. J. Physiol. Endocrinol. Metab.*, 256:E227–230, 1989.

L. Stryer. *Biochemistry*. New York: W.H. Freeman and Company, 5th edition, 2002.

D. Swain. *Old Dominion University's Quest*, 3(2):9–11, 2000.

N. Syed and R. Khandelwal. *Molecular and Cellular Biiochemistry*, 211(1-2): 123–136, 2000.

B. Thorsteinsson. *Danish Medical Bulletin*, 37(2):143–153, 1990.

I. M. Tolić et al. *J. Theor. Biol.*, 207:361–375, 2000.

B. Topp et al. *J. Theor. Biol.*, 206:605–619, 2000.

O. Vahidi et al. Development of a physiological model for patients with type 2 diabetes mellitus. In *American Control Conference*, 2010.

P. Vicini et al. *Am. J. Physiol.*, 273:1024–1032, 1997.

C. Villar-Palasi. *Biochim Biophys Acta.*, 1095(3):261–267, 1991.

C. Villar-Palasí and J. J. Guinovart. *FASEB J.*, 11:544–558, 1997.

R. Weiss et al. *Diabetes*, 54:1735–1743, 2005.

G. Wilcox. *Clin. Biochem.*, 26:19–39, 2005.

H. Yki-Järvinen et al. *J. of Clin. Invest.*, 79:1713–1719, 1987.

B. Zinker et al. *Diabetes*, 42:956–965, 1993.